Thesis work for Dual Master's Degree

Experimental examination of the MONIKA-ORC-Turbine and comparison of the results with thermodynamical calculation

Mardon Pérez, Joaquín
Civil Engineer
Pontificia Universidad Catolica Argentina

Tutor
Dr. Eng. Thomas Schulenberg, ITES Institute

Co-Tutor
Dipl. Wiemer Hans-Achim, ITES Institute

Examiners
Dr. Eng. Thomas Schulenberg, KIT/ITES
Dr. Eng. Andreas Class, KIT/ITES

Karlsruhe

11/04/2022

Declaration by author

I truthfully declare that I have written this thesis independently, that I have fully and accurately cited all and precisely and to have marked everything that has been taken unchanged or with modifications from the work of others.

Date Signature

Acknowledgement

It was a great pleasure to discover the field of geothermal energy. I would like to express my gratitude to Dipl. Ing. Hans-Joachim Wiemer and Prof. Dr. Thomas Schulenberg, who inspired, supervised, and guided me during this process. This work might not have been so interesting without them.

To my colleague Julia Filipe who helped me along the way, and to my colleagues Juan Ignacio Giménez, Eugenio Torres de Ritter, Juan Francisco Gutiérrez and Luciano Gardella.

Finally, I would like to thank to my family and friends who have contributed to this work in one way or another.

Abstract

The aim of this work is to understand the propane turbine behaviour located at MoNiKa facility in Campus North (KIT). Starting with the thermodynamic simulations, continuing with the selection of different load points to evaluate them experimentally on site and ending with the data analysis to finally reach the correction of the Stodola's law equation and the turbine efficiency correction.

The simulations were performed using GESI software developed in MATLAB® by ITES, and in addition, to perform these simulations, all the calculations of the thermodynamic properties were performed with the REFPROP software, NIST fluid properties database. The working medium of this work is either propane or a mixture between propane and nitrogen.

The runs were carried out at the beginning of November 2021, where different types of assays were performed, previously analysed in GESI. First a test of different turbine load points was performed, the following day the response of the turbine was evaluated by progressively opening the turbine control valve and, the last day, another sensitivity test was performed, but this time the turbine was evaluated with the response of a progressive increase of the mass flow rate through the turbine.

Stodola's equation provides a calculation method for the highly nonlinear dependence of the turbine inlet pressure with a flow for a multistage turbine with high backpressure. From its correction we find its behavior for this turbine. In turn, we sought to understand the dependence of the turbine efficiency, and an equation that solves it within certain boundary conditions.

The current experiment performed during winter semester 2021/2022 and is the continuous work of previous thesis and experiments at the facility. Each test performed in MoNiKa brings the possibility to increase the know-how of the facility and optimize the performance of a Binary ORCs (supercritical organic Rankine cycle) power plant with a low temperature geothermal heat source.

Table of content

List of figures

List of tables

List of abbreviations and symbols

Sym.	Description	Unit
b	Small probable errors	
C	Coefficient	
C'	Coefficient	Kg/s
cp	Heat capacity	$J/Kg \cdot K$
ρ	Density	Kg/m^3
E	Energy	J
e	Specific energy	J/Kg
F	Coefficient	$\frac{Kg^2 \cdot K}{s^2 \cdot kPa^2}$
g	Gravity	m/s^2
H	Enthalpy	J
h	Specific enthalpy	J/Kg
$ITES$	Institute for Thermal Energy Technology and Safety	
k	Thermal conductivity	$W/m \cdot K$
L	Length	mm
LGD	Loss given default	
M	Mass	Kg
$\dot{m}$	Mass flow	Kg/s
N	Population	
$NIST$	National Institute of Standard and Technology	
P	Power	W
p	Absolute pressure	kPa
$p\,(r)$	Relative pressure	kPa
$\dot{Q}$	Heat transfer rate	W
Q	Heat transfer	J
$\dot{q}_G$	Energy generated	W/m^3
re_i	Residual	
r	Radius	m
R^2	Coefficient of determination	
$RMSE$	Root Mean Squared Error	
S	Entropy	J/K
s	Specific entropy	$J/Kg \cdot K$
Se	Sum of squared error estimate	
T	Temperature	K
$T-cv$	Turbine control valve	
t	Time	s
u	Specific internal energy	J/Kg
V	Velocity	m/s
v	Specific volume	m^3/kg
$\dot{W}$	Work transfer	W
$\bar{x}$	Average	
$\widehat{ye}$	Fitting response value	
ye	Observed response value	
z	Elevation	m
α	Thermal diffusivity	
δ	Systematic uncertainty	
η	Efficiency	
λ	Thermal conductivity	$W/m \cdot K$
ϕ	Angle	$°rad$
σ_x	Standard deviation	
$\sigma_{\bar{x}}$	Standard deviation of the mean	

Subscript

Amb	Ambient
c	Corrected
crit	Refers to the fluid critical point
DN	Diameter nominal
ext	External
gb	Gear box
g	Generator
int	Internal
k	Conducted
loss	Losses
Obs	Observed
ORC	Organic Rankine Cycle
s	Isentropic prosses
T	Turbine
Point [1]	Inlet pump
Point [2]	Inlet heat exchanger
Point [3]	Inlet turbine by-pass valve
Point [3']	Outlet turbine by-pass valve
Point [3'']	Inlet turbine
Point [4]	Outlet turbine
0	Design parameter

Chemical molecules

C_3H_8	Propane
N_2	Nitrogen

1 Introduction

The increase in energy demand together with the problem of rising temperatures has scientists motivated looking for a different solution. One of the best answers, within the field of renewable energies, is geothermal energy due to the abundant water steam reservoirs below the earth's surface. The heat of these reservoirs can be extracted from the ground with low enthalpy ORC processes due to the temperature of the source. This introduction covers from general geothermal energy to the low enthalpy propane turbine in supercritical organic Rankine cycle processes.

1.1 Geothermal energy

Earth represents a potentially inexhaustible source of energy evident in form of geothermal energy in the form of hot springs, geysers, fumaroles, and volcanos. Currently, conventional drilling techniques are used to reach natural underground reservoirs, that content hot water or steam. Those geothermal fluid are carried to the surfaces where they are either used directly for space or process heating purposes or to produce electricity from a vapor turbine cycle, and then it is reinjected into the geothermal reservoir. These plants have the great advantage, not only of having an inexhaustible source of energy in human terms, but also that the production of energy is cheaper compared to a coal plant, although they have the disadvantage of a high installation cost [1].

There are three types of geothermal power plant technologies to convert hydrothermal fluid heat into electricity. Those categories depend on the chemistry, pressure involved and fluid temperature. Dry steam power plants, first type ever built and relatively rare, use steam fluid for power production, because there are usually available at relatively high temperature and high pressure. This superheated steam can be used directly to drive turbine.

Flash steam power plants are the most common type of geothermal power generation plants in operation. As the fluid is in liquid phase, due to the high pressure, a vapor phase must be created for power conversion. This vaporization is created by flashing it to a lower pressure, in a flash tank, and the Steam is injected into a suitable turbine to produce power. The remaining liquid water and the condensed steam after the turbine are reinjected into the reservoir again.

Finally, and the most important for this master thesis research are the binary cycle power plants. These plants, of low enthalpy sources, operate usually at temperature around 100 to 170 °C hot water reservoir. Therefore, it is not possible to use the fluid directly from the main source, but instead it can exchange heat to another secondary fluid vaporizing at lower temperature than the thermal water from the main source. This secondary fluid, isobutane, halogenated hydrocarbon, propane, etc, which in turn, is injected into a turbine, condensed, and pumped into continuous closed cycle.

1.2 Organic Rankine Cycle

With the same principle as the steam Rankine cycle, the organic Rankine cycle (ORC) use, instead of water, organic working fluids with low boiling points to recover the heat from lower temperature heat sources. Depending on the pressure at which the heat is supplied, the process is either subcritical, with the fluid evaporating as it passes through two-phase regions, or supercritical where the thermodynamic properties at the outlet of the evaporator are above the critical point. Location of the critical point depends on the fluid properties.

Selection of the working fluid depends on its thermo-physical properties and the following criteria should be considered: low critical pressure and temperature (compared to water), low specific volume, high thermal conductivity, non-corrosive, toxic or flammable and stable. In addition, low ozone depletion potential and low greenhouse warming potential are important requirement for the suitability of the working fluid [2]. Figure 1 shows the differences between both configurations, subcritical with bold line and supercritical with dotted line.

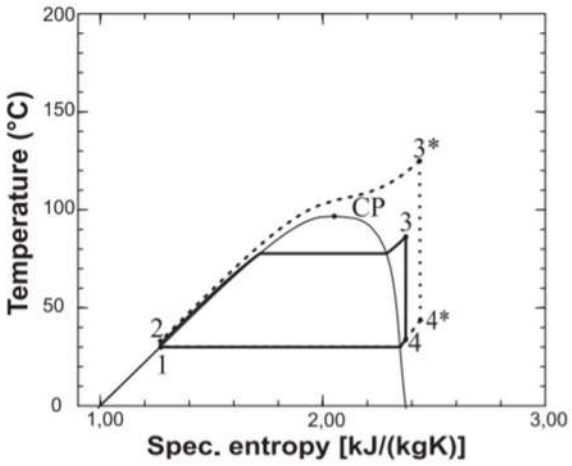

Figure 1: Sub- and supercritical ORC in a T-s diagram [2]

Organic Rankine cycle (ORC), as it was mentioned, use low boiling points. The cycle is configured with an expansion turbine, a condenser, a pump, a boiler, and a superheater (needed depending on the working fluid). In case of "wet" fluid like water usually need to be superheated in order to prevent formation of droplets in the turbine after expansion, while many organic fluids, which may be "dry" or isentropic, do not need to be superheating.

Supercritical Organic Rankine Cycle (*ORCs*) uses, as it was mentioned, working fluid with relatively low critical temperature and pressure. The main reason of thermodynamic properties is that the fluid can be compressed to their supercritical pressure and heated to their supercritical temperature state before the expansion to obtain a better thermal match with heat source. In addition, the heating process does not pass through a distinct two-phase region like the traditional ORC, resulting in a better thermal match in the boiler with less irreversibility. Figure 2 shows the configuration of a supercritical organic Rankine cycle.

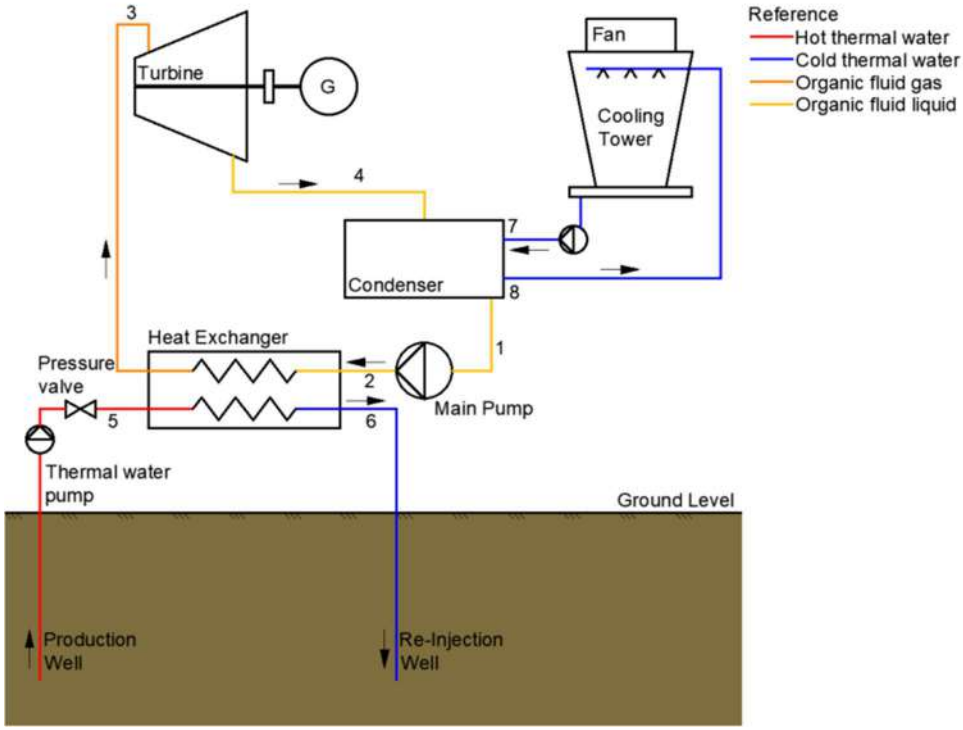

Figure 2: Configuration of an ORCs power plant with geothermal application

The supercritical ORC, related to Figure 2, system consists of a working fluid pump, which increases its pressure (*process 1-2)*, an evaporator driving by a geothermal heat source that heats the working fluid after

the pump outlet to supercritical condition (*process 2-3*), a turbine where the superheated vapor working fluid passes through the expander to generate the mechanical power (*process 3-4*), and a water-cooled condenser to drive the fluid to a liquid phase (*process 4-1*), with the pressure and temperature of the turbine outlet, in order to restart the cycles [3].

The next chapter will focus on the MoNiKa facility (based on the North Campus) with all the components that the installation has, including the instrumentation systems. This installation has the axial turbine whose behaviour is the aim of this work. Previous research works by Luciano Javier Gardella [4], and Christian Vetter [5] have been very important to continue with the investigation of the facility, for which their literature is mentioned repeatedly. Finally, as a method, a software called GESI will be used and then it will be compared with the field experimentation of the installation, focused, as we have already mentioned, on the turbine.

2 Technical description

This chapter provides a general introduction about the ORCs power plant driving by a geothermal source and installed the facilities of KIT Campus North at the ITES institute called MoNiKa, exposing the main objective of the facility, as well as an overview of the components and instrumentation included in it.

2.1 MoNiKa facility

Modular Low Temperature Cycle Karlsruhe is the acronym for MoNika, facility installed in the Institute of Thermal Energy Technology and Safety (ITES) [6]. The main purpose of this facility is to study geothermal power generation and low-temperature electricity generation. With the main individual components studied separately as well as together to find results and thus contribute to increase the economic efficiency of power generation from the low enthalpy geothermal source. Figure 3 illustrates the facility of MoNiKa power plant.

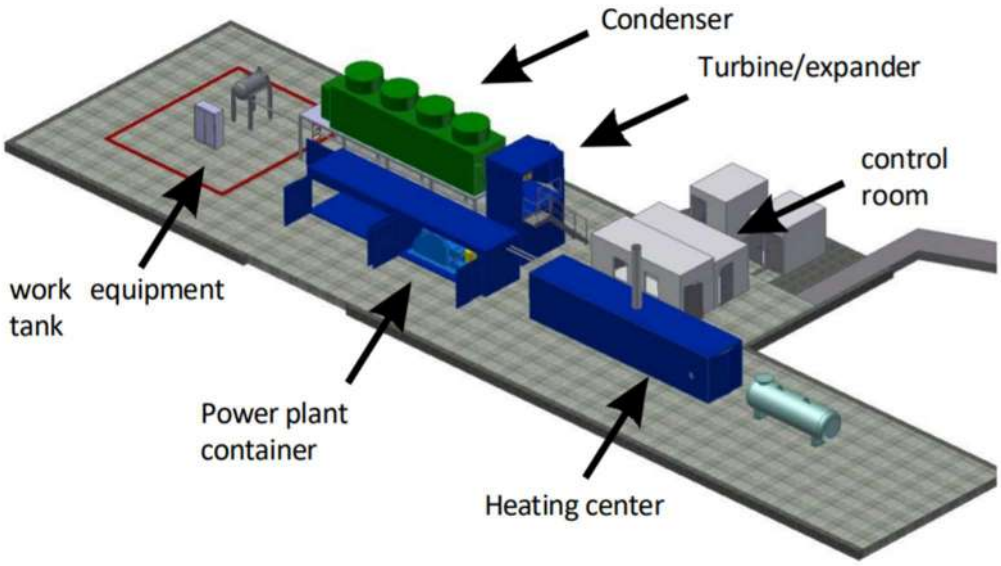

Figure 3: MoNika power plant facility [6]

Previous research show that supercritical live steam parameters power plants present higher efficiency in comparison with subcritical power plants, in particular because of the lower exergy losses during the preheating and evaporation of the working fluid in the heat exchanger. Power plants with supercritical propane configuration can achieve in simulation studies of Vetter et al [2] a net power output of 36.8 kWs/kg, and thermal efficiency of 10.1 %. Therefore, the facility's working fluid is propane. Due to the turbine seal, contamination in the range of a few tenths of a percent by mass with nitrogen cannot be avoided.

The power plant is connected to a boiler that acts as a heat source, instead of been connected to the thermal water circuit. For this reason, the temperature and the mass flow rate can vary between certain limits. Furthermore, certain variables unfavorable to the study can be eliminated, such as corrosion, scale or different compositions of the water from the thermal source [6].

The geothermal power plant is designed to operate at 5.5 MPa and 117 °C live steam pressure and temperature. Considering that propane has a critical pressure of 4.25 MPa (P_{crit}) and a critical temperature of 96.74 °C (T_{crit}). The pump provides a pressure above the P_{crit} and the heat exchanger provide a

temperature above the T_{crit}, as is required to achieve the supercritical condition[1]. All pressures mentioned in this work will be absolute pressures; in case of relative pressures, the same will be detailed.

2.2 Component's description

A schematic diagram for the power plant is presented in Figure 4. As is shown, there are two diagram possible, one (in dot grey line) is presented when the turbine was not in operation. And so, the ORCs went through a valve that expands the steam to the condenser pressure. The second one, the main purpose of this thesis (presented in red line), to study the behaviour of the turbine in the ORCs. As is illustrated, five main components are needed in MoNiKa power plant:

- Condenser
- Propane Tank
- Pumps
- Heat exchanger
- Turbine

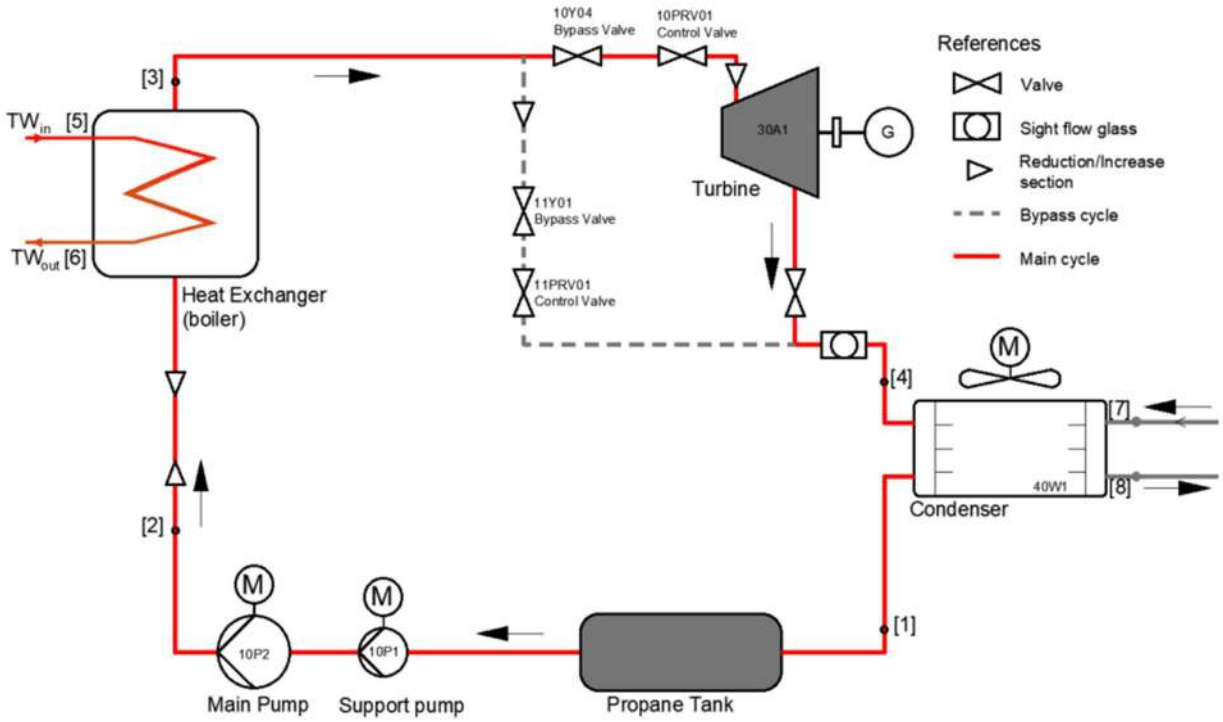

Figure 4: Illustration of MoNiKa power plant main components

The condenser, located between the exit of the turbine and the propane tank, has heat exchange areas built symmetrically in "V" configuration with three chambers, in which the heat exchange between the propane and the air is made. The power consumption of each motor is max. 13 kW at 322 RPM, and a maximum volume flow rate of 44 m^3 /s each one.

Two pumps provide enough pressure to reach supercritical conditions. The main pump, a LEWA triplex M514US G3G, is a piston pump of max. 75 kW with a maximum mass flow of 3.6 kg/s and a design pressure of 6.5 MPa. To avoid cavitation in the main pump, a centrifugal pump, manufactured by Grundfos (CRN20-04 E-FGJ-G-E), is installed with a maximum power of 5.5 kW.

[1] Some literatures call this state transcritical

The heat exchanger, replacing the thermal heat source, is provided by GESMEX. It has the potential to work in both subcritical and supercritical cycle. It is designed for a thermal power of 1000 kW in full operation, with water (simulating the thermal source) as a working fluid with parameter of 0.7-1 MPa and 40-160°C. While the propane side can admit pressures between 4.2 and 6.3 MPa and temperatures between 20 to 130°C (in our experiment we reached 113 °C as maximal temperature). Table 1 shows the differences between the design point, the maximum value, and the maximum reachable value in MoNiKa facility. Last value is due to the limitation of the power plant.

	Propane cycle				Thermal water		
	Max press. p_3 [bar]	Max temp. T_3 [°C]	Min adm. temp. [°C]	Mass flow $\dot{m}_{prop}$ [kg/s]	Max press. p_5 [bar]	Max temp. T_5 [°C]	Mass flow $\dot{m}_{tw}$ [kg/s]
Max ideal values	63	130	-20*	2.90	12**	160	2.60
Max real values	58	113	-	2.85	8.40	160	2.62
Design points	55	117	-	2.90	7-10	150	2.60

*If for any reason the propane has less than -20 °C, all the propane from the pipes must be released.

** Maximum pressure the pipes can support PN16

Table 1: Differences thermodynamic properties between Design, max value, and max. reachable values of MoNiKa power plant

The turbine, the last and most important component of this master thesis, with M+M Turbinen-Technik GmbH as a manufacturer, is installed between heat exchanger and the condenser. The design requirements for max. inlet parameters of 6.3 MPa and 130 °C of pressure and temperature respectively brings a simulated power output of 91 kW [4]. But in practice, as listed in Table 1, we have not been able to reach the desired temperature values due to open issues in the heat exchanger which forces us to operate the power plant in off design.

2.3 Instrumentation

As the main topic of the master thesis is study the behaviour of the turbine, the sensor system important for this research can be found in the turbine container. These sensors meet two requirements, as a power plant control system and as a platform for investigations carried out at the plant. The main indication measured are temperature and pressure at the inlet and outlet of each component as well before the bypass valves, as shown in Figure 5. Mass flow and density of propane is also important for this research, but the flow meter before the turbine FI 10-02 did not deliver reliable data, so we had to use the flow meter FI 10-01, which is located at the outlet of the main pump. In many cases, the outlet of some component refers to the inlet of the next one. But in other cases, the sensors are located at the ends of pipes, which enables to calculate the heat losses in the pipes from temperature differences.

The sensors are directly in contact with the working fluid and for this reason they provide a better measurement of the fluid properties, but there is no possibility to remove the sensor without emptying the fluid inside the piping circuit. As shown in the Figure 5, there are two or three sensors with the same thermodynamic property in each sector of the installation, since it is necessary to be able to take measurements if one of them fails. The measurements in yellow are for pressure, in pink for temperature and in blue for mass flow and density.

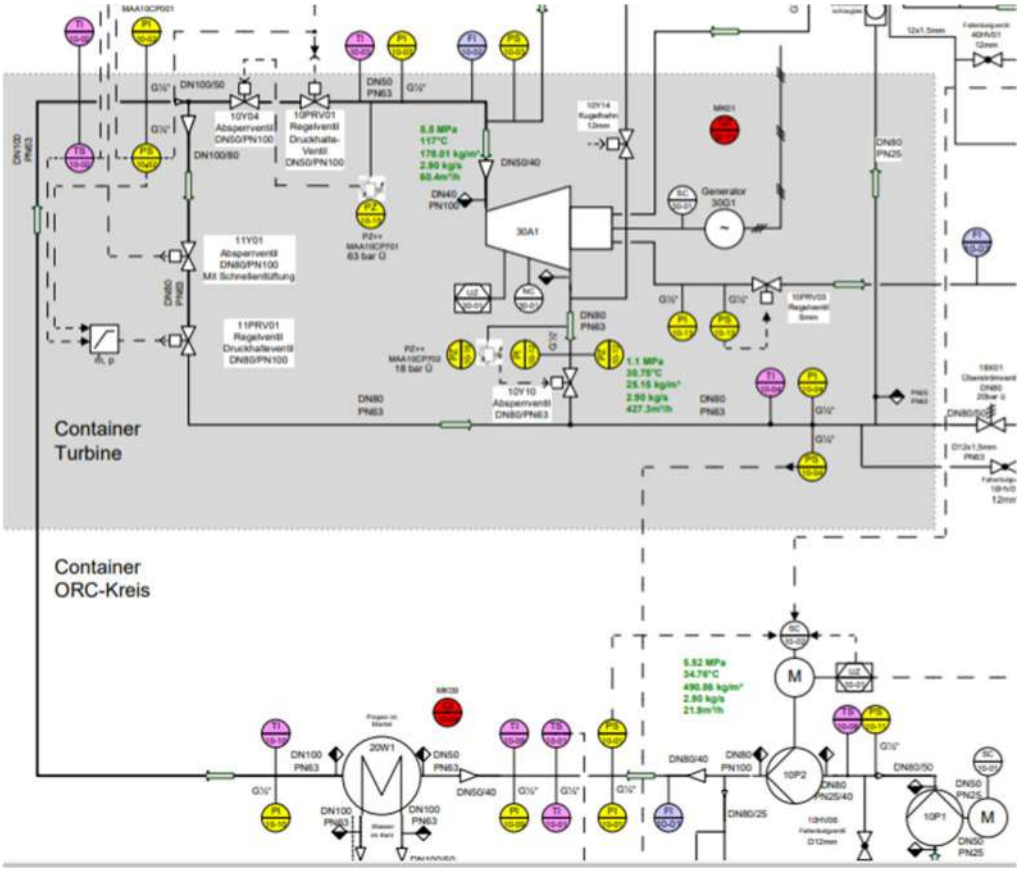

Figure 5: Component's configuration of MoNiKa power plant with the measurement instrumentation

Mass flow rate and density of the working fluid are measured using a Proline Promass 83F sensor. Resonance frequency and Coriolis force are used to have a direct measurement of the mass flow rate, density, and an additional temperature value for the standard density correction.

Temperatures of the working fluid in MoNiKa are measured with WIKA TR34 class A PT100 sensors with resistance thermometer and have an operation range between -50 and 250 °C. They are also compact, resistant to high vibration and have high accuracy in four wire configurations.

Pressure measurements are from VEGA, in particular the models used are the VEGABAR 81 and VEGABAR 82, and can be used for the measurement of gases, vapours, and liquids. They can work in corrosive and hot environment as they have measuring cells. On one hand, VEGABAR 81 is equipped with a chemical seal and Its process consists of diaphragm as well as a transmission liquid. The process pressure acts on the sensor element via the chemical seal. Depending on the measuring range, the sensor element is piezoresistive or a strain gauge system. On the other hand, in VEGABAR 82 the sensor element is the ceramic CERTEC® measuring cell with front flush, abrasion-resistant ceramic diaphragm.

A Humidity and Temperature Transmitter (EE33 series) is responsible for measurement of the ambient conditions in the power plant, from where the conditions can be obtained in situ. Additionally, thermocouples type k are installed in the condenser chambers.

The generator made by MarelliMotori has a control system provided by DEIF, that work in temperatures between -20 °C and 70 °C. The measuring voltage is from 100 to 690 V AC (+/- 20%), and the measuring current is -/1 or -/5 A AC. The current overload is $4xI_n$ in continuous, $20\,xI_n\ in\ 10\ s\ (\max 75A)$, $80xI_n\ in\ 1\ s\ (\max 300A)$ and the measuring frequency is 30 to 70 Hz. To connect the generator with the KIT grid, a Janizta UMG 512 is used as a measurement system.

The three fans inside the condenser are manufactured by WENTECH GmbH, and both three are able to work at temperatures between -40 and +65 °C. The fans are induced draft type with impellers diameter of 2475 mm, and they have a rotation design speed of 322 RPM. The estimated air flow by the manufacturer for that speed is 44 m^3 /s with a fan shaft power of 9.9 kW

The main pump has a frequency converter Siemens Sinamics G180 (type 2X9A-87401-090), and can work between 0 and 40 °C. The support pump (Grundfos) has an external frequency converter for speed control, with RS-485 data bus interface with Grundfos GENI bus protocol.

Table 2 shows each measurement system with the physical type and the magnitude of the measurement, the signal type and the serial number:

Facility code	Model	Physical measurement	Magnitude of measurement	Signal type	Serial number
PS10-02	VEGABAR 81	Chemical seal sensor	Pressure display	4-20 mA	31655353
PI10-03	VEGABAR 81	Chemical seal sensor	Pressure display	4-20 mA	1966071
PS10-03	VEGABAR 81	Chemical seal sensor	Pressure display	4-20 mA	32647408
PI10-12	VEGABAR 82	Ceramic measuring cell	Pressure display	4-20 mA	31655352
TS10-02	TR34 Class A	resistance thermometer	Temperature	TR300(4-20mA)	
TI10-02	TR34 Class A	resistance thermometer	Temperature	TR300(4-20mA)	
FI10-02	PROMASS 83F	Coriolis force with compensation factor due to temperature effects	Temperature	Profibus DP	J1138102000 (fabrication number)
10P1*	SINAMICS G180	Frequency converter	frequency	AC	7506253
10P2**	CRN20-04 E-FGJ-G-E	Frequency converter	frequency	PI controller	96754692

*LEWA Pump
**Grundfos Pump

Table 2: MoNiKa sensors used for this master's thesis

This chapter concludes with the objective of presenting Monika's facility in Campus North with all its measurement systems. Next chapter will talk about the propane turbine technology used at MoNiKa facility and the theory behind the energy balance, the efficiency and the Stodola equation, closing with the software developed by ITES that serves for steady state ORCs cycles calculation at the MoNiKa power plant.

3 Theoretical background

The purpose of this chapter is to review the multi-stage turbine package, designed for the expansion of the propane gas, with gearbox and synchronous generator as well as the required auxiliary systems. Also, we are going to discuss its thermodynamically properties, which are the main objective to understand their behaviour. In addition, this chapter presents the thermodynamic calculation programme (GESI), that has been used in this master thesis to carry out the initial considerations, and the test configuration carried out in the facility. As this work takes the turbine as a black box, a mean line analysis will not be provided.

3.1 Turbine technology

Monika facility has an axial four-stage propane turbine with constant stage pressure (impulse design) of welded construction made by M+M TURBINE-TECHNIK [7]. Enthalpy and pressure is converted to rotational energy by expansion of the propane coming from the boiler. The rotation of the shaft is due to the deflection in the turbine blade caused by the propane working fluid. Figure 6 shows a longitudinal cut of the propane turbine provided by the manufacturer. This illustration shows the 4 stages of the axial turbine.

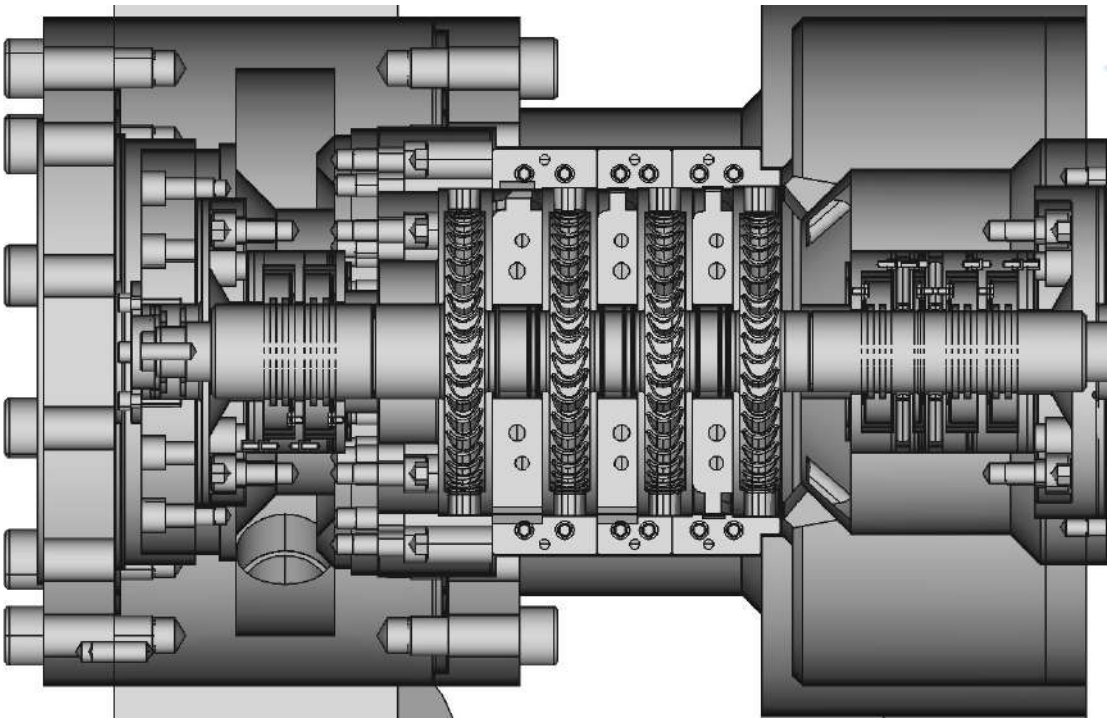

Figure 6: Cut of propane turbine provided by the manufacturer M+M TURBINE-TECHNIK [7]

The axial bearing is made in the steam inlet. Sealing to the outside is achieved by means of carbon seals. The vapour inlet area (front side) is of closed design and has a leakage gas discharge, which is led to the exhaust vapour. In the area of the shaft passage at the coupling connection (gear side), a closed design is not possible. Here, nitrogen is supplied behind the first seal and the nitrogen-propane mixture is discharged behind the second seal. Behind the third seal, atmospheric conditions prevail.

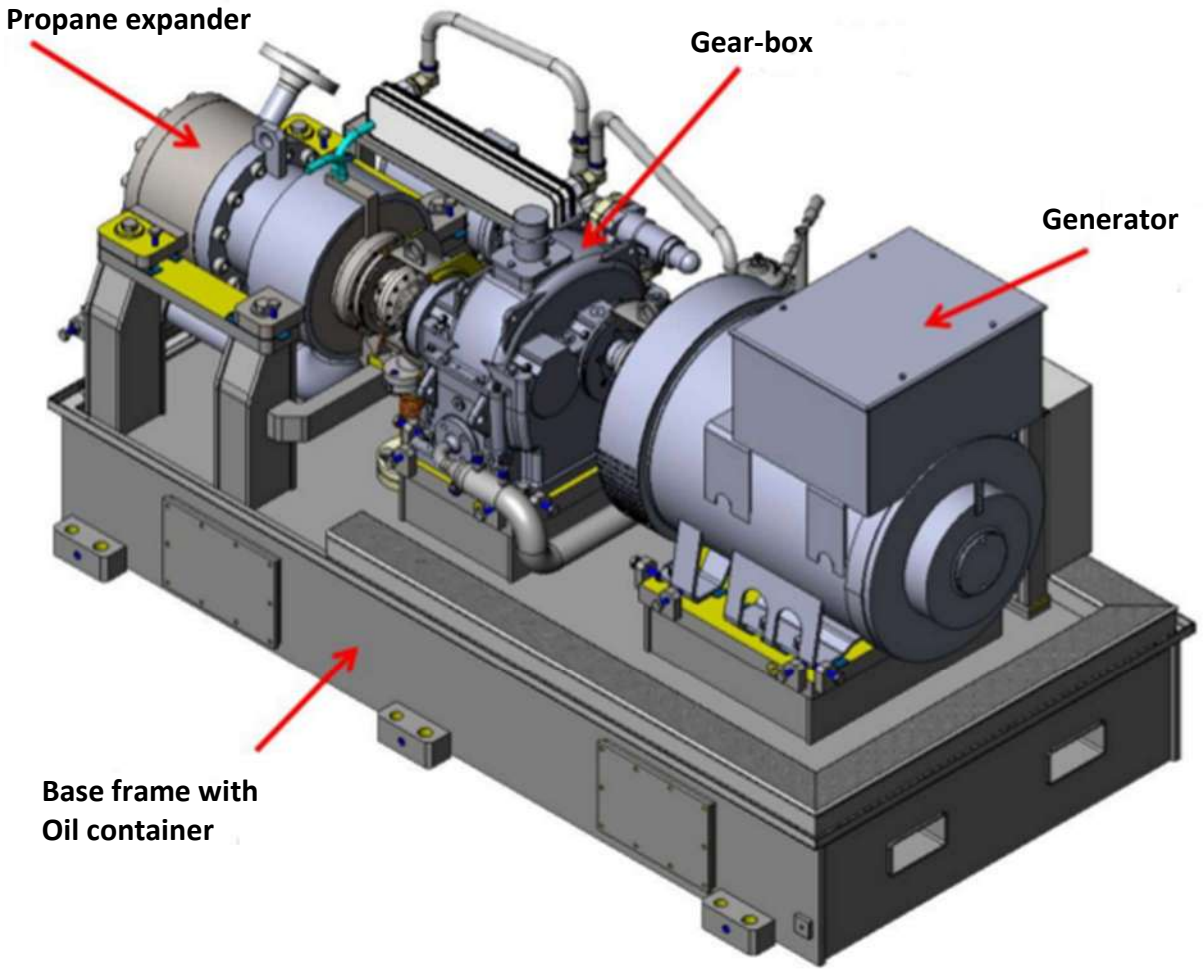

Figure 7: Isometric propane turbine view provided by the manufacturer [7]

Figure 7 shows the isometric view with the different components that integrate the turbine. The generator converts the mechanical energy, extracted by the vapor propane turbine, into electrical energy. Between the turbine and the generator is a single-stage stationary gearbox and it is used to reduce the turbine speed (9960 rpm) to the nominal generator speed (1500 rpm). Lubricating oil must be supplied in the gearbox by the oil system supplies. For this reason, an electrically driven main oil pump delivers oil from the tank via the cooler and the double oil filter to the consumer. Measuring devices are installed on the turbine system for control, regulation, and monitoring, both local and remote.

3.1.1 Energy Balance

We consider an open system including mass flow across certain portion of the system boundary, heat transfer, work interacted, both per unit of time, and portions of the boundary that mass flow crosses. In steady state conditions, $with\ \dot{m}$ as the mass flow rate $\Delta M/\Delta t$, and assuming that more than one inlet and outlet port exits, we arrive at the most general statement of the First Law of Thermodynamics (equation (3. 1)) for an open system. In our case, $\dot{Q}$ is the thermal power given from outside to this component, $\dot{W}$ is the mechanical power produced, $\dot{m}, e, v\ and\ p$ are the mass flow, specific energy, specific volume, and pressure of the working fluid, respectively. Figure 8 shows the control volume in the region contained between inlet and outlet ports [8].

$$\frac{dE}{dt} = \dot{Q} - \dot{W} + \sum_{in} \dot{m}(e + pv) - \sum_{out} \dot{m}(e + pv) \qquad (3.\ 1)$$

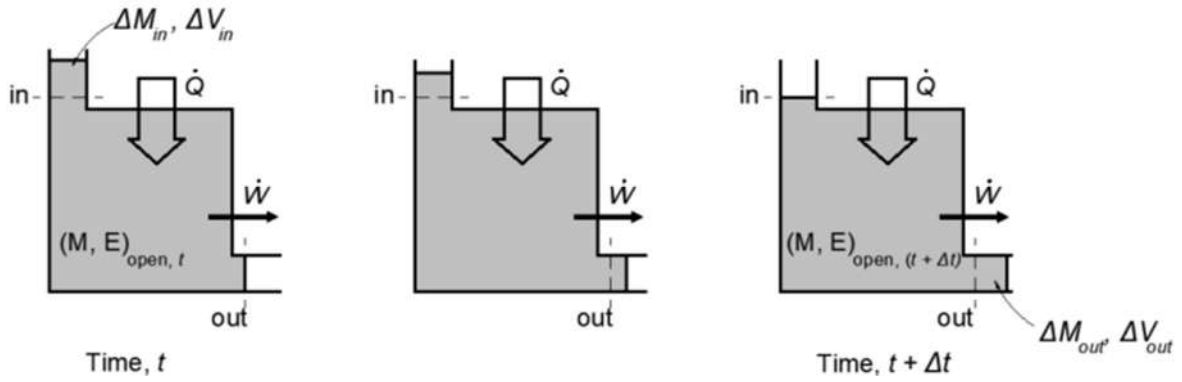

Figure 8: Main characteristics of a thermodynamic open system.

As was mentioned in the previous paragraph, steady state conditions and mass conservation brings next hypothesis:

$$Steady\ State: \quad \frac{dE}{dt} = 0; \qquad \dot{Q} = cte.; \qquad \dot{W} = cte \tag{3. 2}$$

$$Mass\ conservation: \quad \frac{dM}{dt} = 0; \qquad \frac{dM}{dt} = \sum_{in} \dot{m} - \sum_{out} \dot{m} = 0 \tag{3. 3}$$

In the absence of macroscopic forms of energy storage other than kinetic and gravitational, the specific energy *e* can be decomposed into $(u + \frac{1}{2}V^2 + gz)$, these terms represent the specific internal energy (u), the velocity (V), the gravity (g), and the elevation (z). The result of this decomposition is the specific *enthalpy:*

$$h = u + pv \tag{3. 4}$$

Taking in account the term of enthalpy of the equations (3. 4) in the equation (3. 1), appears explicitly in terms explaining energy transfer through mass flow in a steady state condition with the mass conservation.

$$\dot{Q} - \dot{W} + \sum_{in} \dot{m}\left(h + \frac{1}{2}V^2 + gz\right) - \sum_{out} \dot{m}\left(h + \frac{1}{2}V^2 + gz\right) = 0 \tag{3. 5}$$

3.1.2 Stodola's equation

The empirical cone law according to Stodola [9] correlates the mass flow, pressures p and inlet temperature T of a steam turbine as:

$$\left(\frac{\dot{m}_T}{\dot{m}_{T,0}}\right)^2 = \frac{p_{T1}^2 - p_{T2}^2}{p_{T1,0}^2 - p_{T2,0}^2} \frac{T_{T1,0}}{T_{T1}} \tag{3. 6}$$

In Equation (3. 6), index $T1$ designates the state before the turbine, index $T2$ the state after the turbine. In addition, variables indexed with a 0 indicate the design status. The cone law means that if the mass flow deviates, the pressure difference between the turbine inlet and outlet is changed. Therefore, if a pressure-retaining valve in front of the turbine with isenthalpic expansion is assumed another state between the pressure-retaining valve and the turbine can be calculated. This condition is determined by the enthalpy in front of the pressure control valve and the pressure according to Equation (3. 6) . Since the temperature in the pressure-retaining valve changes during isenthalpic expansion, but this is used to calculate the pressure

in Eq. (3. 6) is required, the state must be determined iteratively [9]. In addition, the turbine power is calculated using the next equation:

$$P_T = \eta_T \dot{m}_T \, \Delta h \tag{3. 7}$$

Where, η_T is the turbine efficiency, $\dot{m}$ is the steam flow through the turbine and Δh is the enthalpy drop between inlet and outlet of the expansion process respectively.

3.1.3 Turbine efficiency

Work delivered by a turbine is given as the difference between inlet and exit stagnation enthalpy, in the same way as we do with the GESI software. In the case of a reversible turbine, without mechanical losses, the amount of work delivered by the turbine would be greater at the same outlet pressure than a turbine with mechanical losses. In fact, the efficiency is the ratio between W(work considering mechanical losses) and W_s (isentropic work) [10]:

$$\eta_T = \frac{\dot{W}}{\dot{W}_s} \tag{3. 8}$$

Having the assumption of steady state conditions, conservation of mass flow, and considering that there is only one inlet and one outlet, the kinetic energy and potential energy are small compared to the change in enthalpy and the fluid is considered adiabatic due to the heat generated internally by friction is supposed to stay in the fluid (adiabatic flow). Equation (3. 8) can be rewritten in terms of the equations (3. 5):

$$\eta_T = \frac{\cancel{\dot{Q}} + \sum_{in} \dot{m}_T\left(h_1 + \cancel{\frac{1}{2}\mathcal{V}^2} + \cancel{gz}\right) - \sum_{out} \dot{m}_T\left(h_2 + \cancel{\frac{1}{2}\mathcal{V}^2} + \cancel{gz}\right)}{\cancel{\dot{Q}} + \sum_{in} \dot{m}_T\left(h_1 + \cancel{\frac{1}{2}\mathcal{V}^2} + \cancel{gz}\right) - \sum_{out} \dot{m}_T\left(h_{2,s} + \cancel{\frac{1}{2}\mathcal{V}^2} + \cancel{gz}\right)} = \frac{\dot{m}_T(h_1 - h_2)}{\dot{m}_T\left(h_1 - h_{2,s}\right)} \tag{3. 9}$$

Then the equation (3. 9) reduce to:

$$\eta_T = \frac{\cancel{\dot{m}_T}(h_1 - h_2)}{\cancel{\dot{m}_T}\,(h_1 - h_{2,s})} = \frac{h_1 - h_2}{h_1 - h_{2,s}} \tag{3. 10}$$

Figure 9 illustrates different amount of work in a diagram h-s for two processes with the same working fluid.

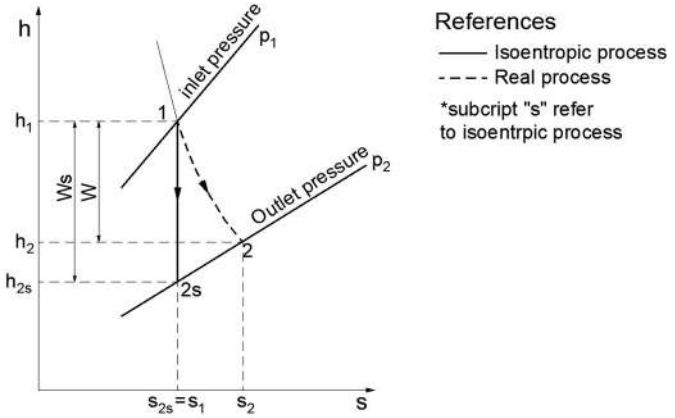

Figure 9: sketched h-s diagram for real and isentropic process in an adiabatic turbine taken [2]

3.2 Geothermal simulation - GESI

Geothermal Simulation (GESI) is a simulation program code developed in MATLAB® by the ITES [11] (Institute for Thermal Energy Technology and Safety) for stationary, zero-dimensional calculation of an ORC in which the heat source is hot thermal water, under given boundary conditions. REFPROP 23, version 9.0, is used as

the data bases software for the calculus of GESI, which is a fluid properties data bases from the NIST (National Institute of Standards and Technology) [12]. The REFPROP data bases contains many gases and fluids, including propane. The software version used in this work is 2.3.6c. It was validated by Christian Vetter [5] via code-to-code comparison with IpsePro (Version 4.0, SimTech Simulation Technology). Vetter concluded: "*The majority of the values show only a relative error of less than 0.02% and the absolute errors of the net power of the processes calculated in GESI corresponds to a relative error of less than 0.2%*", that way it shows a good performance [5]. Additionally, an actualization by Luciano Gardella [4] was made in one sub-program (GESI teillast).

Once the user calls up GESI, the program brings the possibility of using different sub-programs related with ORC cycles, see Figure 10. This master thesis focused only on *Organic Rankine Cycle* and *ORC Partload (teillast),* highlighted with dotted line. Where the second part offers the option of calculating stationary partial load conditions at a given full load point. In addition, those two functions are very important because are the starting point to later start whit the experiment on site (MoNiKa facility).

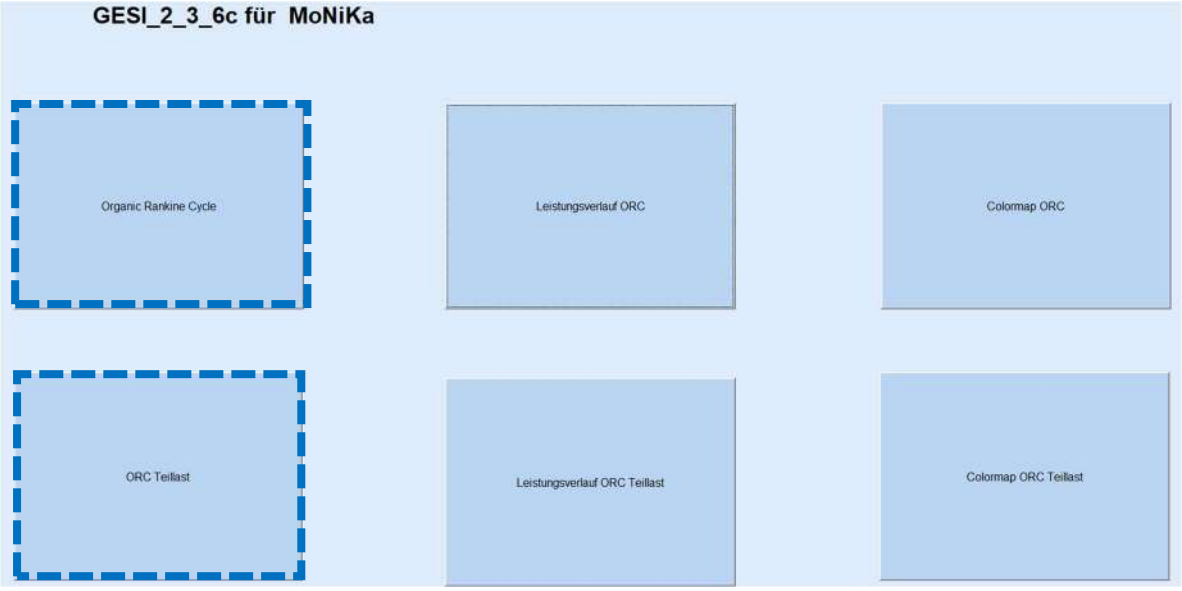

Figure 10: GESI sub-programs (version 2.3.6c)

3.2.1 Organic Rankine Cycle

Without an internal heat exchanger, this program enables the calculation of both sub-critical and supercritical cycles with a particular organic working fluid selected by the user from the REFPROP fluid list. The two-phase area is then displayed in the Graphical User Interface (GUI) in the T-s diagram as well as the pressure and temperature at the critical point of the working selected fluid. The pump inlet is assumed as saturated liquid at a certain temperature. Live steam conditions at turbine inlet brings the possibility on choosing between different variables:

- Pressure and temperature at the turbine outlet
- Pressure and saturated steam at turbine inlet
- Temperature and saturated steam at turbine inlet
- Turbine outlet pressure and turbine outlet steam quality
- Temperature at the turbine outlet and steam content at the turbine outlet

In addition, the user can choose between specify the mass flow or the heat input from thermal water circuit source to the ORC circuit with also indicating the inlet temperature and pressure. Likewise, on the cooling side (condenser, where the lower pressure level of the process is determined by the condensation temperature) the user can select the working cooling fluid between water or air, as well as the pressure and

temperature condenser inlet. Also, in the case of air-cooling, an input is required for the relative humidity, pressure, and temperature. Finally, in both heat exchange processes, it is mandatory to specify a minimum temperature difference.

Together with the specification of the turbine and pump isentropic efficiency and heat exchanger and condenser pressure losses, the state at the characteristic points of the process can be calculated. Figure 11 shows an example of the graphical interface of the software, with all inputs previously identified.

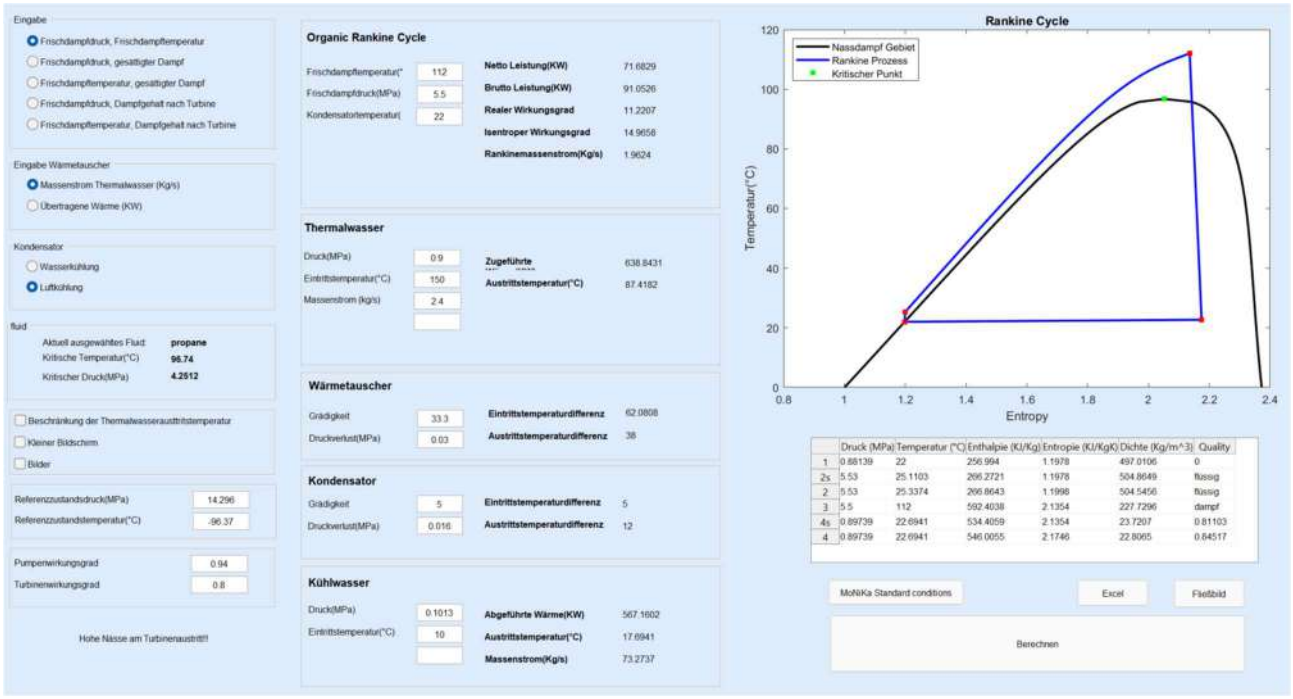

Figure 11: GESI - Organic Rankine Cycle module

3.2.2 ORC Teillast

The last version was modified by Luciano Javier Gardella in his master thesis [4], including three subroutines. Figure 12 shows the user interaction of the GESI ORC Teillast, where the information of the full load operation is given in the first column. The ORC simulation cycle and the ORC points calculations are shown in the middle. Inputs settings for the part load and ambient conditions are in the second column. And finally, the last column shows the calculated parameters, and it includes a box that estimates the components setting in MoNiKa.

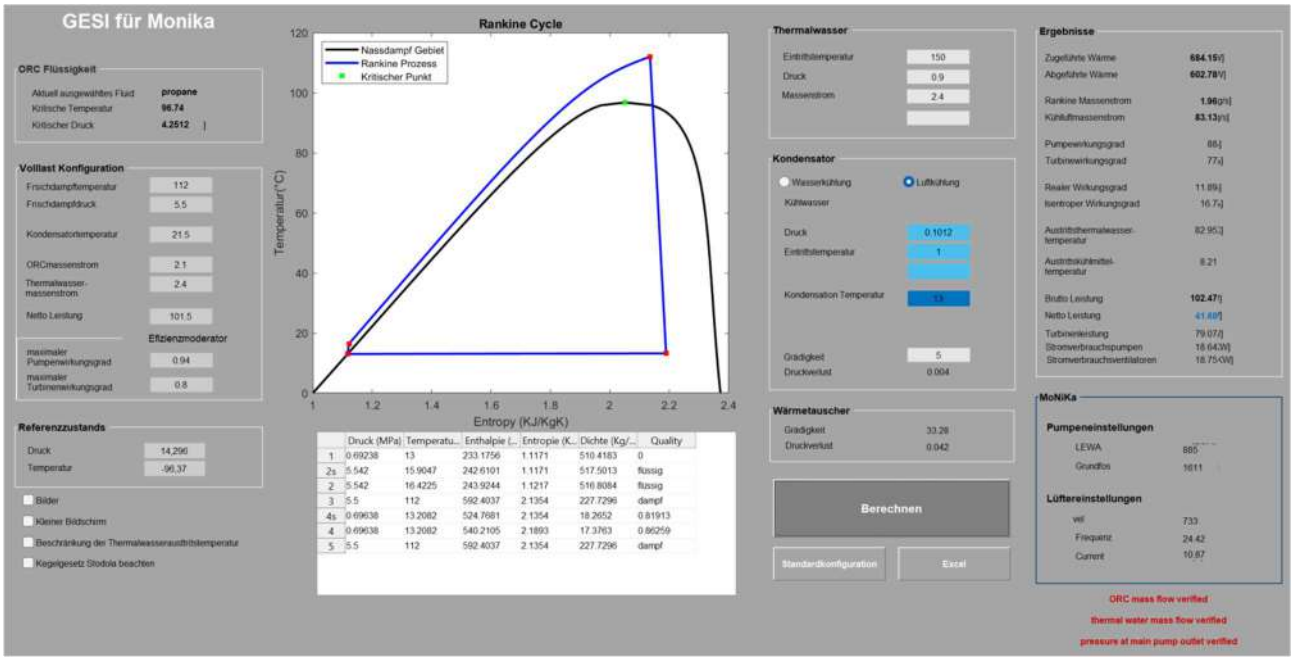

Figure 12: GESI - ORC Teillast module [4]

Figure 13 show the sub-program modify by in Luciano Javier Gardella´s master thesis [4]. The first step estimates the $\dot{m}_{ORC}$ using the information from the actual state of MoNiKa at full load and the inputs of part load, ambient conditions, and condensation temperature. Secondly, the module set the installation characteristics as function of the ORC mass flow. Thirdly, thermodynamics values are calculated (this is the main routine). After real net power generation is calculated including the power need it in the fans and finally, the program checks that the values calculated are in the facility's range.

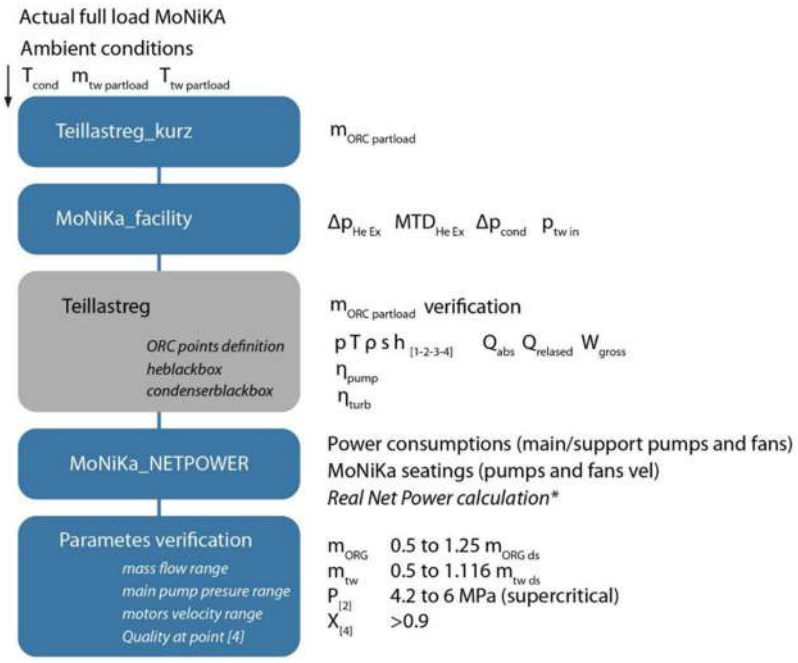

Figure 13: GESI ORCs Teillast block diagram for MoNiKa [4]

This chapter concludes with the theory related to the turbine placed in MoNiKa facility and the software used to simulate the cycle related to the power plant. Next chapter will introduce the theory of errors associated to the measurement system and to, the software calculation and the propagation of them, that have been very important in evaluating the results.

4 Uncertainty analysis of measurement systems

The objective of this chapter is to discuss the uncertainty analysis of measurement systems. Starting with the systematic error of those measurement systems that are sources of error that cause a deviation from the real value. Then, with the statistical analysis to determine the reason of the random error that are dispersed around a mean value, and finally the theory of error propagation, in order to exhibit with this last theory, the ways that was used in this work to calculate the error of the turbine efficiency.

This sums up the systematic and random errors, the size of which can be estimated more reliably using the methods of regression calculation and statistics, the greater the number of repeated measurements [13]. This work uses the statistics methods to estimate the uncertainties.

4.1 Systematic error

Imperfections in the measuring devices and environmental influences are not always avoidable, but they are a regular occurrence with repeated measurements. If they can be recorded in comparisons with other methods, they must be corrected mathematically. This work, being all the measurement provided by electronic devices of different types, has a mathematical correction for this type of error. In addition, once these measurements have been carried out, it is necessary to collect them. This acquisition has a systematic error, and its measurement system has a precision, as well as the program that is very important for the calculation of the thermodynamic property of the working material, the REFRPORP.

4.1.1 Sensor's measurement

This work has an important data base in measurement of certain components before and after the turbine. Table 3 shows a list of MoNiKa sensors that have been used for this thesis and their accuracy provided by the manufacturer.

Magnitude	Facility code	Model	Manufact	Measurement range	Accuracy	Max Abs. error
Pressure	PS10-02	VEGABAR 81	VEGA	0 to 100.0 bar	0.2% full range	0.2 bar
Pressure	PI10-03	VEGABAR 81	VEGA	0 to 100.0 bar	0.2% full range	0.2 bar
Pressure	PS10-03	VEGABAR 81	VEGA	0 to 100.0 bar	0.2% full range	0.2 bar
Pressure	PI10-12	VEGABAR 82	VEGA	-1 to 100.0 bar	0.1% full range	0.1 bar
Temperature	TS10-02	TR34 Class A	WIKA	-30 to 250 °C	±0.15+0,002·|T|	0.4 °C
Temperature	TI10-02	TR34 Class A	WIKA	-30 to 250 °C	±0.15+0,002·|T|	0.4 °C
Temperature	FI10-02	PROMASS 83F	Endress + hauser	-50 to 200 °C	±0.50+0,005·|T|	0.6 °C
Mass flow	FI10-01	PROMASS 83F	Endress + hauser	0 to 2.9 Kg/s[2]	±[0.1+(0.0025/ $\dot{m}$)]· $\dot{m}$/100	0.005 kg/s

Table 3: Type of sensors and their accuracy of MoNiKa power plant

In addition, Figure 14 shows where each of the measurement is located in the schematic presented in Figure 5 with the facility code to see exactly how accurate any of them are. Those marked are the ones used in this work.

[2] The measurement range is larger, but a range up to 2.9 Kg/s has been requested from the manufacturer, which is the design mass flow rate of the MoNiKa power plant.

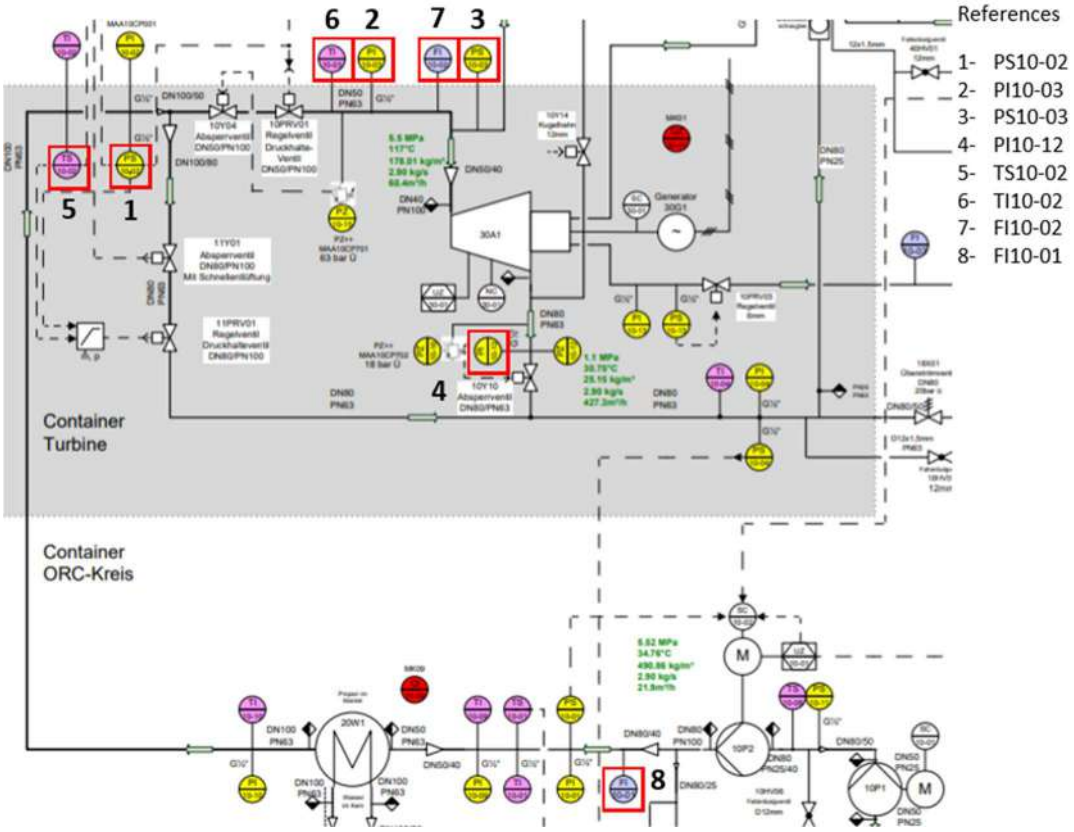

Figure 14: Distribution of each component used in MoNiKa power plant

4.1.2 Data acquisition

PROFIBUS is the standard protocol used in MoNiKa for the data acquisition and the control system. A SIEMENS SERIES S7-300 PLC is implemented as management of the system at MoNiKa. This module, with high resolution and high Common Mode Rejection Ratio, converts the analogy values from the sensor to digital values that can be processed by the PLC. All the information from the sensors works under HART protocol and this communication protocol modulates the current from 4-20mA.

The accuracy of the module is ±0.001220703 mA. The uncertainty of the module is irrelevant compared with the accuracy of the sensors [4]. In order to estimate the accuracy of the data from the PLC a statistical analysis is performed. Once the measurement is exported from the server, the standard deviation of each parameter is calculated with the criteria 2σ. Which means a typical confidence interval of 95.5 % of the population, whereas 1σ includes approx. 68% of the population.

4.1.3 REFPROP accuracy

Thermodynamic and transport properties of pure fluids and mixture substance is calculated by the software REFPROP developed by the National Institute of Standards and Technology (NIST). In this work, this software was used implicitly in the GESI function as well as when calculating the thermodynamic properties of the working fluid in the devices previously shown in Figure 14. As this software was fundamental in the whole process, it is very important to show the error and its influence.

REFPROP “database” [14] uses equations, the most reliable available in the world, for thermodynamic and transport properties to calculate the state points of the fluid or mixture. With the advantage of high accuracy obtained through many coefficients in the equations, but as against the speed of calculation will be slower than other equations. All the equations are valid over the entire steam and liquid regions of the fluid, including supercritical state. In addition, the program does not contain any experimental information, except from the critical and triple point of the pure fluids.

Accuracy of the entropy, enthalpy, cp, density, and any other interest properties for this work depends on the number of numerical digits the software works with (good accuracy need 5 significant digit). MoNiKa power plants is limited by the measurement system that are able to measure with 3 significant numbers of resolution. This scenario indicates that the error is due to the input data, however the REFPROP equations have also an uncertainty, which could not be quantified here.

4.2 Random error

Changes to the measuring device or object, such as wear, friction, or noise, which are not recognizable and cannot be influenced, are unavoidable. When measurements are repeated under the same conditions, they fluctuate irregularly in magnitude and sign [13]. Random error can be evaluated through statistics.

4.2.1 Statistical Analysis

In this work, the MoNiKa PROFIBUS provided a value every second. Three days of experimental data collection provided 41561 samples for each measurement system. Once all the data were obtained, the different runs were sorted, which had an average measurement time of 30 min, and for each run the values that met the steady state condition were chosen. For these data, a statistical analysis was then performed, following the book "Dubbel Taschenbuch für den Maschinenbau" [13].

Repeating a measurement several times increase the reliability of a measurement. Statistics are applied to the multiple measurement to evaluate the uncertainty the measuring quantity in case the error associated with measurement of a quantity are random. Statistics cannot detect systematic errors and should not be used in scenarios where such errors are suspected. Instead, an experimentalist should attempt to reduce systematic errors by using calibration standards and other verification techniques.

For N_i measurements (populations) of a certain quantity x (equation (4. 1)), the best estimate of the actual quantity is the mean value $\bar{x}$ of the measurements (equation (4. 2)) [13]:

$$Population: \qquad N = \sum x_1,\ x_2, x_3, \dots, x_n, \tag{4. 1}$$

$$Average: \qquad \bar{x} = \frac{\sum_i^n x_i}{n} \tag{4. 2}$$

The value $x_i - \bar{x}$ is the deviation of a particular trial from the mean[3], which is not possible to sum the deviation because the construction of the definition of $\bar{x}$ cause the deviation to always sum to zero. The solution, is to square the deviation and sum them, and take the square root of that sum, resulting in a value referred to as the standard deviation, σ_x [13]:

$$\text{Standard deviation:} \qquad \sigma_x = \sqrt{\frac{\sum_{i=1}^n (x_i - \bar{x})^2}{n-1}} \tag{4. 3}$$

The standard deviation estimates the variability of a population from which the sample was drawn. It gives important information about how the distribution of a population is. A large standard deviation indicate that the data points can spread far from the mean and a small standard deviation indicate that there are clustered closely around the mean.

[3] Some literature calls this deviation residual

The mean value calculated in (4. 2) is an estimate for the true value of the quantity x. If I now record different series of measurements, these will yield different mean values. This means that the mean value itself is subject to an error. All mean values which are theoretically possible, are distributed around the true value of x. So, the standard deviation of the mean value can be written as:

Standard deviation of the mean value:
$$\sigma_{\bar{x}} = \sqrt{\frac{\sum_{i=1}^{n}(x_i - \bar{x})^2}{n \cdot (n-1)}} \tag{4. 4}$$

4.3 Error propagation

For a variable y that depends on n independent measured variables $x_1, x_2, \dots, x_n$ with systematic errors $\delta x_1, \delta x_2, \dots, \delta x_n$ according to $y = f(x_1, x_2, \dots, x_n)$, the error δy results at the point of the measured values with the total differential [13]:

$$dy = \sum_{i=1}^{n} f_{xi}\, dx_i \qquad \text{to} \qquad \delta y = \sum_{i=1}^{n} f_{xi}\, \delta x_i \tag{4. 5}$$

The differentials and the true magnitudes are replaced by the sufficiently small errors and the measured values. If the signs of the δx_i are not known, the absolute maximum error δy_{max} applies as the worst case:

$$\delta y_{max} = \sum_{i=1}^{n} |f_{xi}\, \delta x_i\,| \tag{4. 6}$$

Conversely, from the specification of a permissible error δy with equation (4. 5), it is possible to estimate which measuring errors δx_i are to be observed, to then select the measuring devices and the measuring method. Equation (4. 5) is also suitable for estimating the inclusion of rounding errors when calculating numbers, since the rounded digit introduces a systematic error for the individual numbers.

In the case that there are only two variables, and so $y = f(x_1, x_2)$, equation (4. 6) can be written in the next form:

$$\delta y = \left|\frac{\partial f}{\partial x_1}\right| \delta x_1 + \left|\frac{\partial f}{\partial x_2}\right| \delta x_2 \tag{4. 7}$$

For a quantity $y = f(x_1, x_2)$ dependent on two independent measured quantities x_1, x_2, the total differential is formed and squared to calculate statistical error propagation σ_y as an estimate for the standard deviation. For practical purposes the measured values $x_{1Mi}, x_{2Mi}, i = 1, 2, \dots, n$, are to be used for the variables and for dx, dy, dz the small probable errors b_{xi}, b_{yi}, b_{zi} are to be used and summed up.

$$\sum_{i=1}^{n} b_{yi}^2 = \sum_{i=1}^{n} \left(\frac{\partial \mathrm{f}}{\partial \mathrm{x}_1}\right)^2 b_{x_1 i}^2 + \sum_{i=1}^{n} \left(\frac{\partial \mathrm{f}}{\partial \mathrm{x}_2}\right)^2 b_{x_2 i}^2 \tag{4. 8}$$

With $\sum_{i=1}^{n} \frac{\partial \mathrm{f}}{\partial \mathrm{x}_1} \cdot \frac{\partial \mathrm{f}}{\partial \mathrm{x}_2}\, b_{x_1 i} b_{x_2 i} = 0$

because $b_{x_1 i}$ and $b_{x_2 i}$ are equally likely positive and negative. Division by $(n-1)$ and root extraction yield an estimated value

$$\sigma_y = \sqrt{\left(\frac{\partial \mathrm{f}}{\partial \mathrm{x}_1}\right)^2 \sigma_{x_1}^2 + \left(\frac{\partial \mathrm{f}}{\partial \mathrm{x}_2}\right)^2 \sigma_{x_2}^2} \tag{4. 9}$$

for the standard deviation. This is the Gaussian law of error propagation for random error sizes, which can be extended to more than two variables analogously as:

$$\sigma_y = \sqrt{\sum_{i=1}^{n} \left(\frac{\partial \mathrm{f}}{\partial \mathrm{x}_i}\right)^2 \sigma_{x_i}^2} \tag{4. 10}$$

The same equation can be rewritten as:

$$\sigma_y = \sqrt{\left(\frac{\partial \mathrm{f}}{\partial \mathrm{x}_1}\right)^2 \sigma_{x_1}^2 + \left(\frac{\partial \mathrm{f}}{\partial \mathrm{x}_2}\right)^2 \sigma_{x_2}^2 + \cdots + \left(\frac{\partial \mathrm{f}}{\partial \mathrm{x}_n}\right)^2 \sigma_{x_n}^2} \tag{4. 11}$$

4.3.1 Error propagation for thermodynamic variable at MoNiKa

Enthalpy and entropy uncertainty is derived from the measurements of temperature and pressure at MoNiKa can be expressed as follows [15]:

$$\sigma_h = \sqrt{\left(\frac{\partial \mathrm{h}}{\partial \mathrm{p}}\right)^2 \sigma_p^2 + \left(\frac{\partial \mathrm{h}}{\partial \mathrm{T}}\right)^2 \sigma_T^2} \tag{4. 12}$$

$$\sigma_s = \sqrt{\left(\frac{\partial \mathrm{s}}{\partial \mathrm{p}}\right)^2 \sigma_p^2 + \left(\frac{\partial \mathrm{s}}{\partial \mathrm{T}}\right)^2 \sigma_T^2} \tag{4. 13}$$

where σ is the statistical uncertainty, and in turn the partial derivatives of enthalpy (h) and entropy (s), were calculated. Was modelled with a linear function having the assumption that pressure and temperature are independent variables, and the uncertainty variation is very small. Luciano Gardella in his master's thesis calculated the uncertainty of enthalpy and compared it with that of REFPROP and the deviation was 2%. Furthermore, the uncertainties in heat capacity are 0.5% in the liquid phase, 0.2% in the vapor phase, and higher in the supercritical region [14].

4.3.2 Regression analysis

This section will present the Least-Squares Fitting tool provided by Curve fitting Toolbox™ software inside MATLAB [16]. The result of the fitting process is an estimate of the model coefficients. This includes different type of least-square fitting:

- Linear least squares
- Weighted linear least squares
- **Robust least squares**
- Nonlinear least squares

In this thesis, Robust least square method is used, due to the minimal error that brings the comparison with each type of fitting.

To obtain estimate coefficient, the least-squares method minimizes the summed square of residuals:

$$re_i = ye_i - \widehat{ye}_i \tag{4. 14}$$

The residual r_i for each data point is defined as the difference between the observed response value ye_i and the fitted response value $\widehat{ye}_i$. Considering that n is the number of data points included in the fit and S is the sum of squares error estimate, the summed squared of residual result:

$$Se = \sum_{i=1}^{n} re_i^2 = \sum_{i=1}^{n} (ye_i - \widehat{ye}_i)^2 \quad (4.\ 15)$$

To minimize the influence of outliers, rare extreme value due to the assumption that the response error follows a normal distribution, the toolbox provides two robust regression methods:

- Least absolute residuals (LAR): method that finds a curve that minimizes the absolute difference of the residuals, rather than the squared differences. Therefore, extreme value has less influences on the fit.
- Bisquare weights: methods that minimizes a weighted sum of squares, where the weight given to each data points depends on the distance to the fitted line. Which means that points near the line get full weight, and in contrasts with the points that are farther from the line than would be expected by random chance get zero weight.

Figure 15 taken from Leas-Squares Fitting of MathWorks [16] illustrate the comparison between a regular linear fit with a robust fit using bisquare weights. Notice that the robust fit follows the bulk of the data and is not strongly influenced by the outliers.

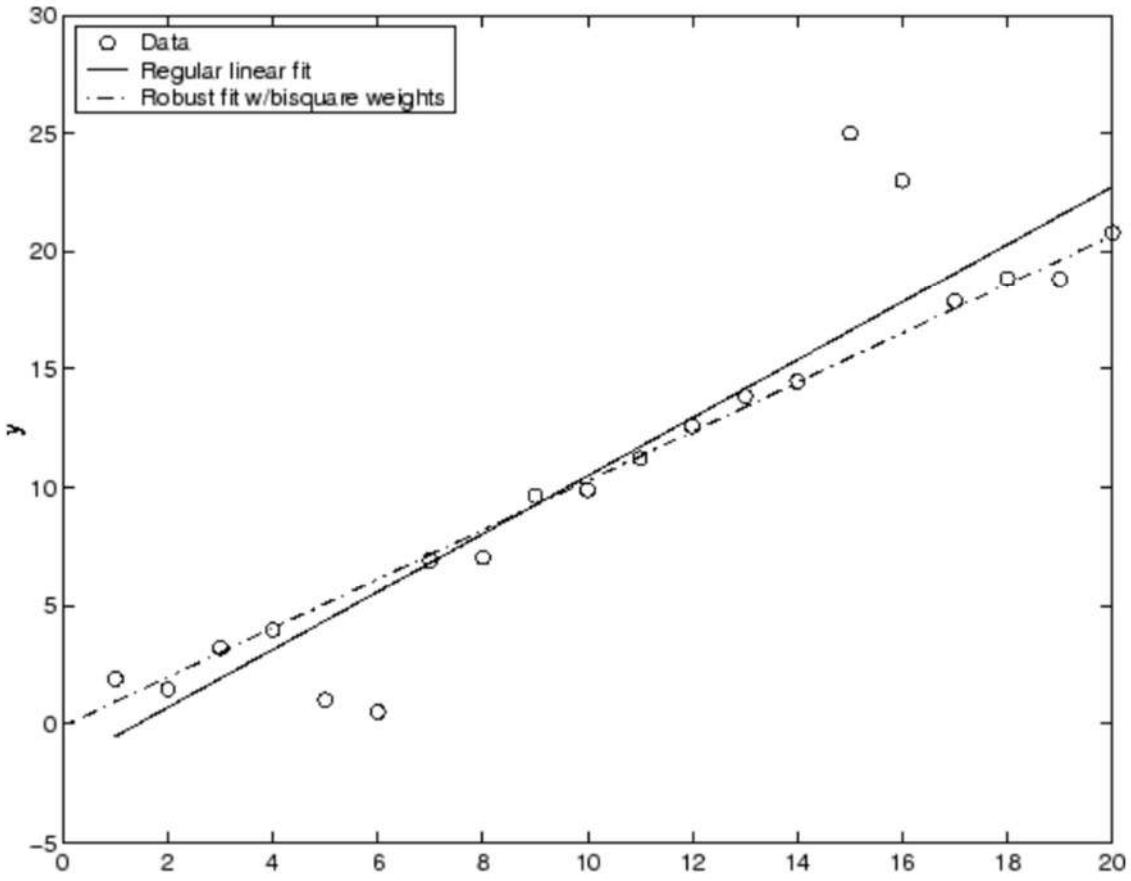

Figure 15: difference between regular linear fit and Robust fit [16]

This model in turn has a precision that measures the accuracy of the predicted probability of LGD (loss given default) values using different metrics [17]:

- R^2 (Coefficient of determination), the model fits a linear regression of the observed LGD values against the predicted LGD values
- $RMSE$ (Root mean square deviation), to compute it, the model uses the following formula where N is the number of observations

$$RMSE = \sqrt{\frac{1}{N}\sum_{i=1}^{N}\left(LGD_i^{obs} - LGD_i^{pred}\right)^2} \tag{4. 16}$$

To conclude this chapter, its important remark that the theory of uncertainty analysis was used to discuss the error of the results calculated for the turbine efficiency and the Stodola's law in the next chapter.

5 Experimental planning and analysis

The objective of this chapter is to show the test plan configuration on site of MoNiKa facility and the preliminary results with the theory behind the practice, this result included the error propagation *(see chapter 4.3)*, as well as the results with the calculations of the entropy and enthalpy in the state 3'' (see Figure 16). This master thesis was performed under the protocol Statute for Safeguarding Good Research Practice at Karlsruhe Institute of Technology [18], all the experimental results were not altered in any aspect.

5.1 Test plan configuration

On November 9, 10 and 11, the experimental part of the master's thesis was carried out. Each day had a different purpose to investigate the turbine. Figure 4 *(see chapter 2.2)* will be taken as a reference point to indicate the thermodynamic variable at each point in the GESI simulation of the ORCs, so that later they can be compared with the experimental data using the references of the Figure 16 where is sketched the process between outlet of the main pump and the outlet of the turbine and the instrumentation used for the working fluid *(see chapter 4.1.1)*. From now on, Figure 16 will be taken as a reference for the states in the different sectors of the cycle.

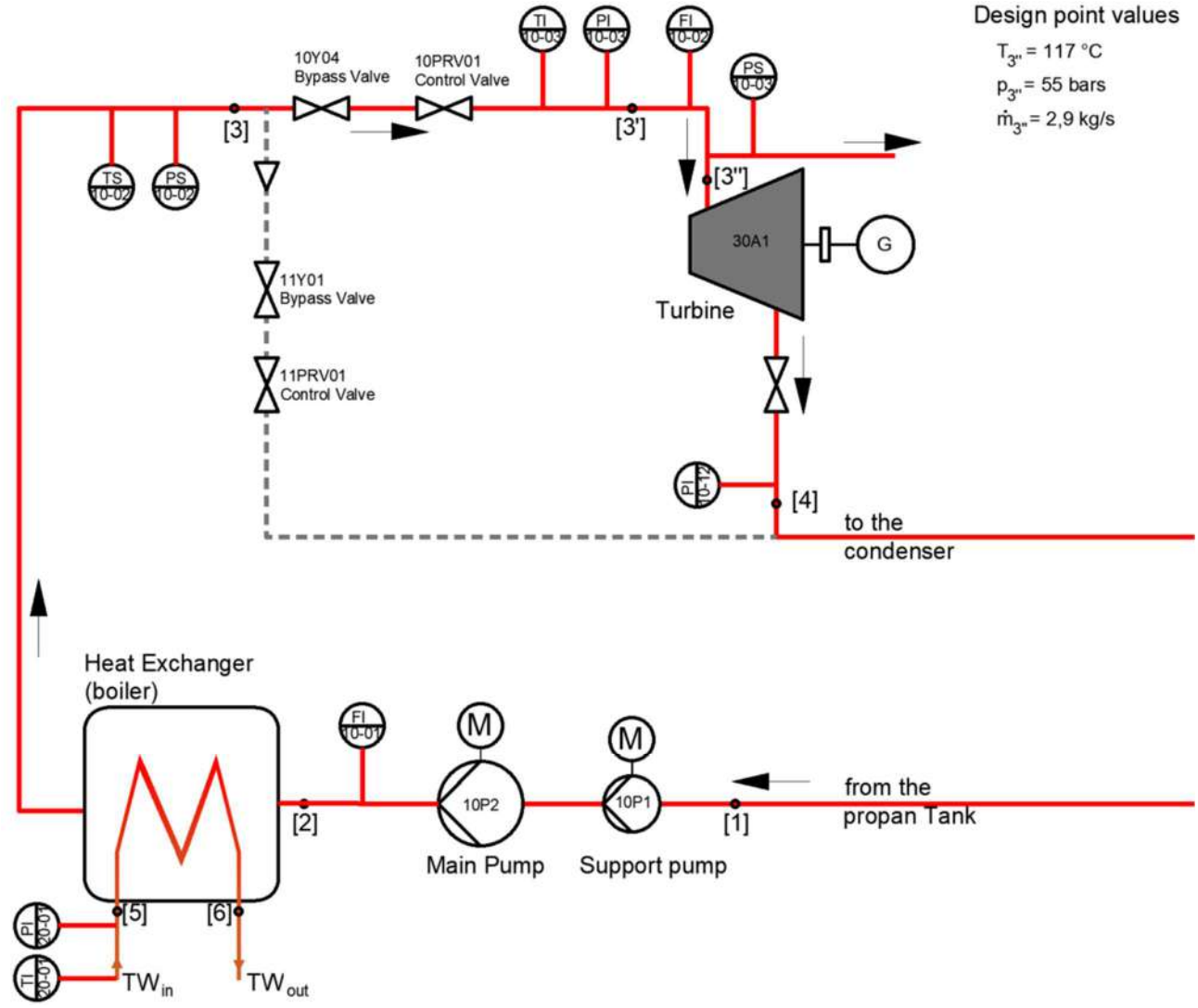

Figure 16: Layout of MoNiKa and the measurement used for the purpose of this thesis

It should be noted that the plant has certain limitations, either with respect to plant safety or thermodynamic values that cannot be reached, which prevent some values planned through the GESI software from being addressed experimentally.

Safety limitations:

- Quality factor at turbine outlet (4) should never be less than $X < 0.80$. in case of occurrence, the formation of droplets inside the blades may cause damage to the blades.
- When the boiler temperature exceeds 160°C, for its own safety, the heating station immediately shuts down.

Thermodynamics value:

- The power plant, due to some problems with the manufacturing of the heat exchanger (boiler), cannot reach a temperature at the inlet of the turbine (3) of more than $113\ °C$ for $\dot{m}_T < 2.2\ kg/s$ and $109\ °C$ for $\dot{m}_T > 2.6\ kg/s$ at given constrains. For comparison, the design point at the inlet of the turbine is $117\ °C$.

5.1.1 First day

Table 4 shows 7 different load points previously simulated in GESI-ORCteillast for steady state conditions. Once the loading points were agreed upon, they were moved to the plant's working conditions. The experiment began with a slow warm up, when the cycle starts in bypass valve and then the boiler is prepared (which acts as the geothermal source of energy). The warmup concludes when the main pump head temperature is less than 0.5 °C for at least 30 minutes, and all the process takes around 4 hours. After warming up, the load points were carried out with an average time of 30 minutes each, and once the 7 load points were completed, the experimental day ended with the regular shutdown.

Date	Time Schedule	Run	ORCs-cycle			Thermal-Water		
			$\dot{m}_T$ [Kg/s]	p_3 [MPa]	T_3 [°C]	$\dot{m}_5$ [Kg/s]	p_5 [MPa]	T_5 [°C]
08.11.21	08:00-12:15	Warm-up	-	-	-	-	-	-
	12:15-12:45	1.1	2.1	5.5	112.0	2.4	0.8	150.7
	12:45-13:34	1.2	2.6	5.5	109.0*	2,4	0.8	150.7
	13:34-14:02	1.3	2.4	5.3	108.0	2.4	0.8	150.0
	14:02-14:40	1.4	2.2	5.3	109.0	2.4	0.8	150.0
	14:40-15:12	1.5	1.9	5.3	110.6	2.4	0.8	150.0
	15:12-15:46	1.6	1.9	5.3	110.6	2.5	0.8	151.0
	15:46-16:15	1.7	2.5	5.3	108.6	2.5	0.8	151.0
	16:15-17:00	Shut down	-	-	-	-	-	-

*In site was no possible to reach more than 109.0 K in the run 1.2

Table 4: Load points proposed at MoNiKa power plant and simulated with GESI – 08.11.2021

During the loading points in the plant, some problems were encountered when trying to reach certain temperature values. This was due to the heat exchanger that did not allow a temperature beyond 109°C with a higher mass flow run.

5.1.2 Second day

The purpose of the second day was a sensibility experiment with the opening of the turbine control valve. As on the first day, the experiment started with a warm-up, which lasted 4 hours. Then by changing the opening of the turbine control valve (*10PRV01* see Figure 16), i.e., opening for each run, the ORCs pressure started to modify.

When the load is above 40% and the turbine control valve has fixed position, e.g., fully open, and the propane temperature is constant, the propane pressure will change proportional to the mass flow according to Stodola's law. This regime is preferred at load above 40% [19]. The next figure shows the two different regimes in MoNiKa power plant when the bypass valve is fully closed during the warm-up. The minimum mass flow rate at which the plant can be operated is $\dot{m}_T = 2.3\ kg/s$. In addition, Figure 18 illustrates the inlet turbine pressure vs the mass flow, and as it is shown the minimal mass flow is around 2.3 kg/s.

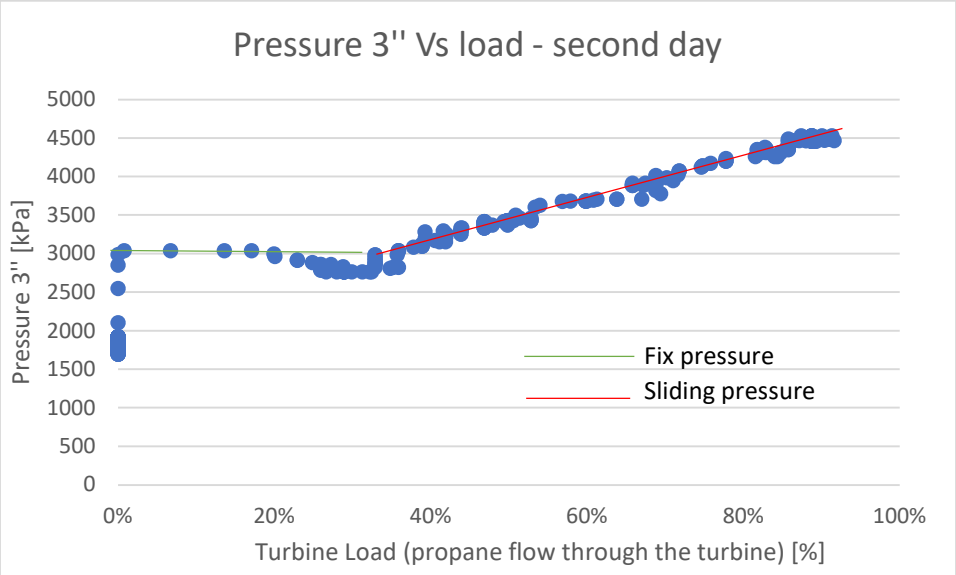

Figure 17: Pressure vs Load during the warm-up

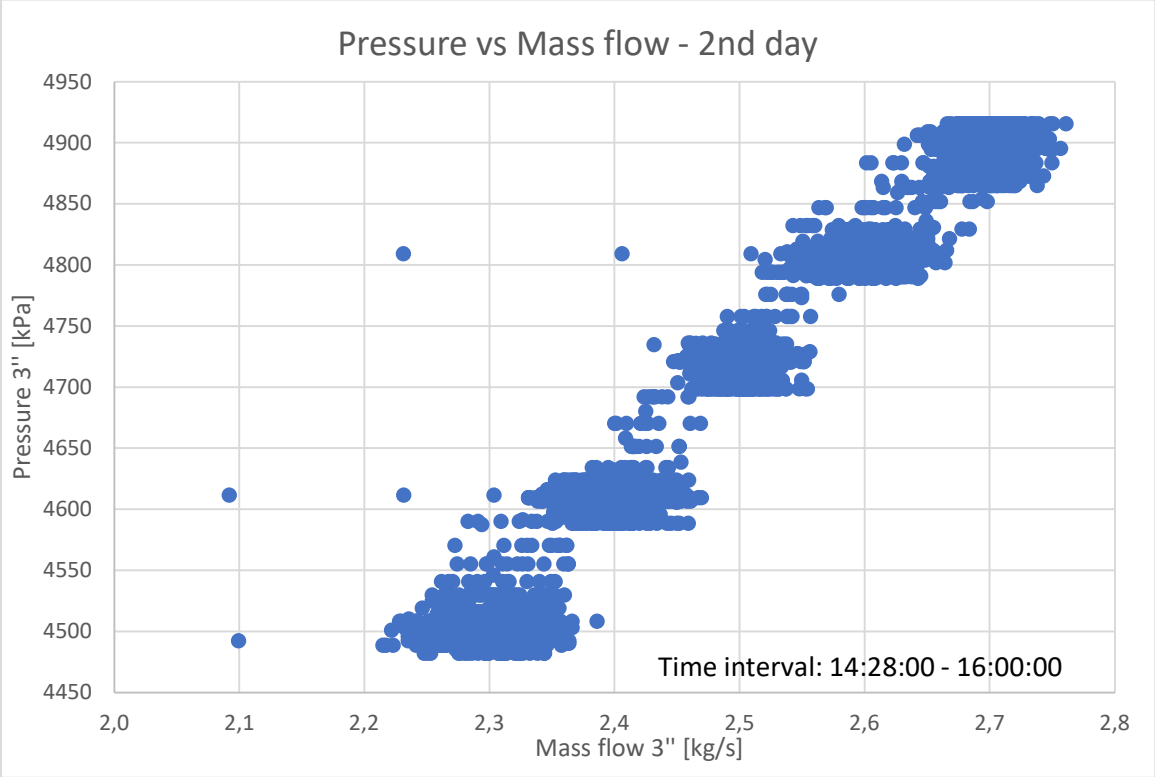

Figure 18: Pressure vs Mass flow - Second day

In this case, data are sampled in time intervals of 15 to 20 minutes each. Starting at 08:00 and finishing at 16:30. Table 5 marks each run of the sensibility tests with the incorporation of the opening of the turbine

control valve (*10PRV01,* see Figure 16). Furthermore, Figure 19 illustrates how the valve was opening throughout the day, ending with the valve completely open.

Date	Time Schedule	Run	ORCs-cycle				Thermal-Water		
			$\dot{m}_T$ [Kg/s]	*T-cv* [%]	p_3 [MPa]	T_3 [°C]	$\dot{m}_5$ [Kg/s]	p_5 [MPa]	T_5 [°C]
09.11.21	08:00-12:08	Warm-up	-	-	-	-	-	-	-
	12:08-12:38	2.1	2.4	16.3	5.5	111.0	2.4	0.8	150.5
	12:38-13:10	2.2	2.4	15.7	5.6	110.9	2.6	0.8	150.5
	13:10-13:43	2.3	2.6	17.0	5.6	111.0	2.6	0.8	150.0
	13:43-13:58	2.4	2.6	18.3	5.5	109.5	2.6	0.8	150.0
	13:58-14:14	2.5	2.6	19.5	5.4	108.7	2.6	0.8	150.0
	14:14-14:30	2.6	2.6	22.2	5.4	107.7	2.6	0.8	150.0
	14:30-14:45	2.7	2.6	27.8	5.4	107.7	2.6	0.8	150.0
	14:45-15:00	2.8	2.6	71.9	5.2	107.0	2.6	0.8	150.0
	15:00-15:15	2.9	2.7	97.3	5.3	106.7	2.6	0.8	150.0
	15:15-15:30	2.10	2.5	99.0	5.1	105.8	2.6	0.8	150.0
	15:30-15:45	2.11	2.4	99.0	4.7	105.0	2.6	0.8	150.0
	15:45-16:30	Shut down	-	-	-	-	-	-	-

Table 5: Sensibility Control Valve experiment at MoNiKa power plant - 09.11.2021

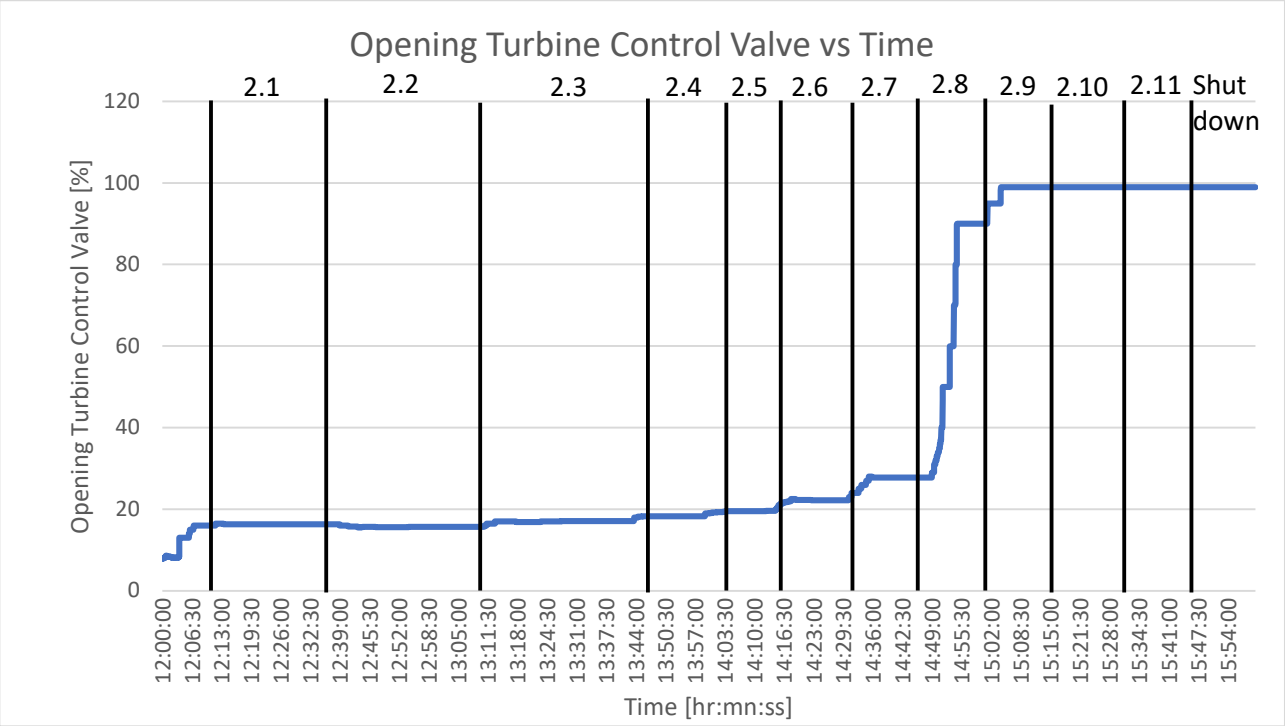

Figure 19: Opening Turbine Control Valve during the sensibility test of MoNiKa

5.1.3 Third day

Experimental work on turbine sensitivity was also planned for the last day, but in this case related to the ORCs mass flow increase. It started with a $\dot{m}_T = 2.1\ kg/s$ and after that it was increased by $0.1\ kg/s$ until a turbine mass flow rate of $2.8\ kg/s$ was reached. As during the previous days, the day started with a slow warm-up but with an issue in the middle of the process: The boiler surpasses 160 °C, so automatically the control system tripped the boiler. Once, the boiler worked more stable, the warm-up finally ended properly. In addition, the boiler had difficulties finding a stable temperature due to failures in the control system, during all day. This caused oscillations in frequencies of 6 minutes (see Figure 20), which caused variation of

other thermodynamic variables, as turbine inlet temperature (T_3), difference of enthalpy between the inlet and the outlet of the turbine, etc.

Once the first loading point was started, an iterative work was done, i.e., before modifying the parameters in the plant, the condition was simulated in GESIteillast to compare the results. Since it was a mass flow sensitivity analysis, the only variable that was increased was the mass flow itself. As the simulation progressed, it was observed that, as the mass flow rate increased and if the turbine inlet temperature did not increase, the cycle could go from supercritical to subcritical. This was a crucial point for the experiment, adding that the boiler could not maintain a constant temperature throughout the day. Table 6 shows the average values of each load point throughout the day and is visibly how the mass flow rate increased by 0.1 kg/s each load point.

Date	Time Schedule	Run	ORCs-cycle			Thermal-Water		
			$\dot{m}_T$ [Kg/s]	p_3 [MPa]	T_3 [°C]	$\dot{m}_5$ [Kg/s]	p_5 [MPa]	T_5 [°C]
10.11.21	08:00-13:34	Warm-up*	-	-	-	-	-	-
	13:34-14:04	3.1	2.1	4.5	100.7	2.4	0.8	152.5*
	14:04-14:43	3.2	2.2	4.6	102.5	2.4	0.8	152.3*
	14:43-15:12	3.3	2.3	4.8	101.8	2.4	0.8	152.2*
	15:12-15:42	3.4	2.4	4.9	102.9	2.4	0.8	151.0*
	15:42-16:02	3.5	2.5	4.9	103.6	2.4	0.8	151.4*
	16:02-16:12	3.6	2.6	5.1	104.4	2.4	0.8	150.5*
	16:12-16:30	3.7	2.7	5.0	104.4	2.4	0.8	149.5*
	16:30-17:02	3.8	2.8	5.0	103.7	2.4	0.8	152.0*
	17:02-17:45	Shut down	-	-	-	-	-	-

*Oscillating temperature, mean values

Table 6: Sensibility ORC mass flow experiment at MoNiKa power plant - 10.11.2021

Figure 20 shows the oscillation of the boiler on the third day. As can be seen in the graph, the temperature difference increased until around 15:30, when the boiler started to stabilize. The data range of the trip during the warm-up does not appear in the figure. In addition, Figure 21 illustrates how the turbine inlet temperature has been varying due to the temperature variation of the heat exchanger.

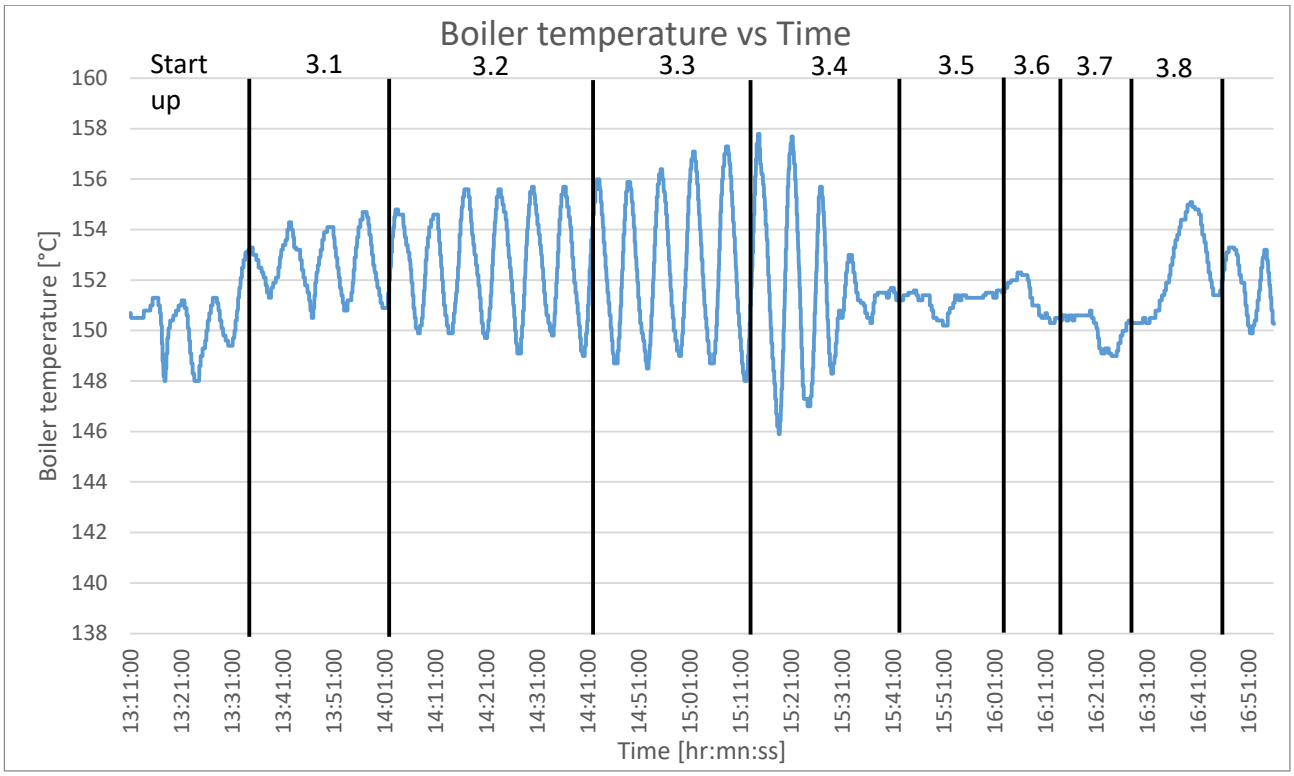

Figure 20: Oscillation in boiler third day

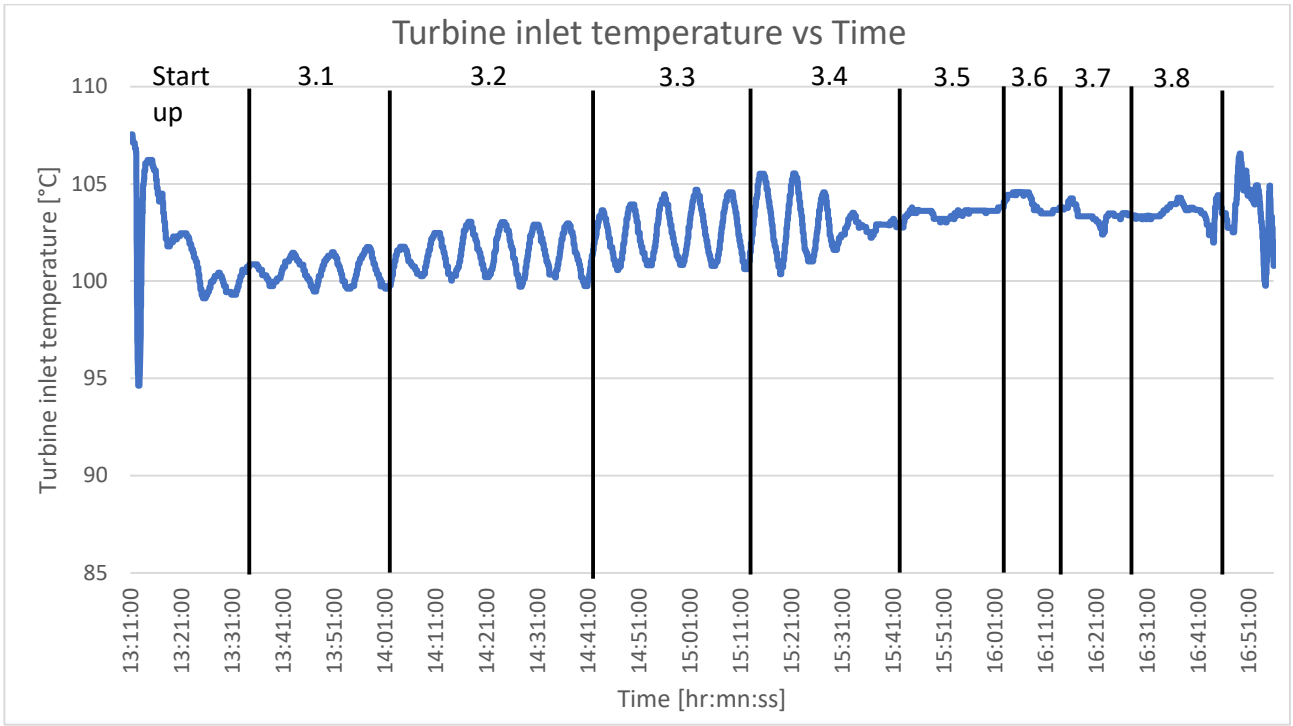

Figure 21: Oscillation turbine inlet temperature due to the oscillation of the boiler's temperature

To conclude this section, it is important to understand how each day of on-site operation was planned, how the previous simulation with GESI and GESIteillast software has been and the problems that have appeared since it has been an experimental work. In addition, the next section will present the analysis, the solution criteria and the calculations of the thermodynamic state each day to continue in the next chapter with the results.

5.2 Analysis

Once the data was collected and processed, the analysis began. The objective of this was to be able to calculate the turbine efficiency of the turbine, so the thermodynamic variables of the equation (3. 10): were needed as a starting point but with the subscripts of Figure 16, so equation (3. 10) results in:

$$\eta_T = \frac{h_{3''} - h_4}{h_{3''} - h_{4,s}} \tag{5. 1}$$

The enthalpy at turbine outlet (h_4) could not be determined, because more than one variable is needed to know a thermodynamic property under saturation conditions. Figure 22 shows the model in GESI for an ORCs [5] with the addition of a red line that illustrates the process of an isentropic turbine. In addition, it shows the turbine outlet properties in the saturation regime. In contrast, $h_{4,s}$ can be determined using the properties entropy and enthalpy at the inlet of the turbine and then assuming an isentropic process, which means that $s_{4,s} = s_{3''}$.

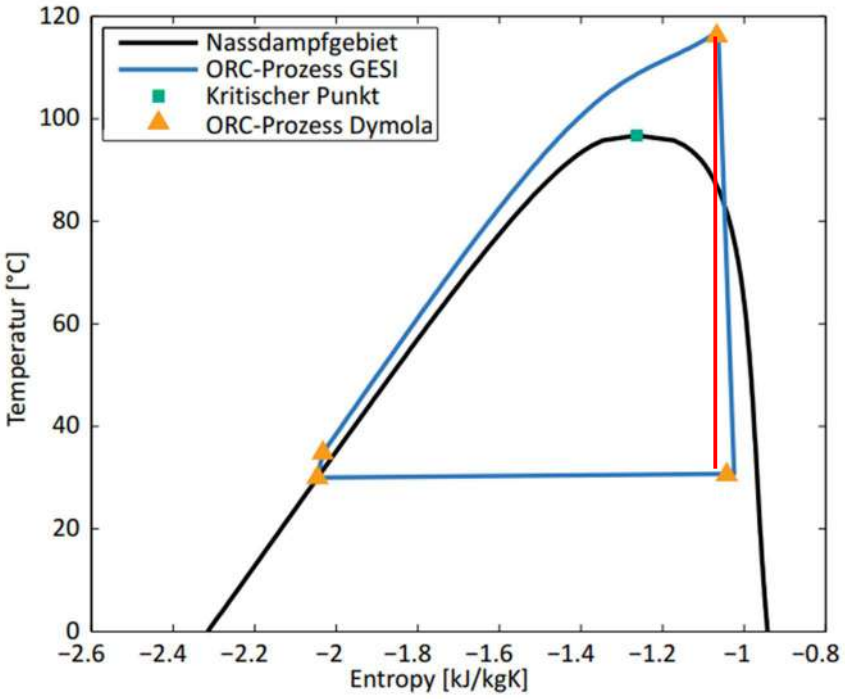

Figure 22: ORCs cycle [5] with the inclusion of the subscripts and the isentropic turbine process

Starting from equation (3. 7), the enthalpic difference of the turbine could be determined knowing the power giving by the turbine and then dividing it by the mass flow through the turbine (It is important to note that the mass flow at the point 3'' is noted $\dot{m}_T$):

$$P_T = \dot{m}_T \cdot (h_{3''} - h_4) \tag{5. 2}$$

The power of the turbine is the measured power of the generator divided by the efficiency of the generator and the efficiency of the gear box ($\eta_{gen} = 94.6\%$ [20] and $\eta_{gb} = 99.2\%$ [7], respectively):

$$P_T = \frac{P_{gen}}{\eta_{gen} \cdot \eta_{gb}} \tag{5. 3}$$

From equation (5. 2) and (5. 3), t the enthalpic difference can be calculated as:

$$(h_{3''} - h_4) = \frac{P_{gen}}{\eta_{gen} \cdot \eta_{gb}} \cdot \frac{1}{\dot{m}_T} = \frac{P_T}{\dot{m}_T} \tag{5. 4}$$

Finally, the efficiency of the turbine (5. 1) can be calculated as:

$$\eta_T = \frac{P_T}{\dot{m}_T} \cdot \frac{1}{(h_{3''} - h_{4,s})} \tag{5. 5}$$

For equation (5. 5), it is possible to measure the power of the turbine and the mass flow rate minus the mass flow that goes through the bypass valve (FI10-01 measurement system, 11PRV01). The enthalpy $h_{3,,}$ can be determined by measuring the temperature and pressure in $3''$ and then calculating the enthalpy with the refprop software as $h_{3,,} = f(P_{3,,}, T_{3,,})$. Following the same criteria, the entropy 3'' was calculated as $s_{3,,} = f(P_{3,,}, T_{3,,})$. The enthalpy 4s, also using Refprop, is a function of the entropy at point $3''$ and the pressure measured at point 4 as $h_4 = f(s_{3,,}, p_4)$. Next lists contain a summary of this values:

- $T_{3''}$ = measured turbine inlet temperature (Measurement system: **FI10-02**)
- $p_{3''}$ = measured turbine inlet pressure (Measurement system: **PS10-03**)
- p_4 = measured turbine inlet pressure (Measurement system: **PI10-12**)
- $\dot{m}_T$ = measured propane mass flow through the turbine (Measurement system: **FI10-01**)
- Bypass valve opening (measurement 11PRV01)
- P_{gen} = measured generator power (Measurement system: **GPC-3 from DEIF**)
- $h_{3''} = f(p_{3''}, T_{3''})$
- $s_{3''} = f(p_{3''}, T_{3''})$
- $h_{4s} = f(s_{3''}, p_4)$

In addition, the enthalpy of h_3 and h_3, was calculated following the same criteria previously mentioned but with the measurement systems corresponding to each one. Which means, for states 3, the temperature TS10-02 and pressure PS10-02 measurement systems were used, and for those of state 4, pressure PI10-12.

Equations (5. 6), (5. 7) and (5. 8) are to demonstrate the calculation procedure of the entropy and enthalpy in one state (this example shows the state 3'' and the enthalpy of 4) with REFPROP in MATLAB software:

$$h_{3''} = refpropm('h', 'T', FI10-02, 'p', PS10-03, 'propane'); \tag{5. 6}$$

$$s_{3''} = refpropm('s', 'T', FI10-02, 'p', PS10-03, 'propane'); \tag{5. 7}$$

$$h_{4s} = refpropm('h', 'p', PS10-12, 's', s_{3''}, 'propane'); \tag{5. 8}$$

For the three days, the thermodynamic properties previously mentioned were calculated for each state. Then, the turbine efficiency was calculated, following the equation (5. 5), which in many points was greater than one, which is physically impossible. Notably, a significant difference in enthalpy was noticed between states 3 and 3'', whereas only two valves and one piping system were found between the two states. The following section will discuss this enthalpy error between both states given by Refprop.

5.2.1 Refprop and thermodynamic error calculation

In this section we will discuss the problem, due the large error in the enthalpy or entropy calculation with small systematic errors in temperature or pressure, for the mixture working fluid composed of propane and nitrogen (99.8% and 0.2% respectively).

The turbine efficiency η_T is determined from individual data points $T_{1,i}$, $p_{1,i}, p_{2,i}$, $\dot{m}_i, P$ and thus its variance can be determined from the variances of $T, p, \dot{m}$ and P, as is shown in the next equation, with the equation (4. 11) of the statistical error propagation theory (see chapter 4.3):

$$\sigma_{\eta,i} = \sqrt{\left(\frac{d\eta}{dT_{3,i}}\right)_{p3,p4,\dot{m},P}^{2} \sigma_T^2 + \left(\frac{d\eta}{dp_{3,i}}\right)_{T,p4,\dot{m},P}^{2} \sigma_{p3}^2 + \left(\frac{d\eta}{d\dot{m}_i}\right)_{p3,p4,T,P}^{2} \sigma_{\dot{m}}^2 + \left(\frac{d\eta}{dp_{4,i}}\right)_{p3,T,\dot{m},P}^{2} \sigma_{p2}^2 + \left(\frac{d\eta}{dP_i}\right)_{p3,p4\dot{m},T}^{2} \sigma_P^2} \quad (5.\ 9)$$

Where T represents the temperature, p the pressure, $\dot{m}$ the mass flow, P refers to the power output of the turbine and subindices *3* and *4* indicate turbine inlet and outlet respectively. In addition, $\frac{d\eta}{dT}, \frac{d\eta}{dp}, \frac{d\eta}{dp4}, \frac{d\eta}{d\dot{m}}, \frac{d\eta}{dP}$ were determined with the same solution:

- $\frac{d\eta}{dT_{3,i}}$ by changing ± 1 K and calculating the efficiency as: $\frac{\Delta\eta}{\Delta T_{3,i}}$, (with the other variable cte.)
- $\frac{d\eta}{dp_{3,i}}$ by changing ± 100 kPa and calculating the efficiency as: $\frac{\Delta\eta}{\Delta p_{3,i}}$, (with the other variable cte.)
- $\frac{d\eta}{dp_{4,i}}$ by changing ± 100 kPa and calculating the efficiency as: $\frac{\Delta\eta}{\Delta p_{4,i}}$, (with the other variable cte.)
- $\frac{d\eta}{d\dot{m}_i}$ as is proportional, the variance is: $\frac{\Delta\eta}{\dot{m}_i}$, (with the other variable cte.)
- $\frac{d\eta}{dP_i}$ as is proportional, the variance is: $\frac{\Delta\eta}{\Delta P_i}$, (with the other variable cte.)

Where the scatter of the turbine power is a problem with the data transfer accuracy, which means the PROFIBUS.

In order to see the problem of the calculation of the thermodynamical properties h and s, a time interval was taken, run1.7 between 16:07:00 and 16:15:00 (see Table 4), within the first day where the temperature and pressure would indicate that they were above of the propane critical point ($T_{crit} = 96.74\ °C$ and $p_{crit} = 4.25\ MPa$). For that time interval, the temperature and pressure of 3, 3' and 3'' were plotted (see Figure 23 and Figure 24 respectively).

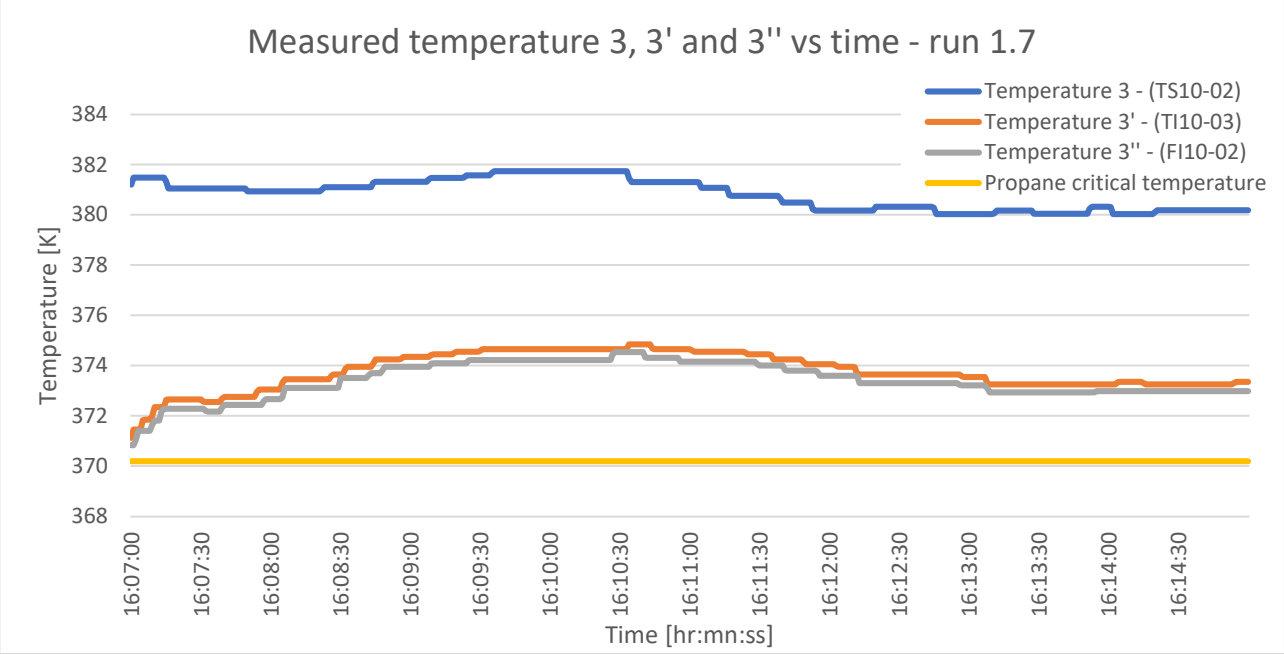

Figure 23: Temperature values 3, 3', 3'' - first day, run 1.

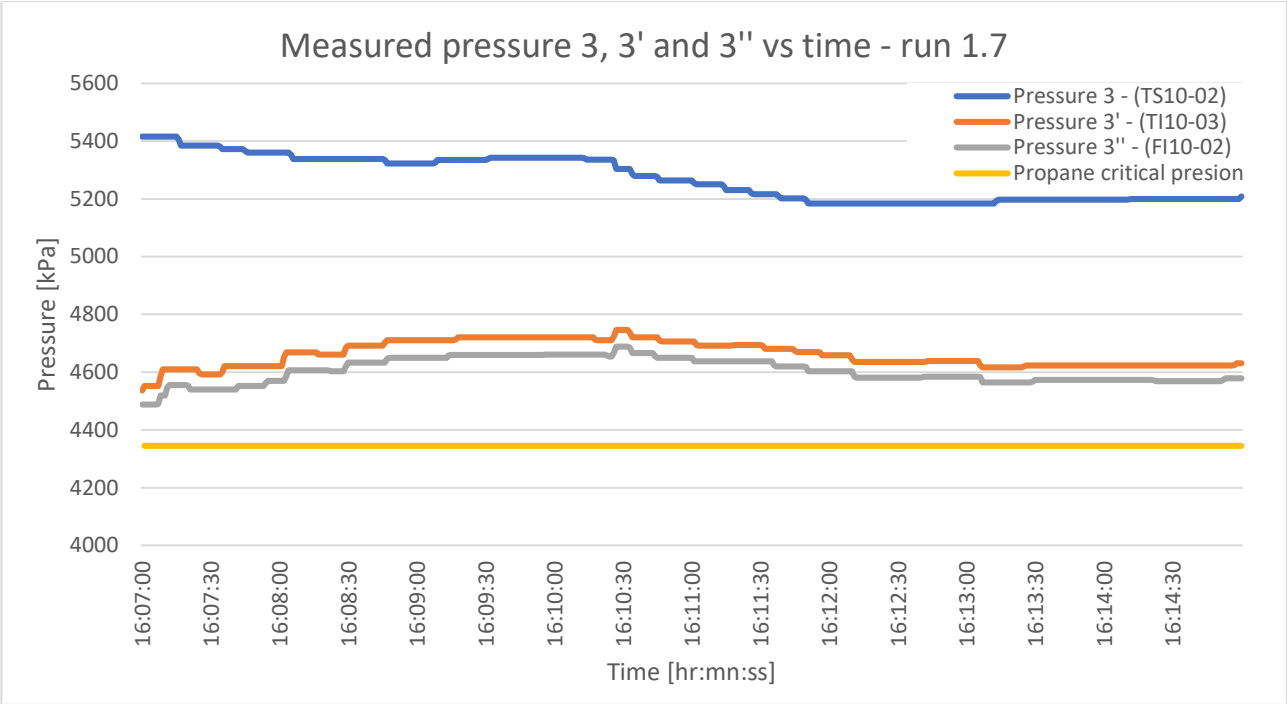

Figure 24: Pressure values 3, 3', 3'' - first day, run 1.7

Then, for the same time interval, the entropy and enthalpy, previously calculated (see equations (5. 6) and (5. 7)). with refprop, were plotted in Figure 25 and Figure 26.

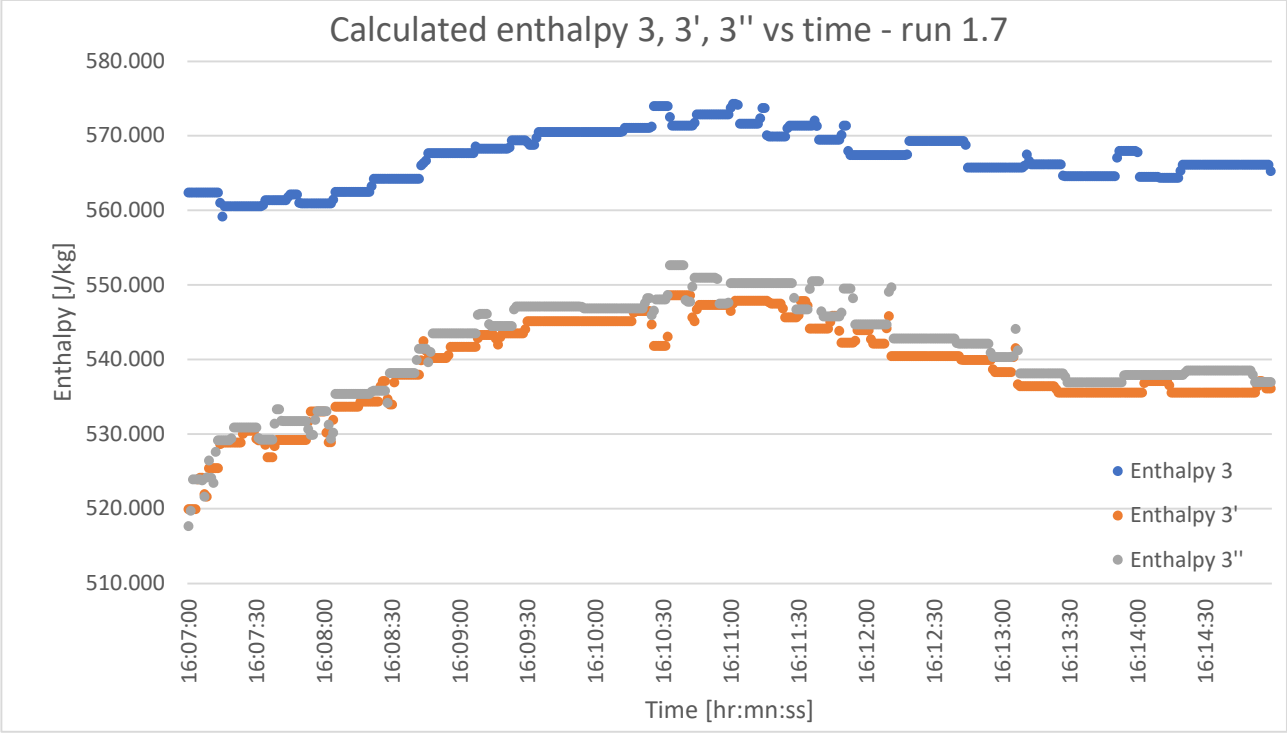

Figure 25: Enthalpy calculated 3, 3', 3'' - first day, run 1.7

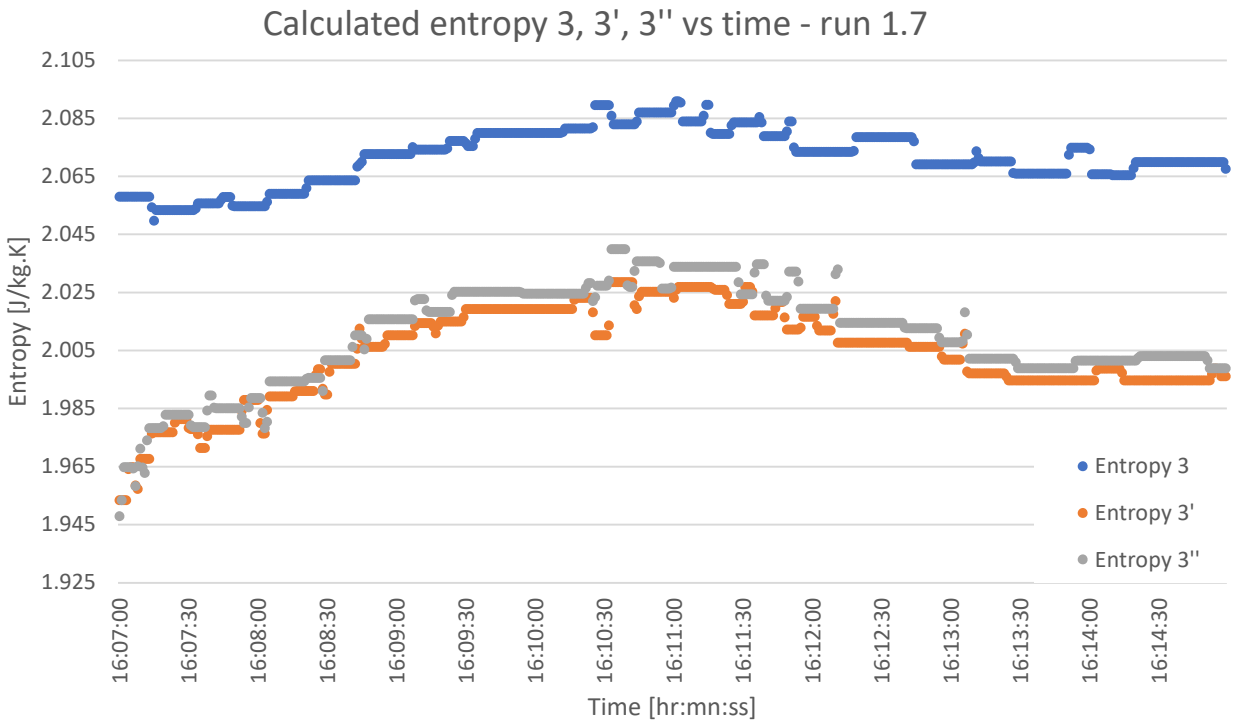

Figure 26: Entropy 3, 3', 3'' - first day, run 1.7

Equation (5. 10), determines the heat loss between state 3 and 3'', i.e., through the valve and pipes, due to the enthalpy difference multiplied by the mass flow rate flowing through that section. The next illustration, Figure 27, shows this heat loss of the process 3-3'' in detail. Initial values in Figure 23 show that the working fluid is close to the pseudo-critical point and looking at Figure 27 it is possible to see how there is an increase in heat loss in the vicinity of the critical point.

$$\dot{Q}_{loss\ 3-3''} = (h_3 - h_{3''}) \cdot \dot{m}_T \qquad (5.\ 10)$$

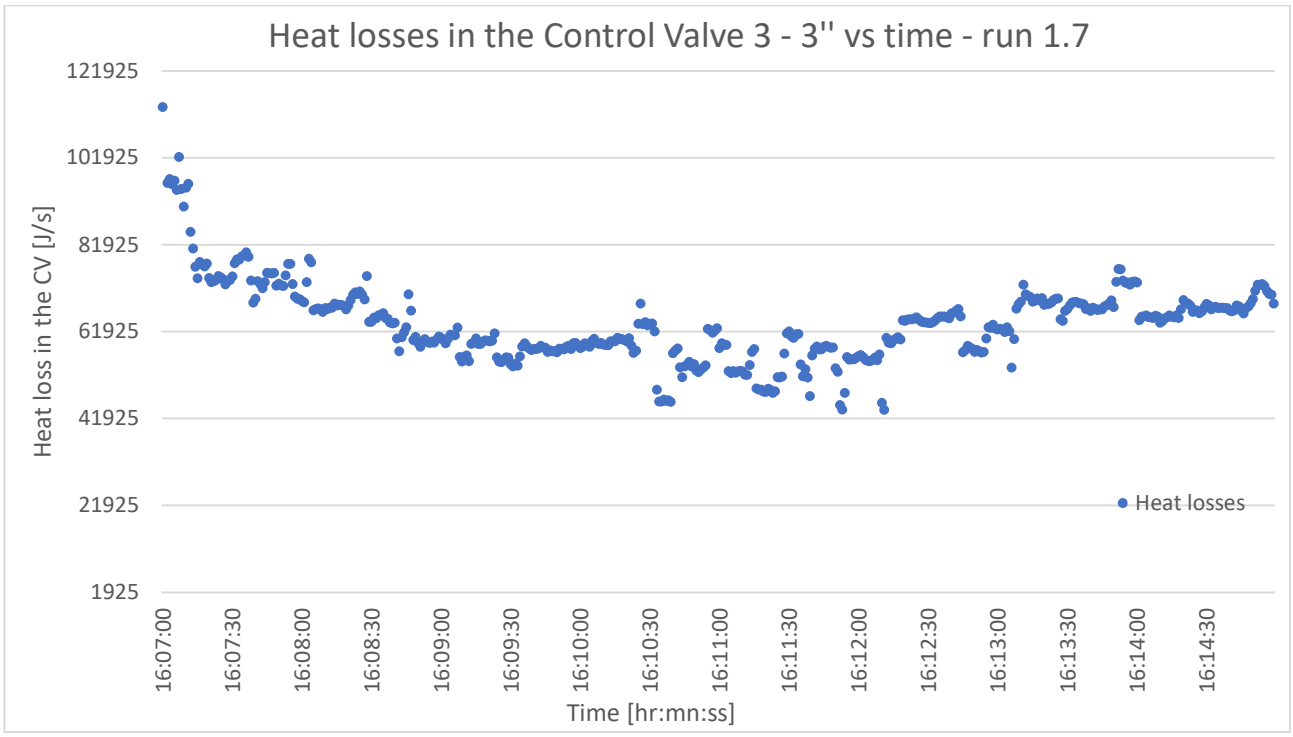

Figure 27: Heat losses in 3 - 3'' - first day, run 1.7

In order to understand the problem of high heat loss values between points 3 - 3'', I calculated and plotted the heat capacity and density values for temperatures and pressures close to the critical point (as shown in Figure 23 and Figure 24, the values of temperature and pressure are above the critical point but not so far away). Figure 28 shows the heat capacity of the working fluid between the temperatures of 350 and 400 K at three different pressures, and Figure 29 the density of the working fluid in the same parameter range.

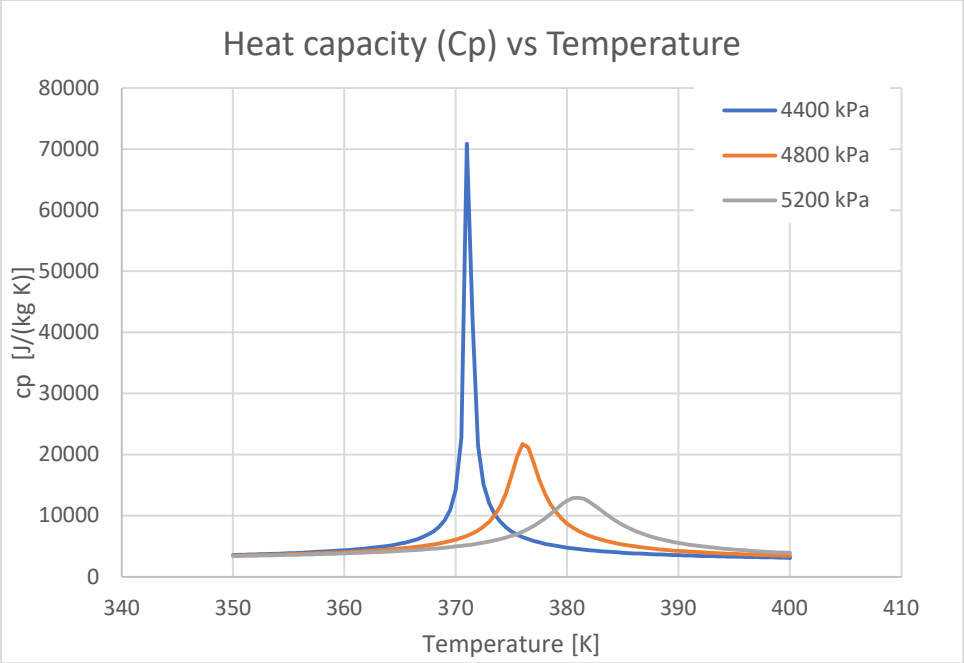

Figure 28: cp vs T for pressures 4400, 4800 and 5200 kPa of a mixture (C_3H_8 99.8% and N_2 0.2%)

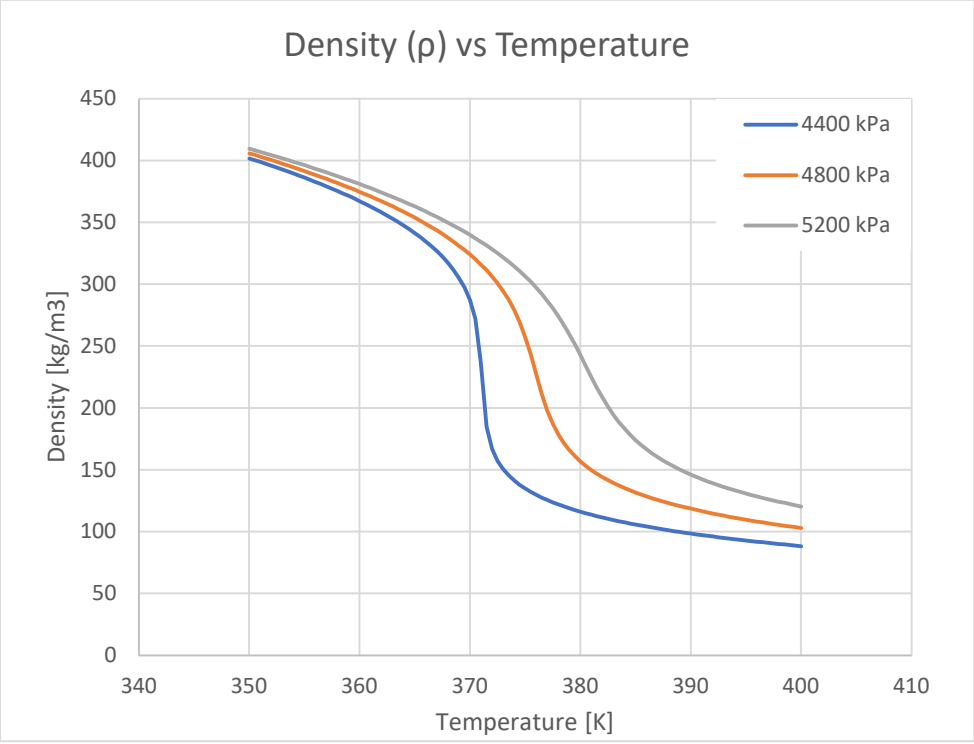

Figure 29: ρ vs T for pressures 4400, 4800 and 5200 kPa of a mixture (C_3H_8 99.8% and N_2 0.2%)

Figure 28 shows that the working fluid heat capacity has a maximum, which is increasing when approaching the critical point. On the left side of the peak, the fluid is pseudo-liquid and on the right side the fluid it is pseudo-steam, and the maximum is called pseudo-critical point. Looking again at Figure 23, both upstream

and downstream the valve, the working fluid manage to reach a temperature almost exactly at the pseudo-critical temperatures. Any temperature error dT is causing and enthalpy error dh (see equation (4. 7)) as a linear error propagation:

$$dh = \left(\frac{dh}{dT}\right)_p \cdot dT = cp \cdot dT \tag{5. 11}$$

Which means that a systematic error of 1 K of the temperature measurement could cause an enthalpy error of 10kJ/kg at 5200 kPa, 20kJ/kg at 4800 kPa, or even 70kJ/kg at 4400 kPa. Therefore, it is concluded that it is difficult to measure the enthalpy at turbine inlet precisely with the used sensors under these conditions.

To solve this problem of enthalpy and entropy calculation due to the measurement systems near the critical temperature point, the data at point 3 shall be taken and the properties at point 3'' shall be calculated instead. As the valve is assumed to be isenthalpic, the enthalpy at 3'' can be determined from the enthalpy at point 3 minus the heat losses in between. The following section will calculate the heat loss between measurement systems 3 and 3'' according to the heat loss of the components by to their physical properties (pipe, insulation, etc.).

5.2.2 Heat losses of the components

Thermal diffusion or conduction happened in the pipe between 3 and 3'', which means, from an engineering point of view, heat propagation can be predicted by Fourier's law [21] according to next equation:

$$\nabla^2 T + \frac{\dot{q}_G}{k} = \frac{1}{\alpha}\frac{\partial T}{\partial t} \tag{5. 12}$$

Where $\dot{q}_G$ the rate of energy generation per unit volume inside the control volume, α is the thermal diffusivity define as:

$$\alpha = \frac{k}{\rho c} \tag{5. 13}$$

If the system is in the steady state and no heat is generated internally, as for the process 3 – 3'', the conduction equation (5. 12) further simplifies to (known as the *Laplace equation*):

$$for\ rectangular: \qquad \nabla^2 T = \frac{\partial^2 T}{\partial x^2} + \frac{\partial^2 T}{\partial y^2} + \frac{\partial^2 T}{\partial z^2} = 0 \tag{5. 14}$$

$$for\ cilindrical: \qquad \nabla^2 T = \frac{1}{r}\frac{\partial}{\partial r}\left(r\frac{\partial T}{\partial r}\right) + \frac{1}{r^2}\frac{\partial^2 T}{\partial \phi^2} + \frac{\partial^2 T}{\partial z^2} = 0 \tag{5. 15}$$

Cylindrical coordinate system for the general equation is showed in Figure 30:

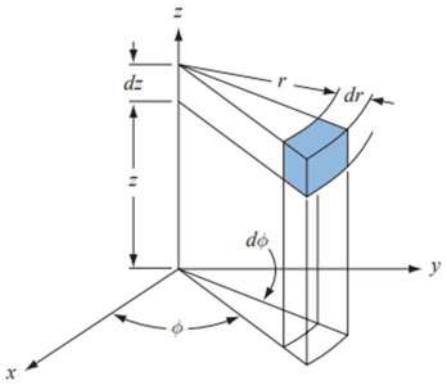

Figure 30: Cylindrical coordinate system for general conduction equation [21]

If the heat flux in a cylindrical shape is only in the radial direction, the equation (5. 15) simplifies and the steady-state conduction equation for cylindrical coordinate is:

$$\frac{d}{dr}\left(r\frac{dT}{dr}\right) = 0 \tag{5. 16}$$

The heat transferred by conduction through the cylinder of length L, illustrated in Figure 31, is:

$$q_k = 2\pi Lk\,\frac{(T_i - T_o)}{ln(r_0/r_i)} \tag{5. 17}$$

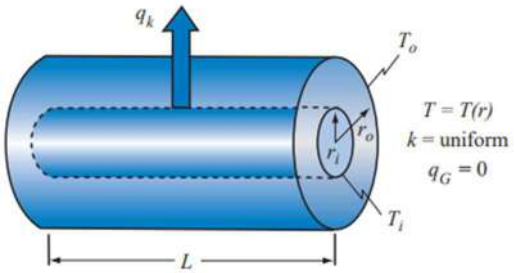

Figure 31: Radial heat conduction through a cylindrical pipe

The calculation of the heat losses between points 3 and 3'' was carried out using the drawings "Zulauf Turbine" (*Appendix 9.1*), which details the piping from the PI10-10 sensors to the turbine inlet. The only heat resistance was assumed to be given by a thermal insulation of 50 mm thickness covering all the pipe, with a function of the thermal conductivity of the insulation given by Table 7:

Temperature [°C]	40.0	50.0	100.0	150.0
$k\ [W/(m \cdot K)]$	0.035	0.037	0.043	0.050

Table 7: Thermal insulator of the piping system according to Rohrschale ROCKWOOL 800

Heat resistances inside the pipes, inside the steel and outside the insulation were neglected. Starting from equation (5. 17), we arrive at the following equation which is the heat loss associated with the mass flow rate through the piping system seated at MoNiKa power plant between the state 3 and 3'':

$$q_{loss,i} = 2\pi k_i\left(T_{inlet,i} - T_{Amb,\infty}\right)\sum \frac{L_{pipe,i}}{\ln\left(r_{int,i}/r_{ext,i}\right)} \tag{5. 18}$$

Where, k_i is function of the temperature of the working fluid (see Table 7), $T_{inlet,i}$ is the fluid temperature at the state 3, $T_{Amb,\infty}$ is the ambient temperature, $L_{pipe,i}$ is the longitude of each pipe between those states,

$r_{int,i}$, is the radio external of the pipes, and $r_{ext,i}$ is the external radios of the pipe plus the thickness of the thermal insulator (50 mm). The resolution of the term $\sum \frac{L_{pipe,i}}{\ln (r_{int,i}/r_{ext,i})}$ can be seen in the following table.

Pipe	ID*	Length [mm]	Tube DN [mm]	Dtube [mm]	Tube Surface [m²]	Insulation [mm]	Da [mm]	ln(Da/Dtube)
1	2-2	227.0	100.0	114.3	0.08	50.0	214.3	0.6
2	2-2	317.0	100.0	114.3	0.11	50.0	214.3	0.6
3	2-3	210.0	100.00	114.3	0.08	50.0	214.3	0.6
4	2-3	100.0	80.0	88.9	0.03	50.0	188.9	0.8
5	1-3	152.0	50.0	60.3	0.03	50.0	160.3	1.0
6	1-3	808.0	50.0	60.3	0.15	50.0	160.3	1.0
7	1-4	842.0	50.0	60.3	0.16	50.0	160.3	1.0
8	1-4	376.0	50.0	60.3	0.07	50.0	160.3	1.0
9	1-4	844.0	50.0	60.3	0.16	50.0	160.3	1.0
10	2-5	806.0	50.0	60.3	0.15	50.0	160.3	1.0
11	2-5	832.0	50.0	60.3	0.16	50.0	160.3	1.0
12	2-5	2700.0	50.0	60.3	0.51	50.0	160.3	1.0
13	2-5	829.0	50.0	60.3	0.16	50.0	160.3	1.0
14	2-5	409.0	50.0	60.3	0.08	50.0	160.3	1.0
15	2-5	1133.0	50.0	60.3	0.21	50.0	160.3	1.0
16	1-5	679.0	50.0	60.3	0.13	50.0	160.3	1.0
17	1-5	86.0	50.0	60.3	0.02	50.0	160.3	1.0

Summarizing by Dtube

Pipe	Length [mm]	Tube DN	Dtube [mm]	Tube surface [m²]	Insulation [mm]	Da [mm]	ln(Da/Dtube)
1	754.0	100.0	114.3	0.27	50.0	214.3	0.6
2	100.0	80	88.9	0.03	50.0	188.9	0.8
3	10496.0	50	60.3	1.99	50.0	160.3	1.0

*ID and document page

Table 8: $\sum((Lpipe,i)/(ln\ (rint,i)\ /\ (rext,i))$ between state 3 and 3'

Resulting $\sum \frac{L_{pipe,i}}{\ln (r_{int,i}/r_{ext,i})} = 12.1\ m$

Once the heat loss was calculated for each run, the enthalpic loss due to heat [8] between point 3 and 3'' was calculated as:

$$h_{loss,i} = \frac{q_{loss,i}}{\dot{m}_T} \tag{5. 19}$$

It can be concluded that, because the working fluid downstream of the control valve is very close to the critical point, this causes the enthalpy to have very large errors and therefore it is almost impossible to measure the enthalpy at turbine inlet precisely under these conditions (they were in the order of 40000 J/s see Figure 27). Therefore, the enthalpy loss was calculated as the heat loss in the pipes. This gives values of enthalpy loss around 200 J/s in relation to the equation (5.19), so there is a very large difference between one procedure and the other (are 200 times smaller).

With this assumption, the enthalpy at the inlet of t|he turbine is calculated as:

$$h_{3''} = \ h_3 - h_{loss,i} \tag{5. 20}$$

Then, the entropy can be calculated as a function of the enthalpy and the pressure with Refprop:

$$s_{3''} = refpropm('s', 'h', h_{3''}, 'p', PS10-03, 'propane'); \tag{5. 21}$$

Finally, the isentropic enthalpy at the outlet will be function of the entropy $s_{3''}$, and the turbine outlet pressure:

$$h_{4s} = refpropm('h', 's', s_{3''}, 'p', PI10-12, 'propane', 'nitrogen', 0.998, 0.002); \tag{5. 22}$$

This chapter concludes with all the thermodynamic state variables required to continue in the next chapter with the calculation of the turbine efficiency and the equation of Stodola's, to take a further step in understanding the turbine.

6 Results

The main objective of this chapter is to analyse the different test runs of each day under steady state conditions to see on which parameters the efficiency depends. Concluding with the calculus of the turbine efficiency (with their limitations) and the Stodola's law equation.

Turbine efficiency analysis

Steady state points were selected, having established as a criterion the continuous values of around 2 to 3 minutes that have a very low variation (around 2%) both in its intensive properties and in its extensive properties.

The following table shows for each run the steady state times that were selected, and the mean values measured for turbine mass flow ($\dot{m}_3$), temperature upstream the control valve (T_3), pressure upstream the control valve (p_3), opening of the bypass valve, generator power output (P_{gen}), and pressure at the outlet of the turbine (p_4).

Day	Run	Time interval [hr:mn:ss]		Time [hr:mn:ss]	$\dot{m}_T$ [kg/s]	T_3 [K]	p_3 [kPa]	P_{gen} [kW]	Bypass Valve [%]	p_4 [kPa]
1°	1.1	12:29:18	12:31:30	00:02:12	2.1	384.6	5504.1	86.9	1.0	965.7
	1.2	13:08:00	13:11:00	00:03:00	2.6	382.3	5525.0	96.4	1.6	1013.3
	1.3	13:54:30	13:56:40	00:02:10	2.4	381.2	5254.9	97.0	0.7	1029.4
	1.4	14:30:00	14:32:45	00:02:45	2.2	381.2	5191.3	90.1	0.0	1035.0
	1.5	15:04:00	15:06:30	00:02:30	1.9	382.9	5226.8	77.6	1.3	1035.0
	1.6	15:36:00	15:39:00	00:03:00	1.9	383.0	5192.0	78.5	0.0	1039.5
	1.7	16:10:00	16:13:00	00:03:00	2.5	380.7	5237.1	97.0	0.0	1062.5
2°	2.1	12:28:19	12:31:00	00:02:41	2.4	383.5	5517.7	91.8	0.2	1106.4
	2.2	12:56:00	12:58:00	00:02:00	2.4	384.5	5611.2	91.3	0.0	1103.6
	2.3	13:23:00	13:26:00	00:03:00	2.6	383.4	5628.9	95.9	0.0	1115.6
	2.4	13:52:30	13:54:20	00:01:50	2.6	382.4	5501.0	96.3	0.0	1117.0
	2.5	14:08:30	14:10:30	00:02:00	2.6	382.0	5429.4	97.0	0.0	1119.9
	2.6	14:24:45	14:26:45	00:02:00	2.6	380.7	5296.9	96.7	0.0	1121.4
	2.7	14:38:15	14:39:53	00:01:38	2.6	379.8	5198.4	97.4	0.0	1123.6
	2.8	14:52:46	14:55:00	00:02:14	2.6	379.0	5132.5	97.2	0.0	1124.3
	2.9	15:02:56	15:06:46	00:03:50	2.7	379.8	5221.5	98.0	0.0	1128.5
	2.10	15:22:30	15:25:00	00:02:30	2.5	378.9	5048.5	97.6	0.0	1124.2
	2.11	15:38:05	15:39:35	00:01:30	2.4	377.9	4936.4	96.0	0.0	1120.7
3°	3.1	13:42:37	13:43:43	00:01:06	2.1	374.3	4546.9	89.9	0.0	1071.9
	3.2	14:20:52	14:22:33	00:01:41	2.2	373.4	4599.8	87.1	0.0	1073.6
	3.3	15:00:52	15:03:27	00:02:35	2.3	377.0	4825.8	96.3	0.0	1078.2
	3.4	15:37:27	15:40:29	00:03:02	2.4	375.8	4841.0	92.7	0.0	1078.0
	3.5	15:50:44	15:53:27	00:02:43	2.5	376.2	4921.4	93.2	0.0	1077.6
	3.6	16:05:05	16:06:52	00:01:47	2.6	377.5	5057.9	96.1	0.7	1077.4
	3.7	16:26:55	16:29:18	00:02:23	2.7	376.3	5006.9	93.0	1.5	1071.6
	3.8	16:39:44	16:41:43	00:01:59	2.8	376.6	4986.2	94.3	2.0	1069.3

Table 9: Steady-state selected points in each run

With the data points listed in Table 9, and with chapter 5.2.2, where the way to determine the enthalpy and the entropy downstream and upstream of the turbine is shown in equation (5. 5), it was possible to determine the efficiency of the turbine. In addition, equation (5. 5) details the error propagation of the efficiency calculation. In this work the systematic error was neglected, and I considered the propagation of random error as is can be seen in Figure 22.

The following graph shows the efficiency values with respect to time (day two run 2.3, see Table 9), and the graph also contains the error bars calculated with the previously mentioned error propagation.

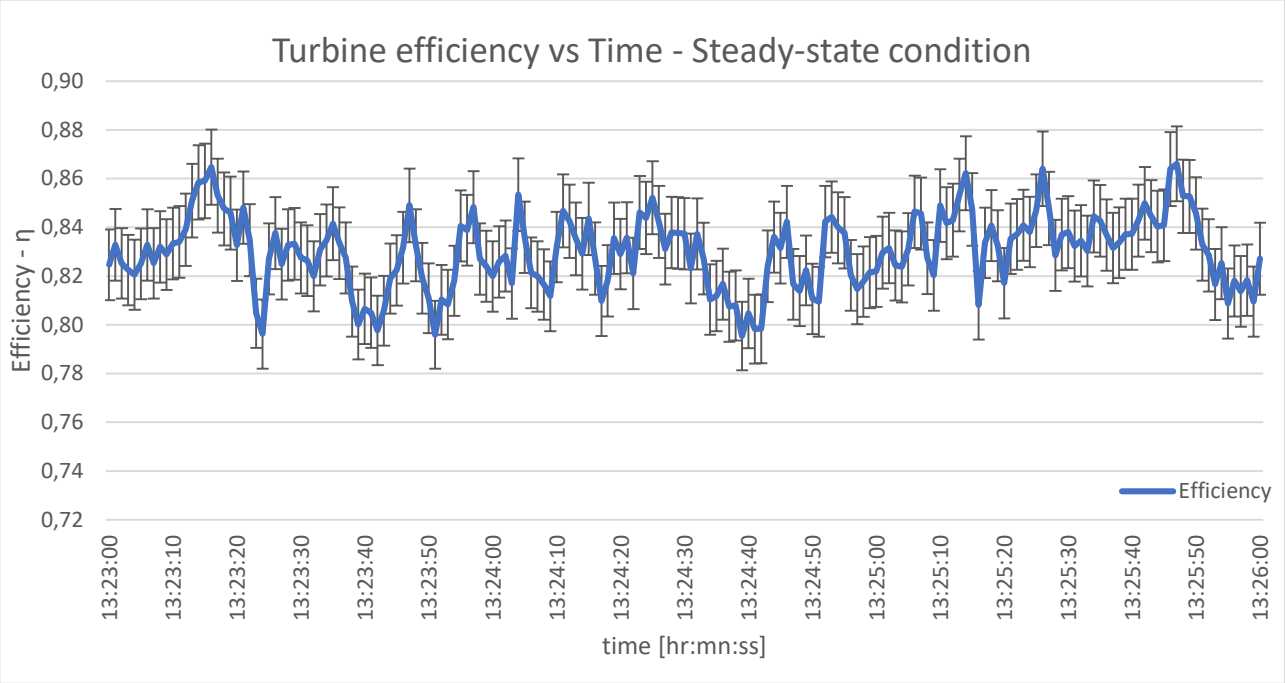

Figure 32: Turbine efficiency vs time in steady state condition - 2° day, run 2.3

In the Figure 32, which is a representative graph of all those that have been made by each run, the efficiency value is between 0.80 and 0.88. Furthermore, it can also be seen that the error bars are in the same magnitude than the scatter, in Appendix chapter 9.2 it is possible to see the Turbine efficiency vs time graph of all the runs.

Efficiency, it is calculated (see equation (5. 5)), is a function of different thermodynamic variables. Once the efficiency was already calculated and plotted (Figure 32), the procedure continued with a plot of the efficiency as a function of mass flow rate for the same run (2° day, run 2.3). As can be seen in the following Figure 33, the efficiency increases for decreasing values of mass flow rate for this measured range, which was not expected.

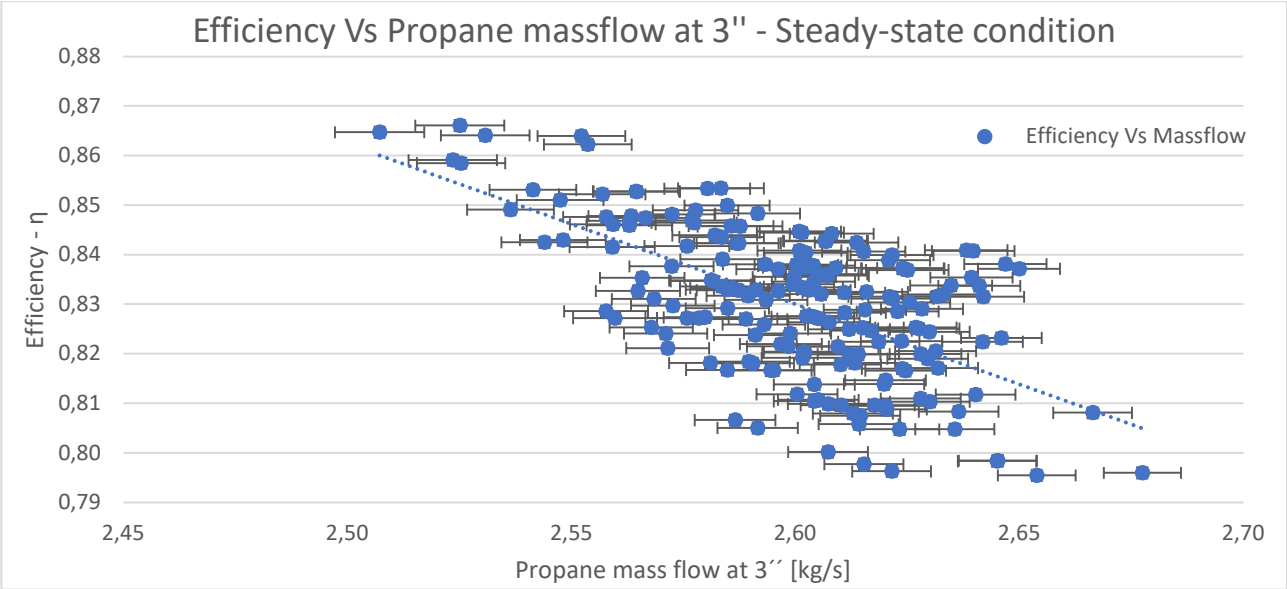

Figure 33: Efficiency vs Mass flow at 3'', in steady state condition - 2° day, run 2.3

The correlation between mass flow rate and efficiency previously mentioned can be seen in Figure 33. On the third experimental day, a turbine mass flow rate sensitivity test was performed, as the turbine mass flow rate was increased by 0.1 kg/s. We proceed to plot the 8 steady state runs of the 3rd day (*chapter 5.1.3*).

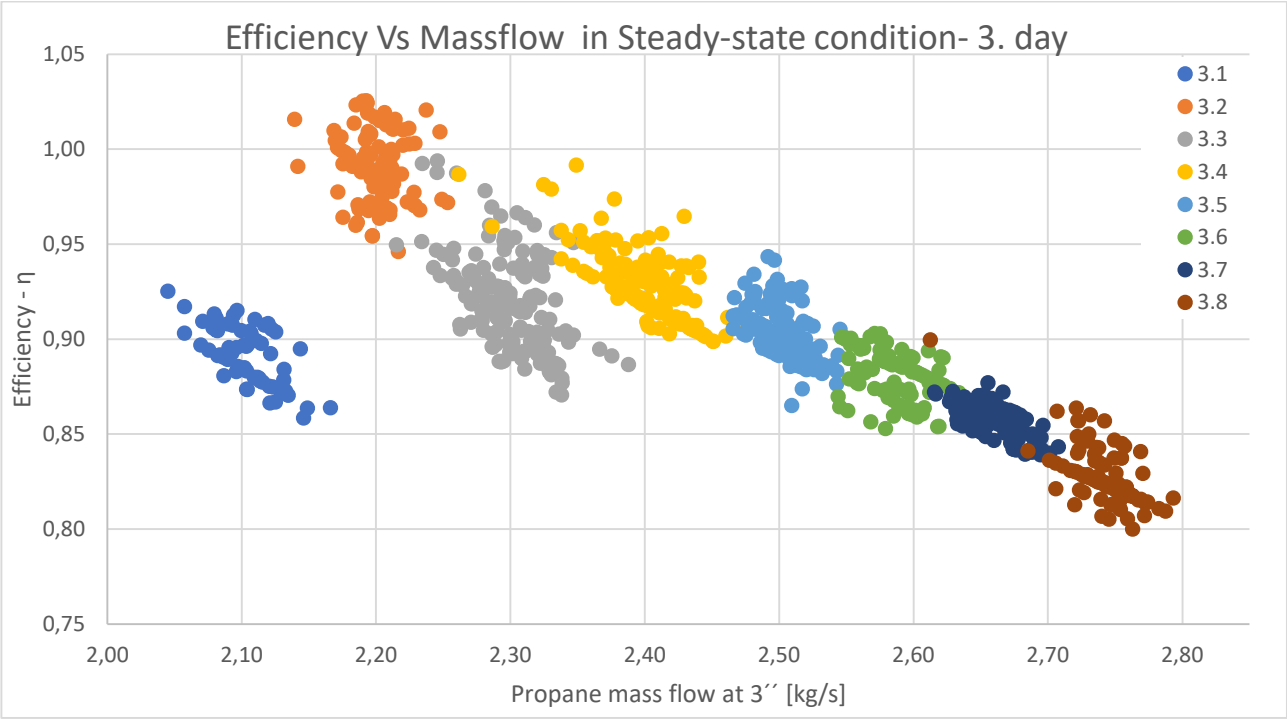

Figure 34: Turbine efficiency vs Mas Flow at 3'', in steady state condition - 3° day all runs

Here can be observed again the previously discussed efficiency increase with decreasing turbine mass flow rates. In particular, run 3.1 has a different behaviour because pressure and temperature at point 3'' are quite close to the critical point, which means a bigger error in the calculation of the enthalpy and entropy with REFPROP (see *chapter 5.2.1).*

Additionally, is important to remark that run 3.2 surpasses the maximum value possible of efficiency, that is greater than 1. The main reason for this behaviour is what was mentioned in section 5.2.1, by having temperature values at point 3'' very close to the critical point, the enthalpy calculation has very high

systematic errors. The range of this error in all day was higher in the points 3.1, 3.2 and 3.3 (2,4%, 3,5% and 5,5% respectively) and in the range of 1,6% for the other runs.

To see another relationship between both parameters, the next graph shows the correlation, again, of the efficiency and the mass flow rate in steady state condition on the second day, in which both the pressure and the temperature at the turbine inlet were changing. Runs 2.1 and 2.2 have a notorious difference with the other runs due to the fact that they are up to 200 kPa different from each other. The systematic error is around 1,4 % for the run 2.3 to 2.8 and 2.10 to 2.11, and this error increase to 2.2% in the run 2.1 and 2.2, and around 3.5% in the run 2.9.

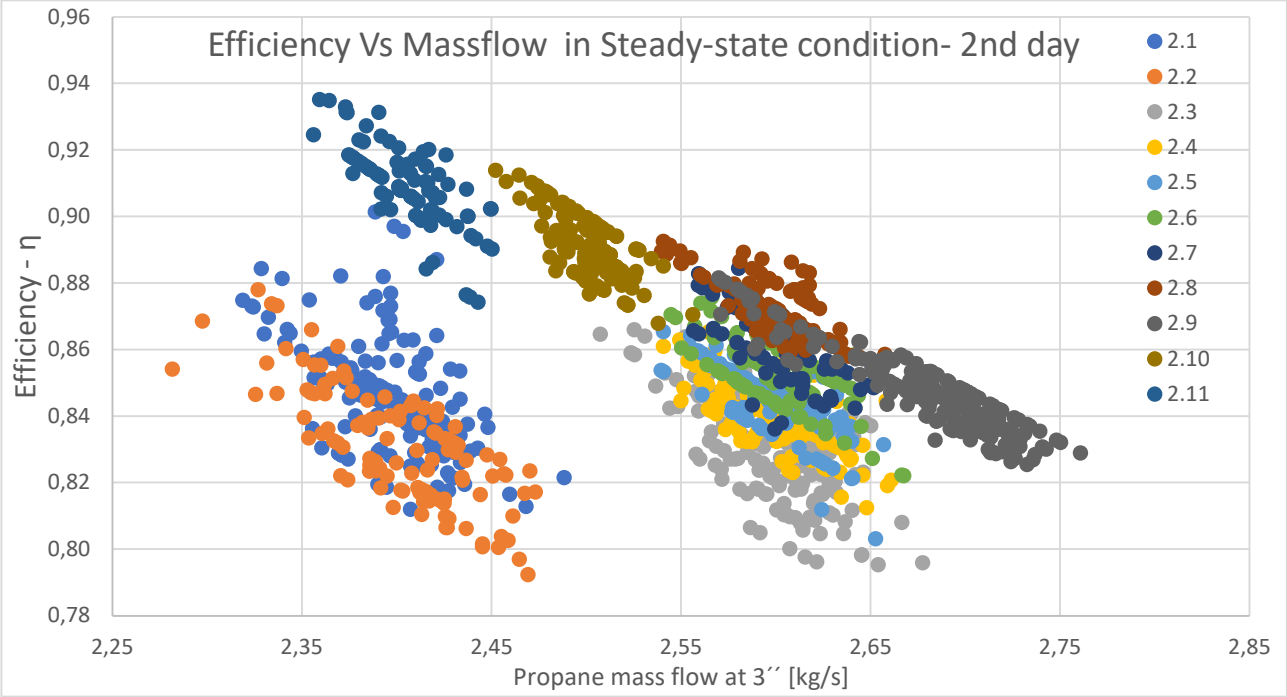

Figure 35: Efficiency vs Mas Flow at 3'', in steady state condition - 2° day all runs

In this last image it can be seen that there is another variable in addition to the mass flow rate. Table 10 shows the mean values of pressure ($p_{3''}$), temperature ($T_{3''}$), turbine mass flow rate ($\dot{m}_T$) and turbine efficiency (η) in each of the 2nd day runs.

	Mass flow [kg/s]	Temperature [K]	Pressure [kPa]	Efficiency
	Turbine	FI10-02 - 3''	PS10-03 - 3''	
2.1 - Steady State	2.4	372.3	4556.6	0.85
2.2 - Steady State	2.4	372.3	4537.0	0.83
2.3 - Steady State	2.6	374.9	4770.8	0.83
2.4 - Steady State	2.6	375.1	4778.6	0.84
2.5 - Steady State	2.6	375.4	4791.4	0.84
2.6 - Steady State	2.6	375.3	4785.8	0.85
2.7 - Steady State	2.6	375.6	4805.3	0.86
2.8 - Steady State	2.6	375.6	4804.2	0.87
2.9 - Steady State	2.7	376.5	4889.8	0.85
2.10 - Steady State	2.5	375.2	4722.2	0.89
2.11 - Steady State	2.4	374.1	4615.8	0.91

Table 10: Steady state run 2° day, values of mass flow, temperature, pressure, and efficiency

From Table 10 and Figure 35 it can be seen that the mass flow trend line moves in a parallel plane to different values of temperature or pressure (indicated in colour scale). At increasing values of pressure and temperature, the trend line moves to the right. Knowing that the measured turbine inlet temperature is systematically too low, the correlation of the turbine efficiency will be as a function of mass flow and turbine inlet pressure instead:

$$\eta_T = f(\dot{m}_T, p_{3''}) \quad (6.\ 1)$$

In the first considerations it was believed that the efficiency increased with increasing mass flow rate but looking at the graphs in this section we can see a behaviour contrary to the assumption. The problem with this is that the increase in mass flow produces a higher liquid content at the outlet of the turbine, which in addition to damaging the turbine, might produce a decrease in efficiency in the parameter range that has been studied.

The following section will calculate the efficiency correction with a multiple regression analysis provided by MATLAB and named in *chapter 4.3.2*

6.1 Turbine efficiency with multi regression analysis

Multiple regression is a statistical technique that can be used to analyse the relationship between a single dependent variable and several independent variables. The objective of multiple regression analysis is to use the independent variables whose values are known to predict the value of the single dependent value. In our case of study, and as it was mentioned in equation (6. 1), the efficiency is the dependent variable and is function of $\dot{m}_T$ and $p_{3''}$.

With Least-Squares Fitting [16] application provided by MATLAB (Curve fitting Toolbox™ software), the multiple correlation was made, where the steady state values of turbine inlet pressure, turbine inlet mass flow and efficiency calculation in the following variables were loaded.

- X data: Turbine inlet mass flow [kg/s]
- Y data: Turbine inlet pressure [kPa]
- Z data: Efficiency (dependent variable)

Inside the toolbox I selected the method Least absolute residuals (LAR) rather than Bisquare method, because the error was small for our fitting of each day, but with the problem of the LAR in comparison with the Bisquare is that extreme values have less influence on the fit.

Multiple regression was performed for all experiment days, of which this master-thesis will present the first two days, since the third day, due to fluctuations with the heat exchanger, obtained a worse FIT. All multiple regression has confidence limits, provided by the software, of 95 %.

6.1.1 Fitting first day

With the data of pressure, mass flow rate and the calculated efficiency of the second day, we proceeded to perform the fitting with curve fitting Toolbox™ software, in which the best results were obtained by the linear multiple regression. Figure 36 illustrate for a Polynomial selection LAR with degree 1 in mass flow and 1 in pressure, where R^2 is 0.9930 and $RMSE$ = 0.0047 [17], both provided by the fitting Toolbox an explained in *chapter 4.3.2*. In the software output R-squared means R^2.

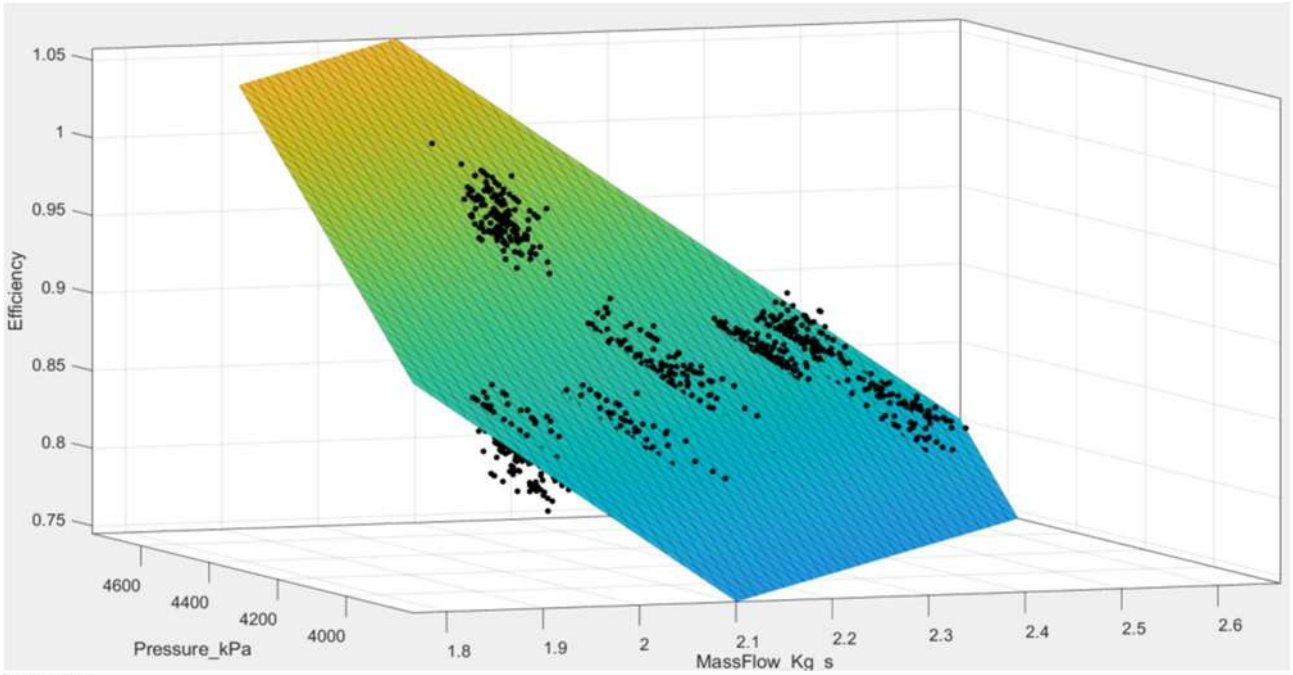

Table of Fits

Fit name	Data	Fit type	SSE	R-square	DFE	Adj R-sq	RMSE
untitled fit 2	Efficiency vs. MassFlow_...	poly11	0.0243	0.9930	1121	0.9930	0.0047

Figure 36: Polynomial with mass flow = 1 degree and pressure = 1, LAR selection – 1st day

6.1.2 Fitting second day

With the same procedure of the first day but in this case best results were obtained for two different types of fitting (the others were discarded):

- linear multiple regression (grade 1 in mass flow and grade in pressure).
- multiple regression (grade 2 in mass flow and grade 1 in pressure)

Figure 37 illustrate for a Polynomial selection LAR with degree 1 in mass flow and 1 in pressure, where R^2 is 0.5756 and $RMSE$ is 0.168. This is not a reasonable fit, but with a linear function there is no better fit, in case of higher degree, has less error buy must be in the range of the data, otherwise the error would grow much larger.

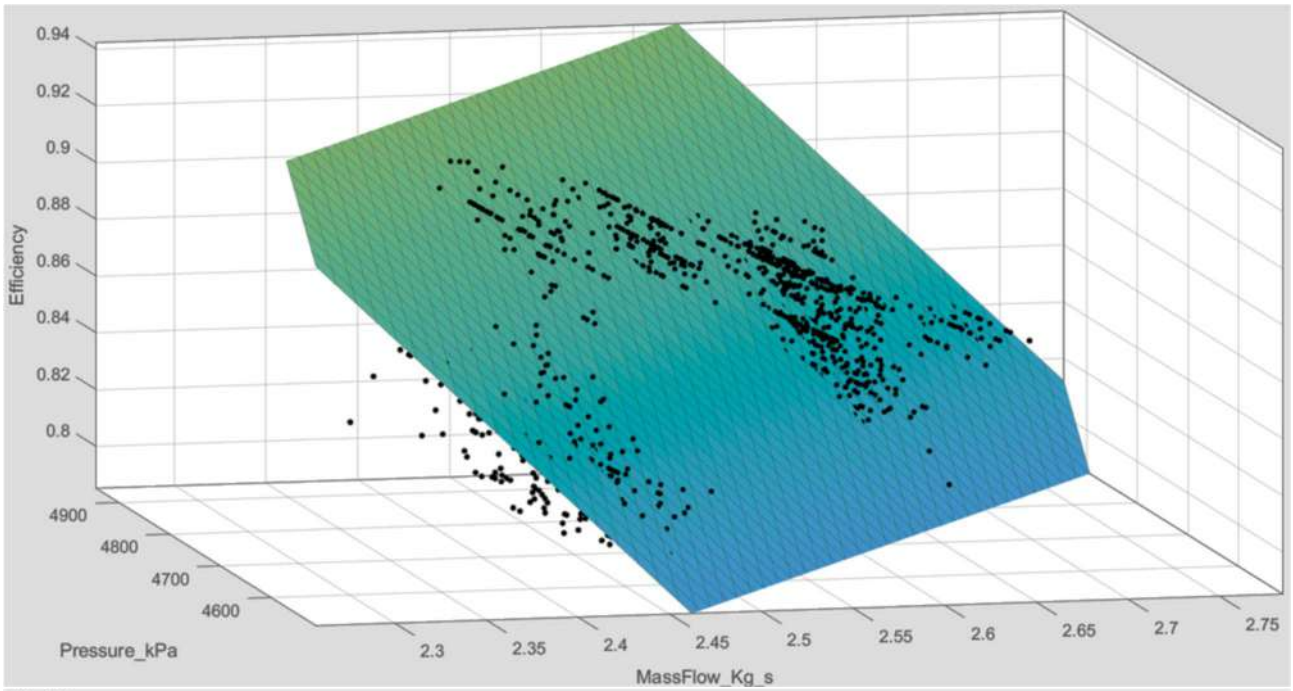

Table of Fits

Fit name	Data	Fit type	SSE	R-square	DFE	Adj R-sq	RMSE	# Coeff
untitled fit 1	Efficiency vs. MassFlow_...	poly11	0.4259	0.5756	1509	0.5750	0.0168	3

Figure 37: Polynomial with mass flow = 1 degree and pressure = 1, LAR selection - 2nd day

Figure 38 illustrate for a Polynomial selection LAR with degree 2 in mass flow and 1 in pressure a very good fit, where R^2 is 0.9899 and $RMSE$ = 0.026. [17]

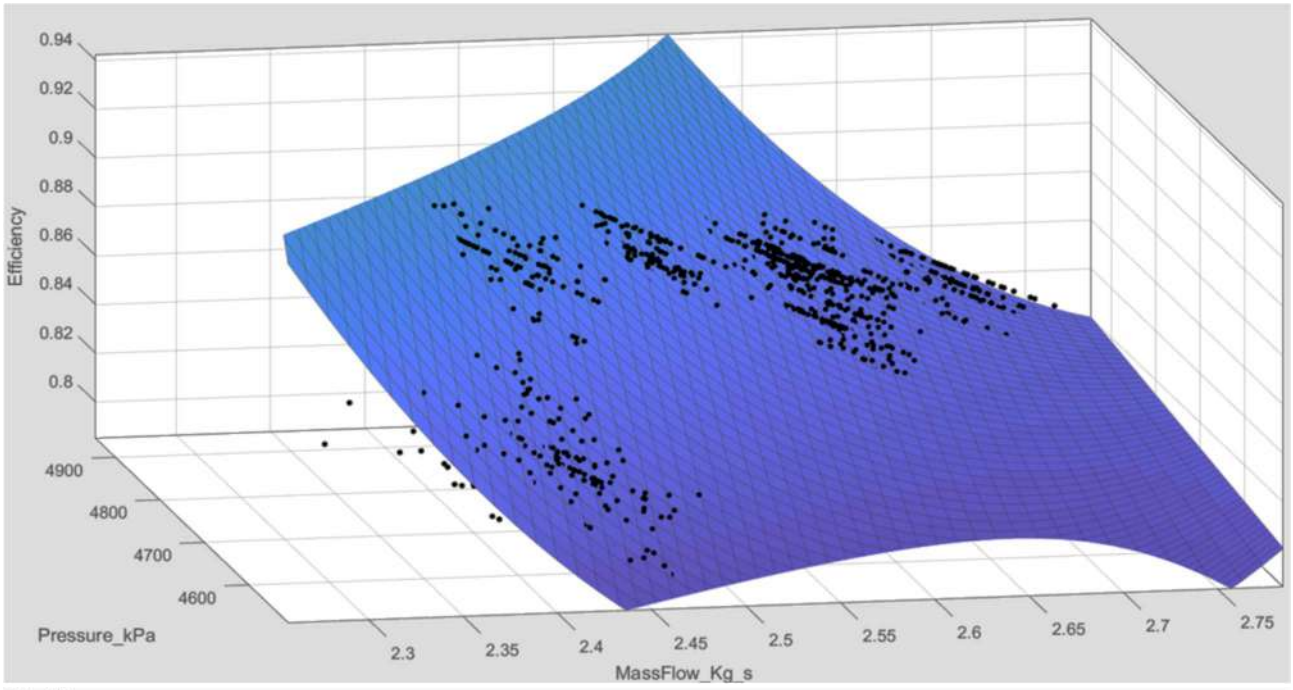

Table of Fits

Fit name	Data	Fit type	SSE	R-square	DFE	Adj R-sq	RMSE	# Coeff
untitled fit 1	Efficiency vs. MassFlow_...	poly21	0.0101	0.9899	1507	0.9899	0.0026	5

Figure 38: Polynomial with mass flow = 2 degree and pressure = 1, LAR selection - 2nd day

In this case, the problem with the fit is outside the data range, where the error is bigger than when it is a linear multiple regression.

6.1.3 Selection of the corrected formula

Considering the fitting of the first 2 days and having discarded the 3rd day for having values very close to the critical temperature of the working fluid, the efficiency correction formula was calculated with the software. The selection of the efficiency correction was based on having an R^2 quite similar to 1 (see *chapter 4.3.2)* since it presents less errors, and to look for a linear equation of two variables, so as not to present so much error in the extreme values measured. The following equation was taken from the section *6.1.1 – First day fitting*, which was the one selected due to the criteria previously mentioned:

$$\eta_c = 0.4412 - 0.4399 \cdot \dot{m}_T + 0.0003229 \cdot p_{3''} \quad (6.\ 2)$$

The equation ins within the next limits of application:

- Mass flow: 2.10 < $\dot{m}_T$ < 2.6 [kg/s]
- Pressure: 3860 < $p_{3''}$ < 4640 [kPa]
- Temperature: 363.5 < $T_{3''}$ < 374 [k]

The software also brings two planes to have the 95% of confidence bounds:

$$\eta_{c,lower\ limit} = 0.4338 - 0.4457 \cdot \dot{m}_T + 0.0003184 \cdot p_{3''} \quad (6.\ 3)$$

$$\eta_{c,upper\ limit} = 0.4486 - 0.4342 \cdot \dot{m}_T + 0.0003275 \cdot p_{3''} \quad (6.\ 4)$$

Where the values 3'' refer to the turbine inlet as shown in Figure 16, and in addition, the following table details the unit of each of the variables or constants:

Correction plane	Upper limit	Lower limit	Type	Unit
0.4412	0.4338	0.4486	Constant	-
-0.4399	-0.4457	-0.4342	Constant	s/Kg
$\dot{m}_T$	$\dot{m}_T$	$\dot{m}_T$	Variable	Kg/s
0.0003229	0.0003184	0.0003275	Constant	1/kPa
$p_{3''}$	$p_{3''}$	$p_{3''}$	Variable	kPa

Table 11: Variables and constants of the corrected efficiency

6.2 Stodola´s law correction

The aim of this section is correct the Stodola's law due to the real behaviour of the turbine compared with the ideal Stodola's equation (3. 6) presented in *chapter 3.1.2*. Also, in this section the subscripts will be adjusted according to Figure 16, so equation (3. 6) will be rewritten as:

$$\left(\frac{\dot{m}_T}{\dot{m}_0}\right)^2 = \frac{p_{3''}^2 - p_4^2}{p_{3'',0}^2 - p_{4,0}^2} \frac{T_{3'',0}}{T_{3''}} \quad (6.\ 5)$$

In Equation (3. 6), index $3''$ designates the state before the turbine, index 4 the state after the turbine. In addition, variables indexed with a 0 indicate the design status. The turbine design data is detailed below according to the data sheet provided by the turbine manufacturer [7]:

- $\dot{m}_0$ = 2.9 kg/s
- $p_{3'',0}$= 5500 kPa
- $p_{4,0}$ = 1080 kPa
- $T_{3'',0}$ = 117 °C

The mass flow rate of the turbine can be written, by solving Equation (6. 5), as:

$$\dot{m}_T{}^2 = \frac{m_0^2 \cdot T_{3'',0}}{p_{3'',0}^2 - p_{4,0}^2} \cdot \frac{p_{3''}^2 - p_4^2}{T_{3''}} \tag{6. 6}$$

The first term, being design parameters, can be taken as a constant:

$$\frac{m_0^2 \cdot T_{3'',0}}{p_{3'',0}^2 - p_{4,0}^2} = F \tag{6. 7}$$

So, the equation (6. 6) can be written as:

$$\dot{m}_T{}^2 = F \cdot \frac{p_{3''}^2 - p_4^2}{T_{3''}} \tag{6. 8}$$

Solving the square of the mass flow rate, equation (6. 8) is:

$$\dot{m}_T = \sqrt{F} \cdot \sqrt{\frac{p_{3''}^2 - p_4^2}{T_{3''}}} \tag{6. 9}$$

Considering that equation (6. 9) can be written as a linear equation as $y = ax + b$, where $\dot{m}_{3,,} = y$, $\sqrt{F} = a$ (where the square roots of the constants as $\sqrt{\mathrm{F}}$ = 0.010622 $\left[\frac{Kg \cdot K^{1/2}}{s \cdot kPa}\right]$) and $\sqrt{\frac{p_{3''}^2 - p_4^2}{T_{3''}}} = x$, and b is a constant when pressure difference is equal to 0. Figure 39 shows the differences between both equations (the ideal Stodola's law and the corrected Stodola's law).

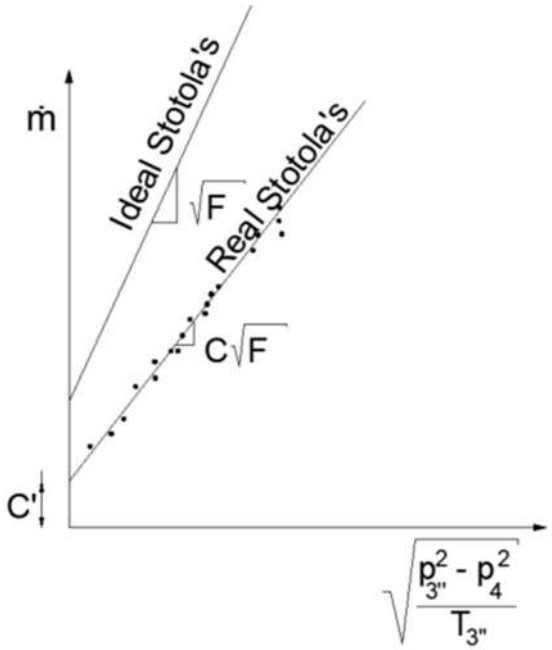

Figure 39: Differences between ideal Stodola's law and Corrected Stodola´s law

As it is shown in Figure 39, the ideal equation of Stodola's law passes through the origin, which means that the term b is equal to cero 0. The real equation of Stodola's law is given by the mean value of mass flow through the turbine in each day and the value of each point of the equation (6. 9) corrected by a factor C and displaced by a factor C' as is written in the next equation:

$$\dot{m}_T = C * \sqrt{F} \cdot \sqrt{\frac{p_{3''}^2 - p_4^2}{T_{3''}}} + C' \quad (6.\ 10)$$

Table 12 shows the mean value of each point in the graph as is marked in Figure 40 for the real values of Stodola's law.

Run	$\dot{m}_{3''}$	$\sqrt{F} \cdot \sqrt{\frac{p_{3''}^2 - p_4^2}{T_{3''}}}$
1.1	2.1	2.2
1.2	2.6	2.5
1.3	2.4	2.4
1.4	2.2	2.3
1.5	1.9	2.1
1.6	1.9	2.1
1.7	2.5	2.5
2.1	2.4	2.4
2.2	2.4	2.4
2.3	2.6	2.5
2.4	2.6	2.6
2.5	2.6	2.6
2.6	2.6	2.6
2.7	2.6	2.6
2.8	2.6	2.6
2.9	2.7	2.6
2.10	2.5	2.5
2.11	2.4	2.5
3.1	2.1	2.3
3.2	2.2	2.3
3.3	2.3	2.4
3.4	2.4	2.4
3.5	2.5	2.5
3.6	2.6	2.5
3.7	2.7	2.5
3.8	2.7	2.5

Table 12: Real values of Stodola's equation

Figure 40 shows the trend line of the real values of Stodola's law, and the trend equation that is $y = ax + b$ and is equal to (6. 10).

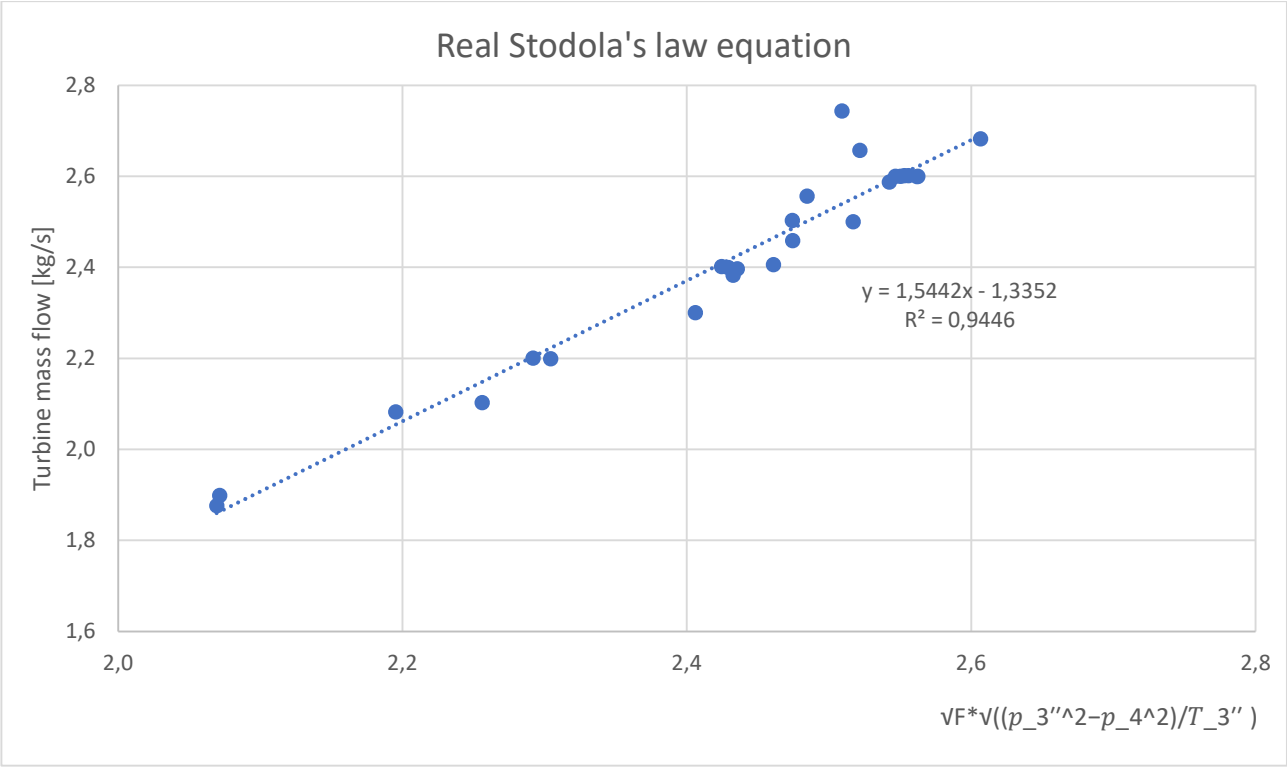

Figure 40: Trend line of real values of Stodola's equation

By equating the trend line equation of the Figure 40 and equation (6. 10), the variables C and C' can be solved, which results:

- C = 1.5442
- C' = -1.3352 kg/s

So, with the value of the constants C and C' and the equation (6. 10), it is possible to write the corrected Stodola's law equation as:

$$\underbrace{\dot{m}_T}_{y} = \underbrace{1{,}5442}_{C} * \underbrace{\sqrt{F} \cdot \sqrt{\frac{p_{3''}^2 - p_4^2}{T_{3''}}}}_{x} \underbrace{- 1{,}3352\ kg/s}_{C'} \tag{6. 11}$$

With the next range for mass flow, pressure, and temperature at the turbine inlet:

- Mass flow: 1.88 < $\dot{m}_T$ < 2.74 [kg/s]
- Pressure: 3860 < $p_{3''}$ < 4900 [kPa]
- Temperature 363.5 < $T_{3''}$ < 376.5 [K]

In addition, it is possible to write equation (6. 11) as it was presented in the original equation of Stodola's but corrected with the coefficient:

$$\left(\frac{\dot{m}_T + C'}{\dot{m}_0}\right)^2 = \frac{p_{3''}^2 - p_4^2}{p_{3'',0}^2 - p_{4,0}^2} \frac{T_{3'',0}}{T_{3''}} \cdot (C^2) \tag{6. 12}$$

And replacing the variables already known C and C', the equation (6. 12) is:

$$\left(\frac{\dot{m}_T + 1.3352kg/s}{\dot{m}_0}\right)^2 = \frac{p_{3''}^2 - p_4^2}{p_{3'',0}^2 - p_{4,0}^2} \frac{T_{3'',0}}{T_{3''}} \cdot (1.5442^2) \quad (6.\ 13)$$

Both the corrected Stodola equation and the equation of the real efficiency of the turbine, serve to model the behaviour of the same within the conditions presented by the MoNiKa power plant in certain conditions with the environment.

7 Conclusions

This research aimed to understand the behaviour of the propane turbine placed in the MoNiKa power plant. To reach the understanding of such behaviour, the work was divided in different processes, as the simulation, the runs, and the data analysis with its results.

The GESI software was a great tool to analyse the ORCs cycle of the MoNiKa power plant in steady state condition. It helped to provide the load points and take precautions to prevent the liquid content to be higher than 20% at the turbine outlet. However, certain values, such as turbine efficiency, has to be set as input. In the case of the runs, although it is the field of experimentation in the plant, we have had problems to reach certain desired values at the outlet of the boiler, this is due to a failure within the control system of the heating station.

The analysis of the data was possible thanks to the measurement of different thermodynamic variables, with which the values of the state functions corresponding to the enthalpy and entropy between the turbine inlet and outlet have been found. The results were in line with expectations, although in the middle of the process the theory had to be adapted, due to large errors in the calculation of these state functions in the vicinity of the critical point using the software. In addition, the process and results indicate that turbine efficiency and Stodola's law have certain limits in their applications.

The turbine inlet values (3'') were very close to the critical point, due to the failure of the boiler in operation, that when calculating the state functions, the REFPROP software has very large errors and this causes two considerable problems at the time of calculation in some of the cases. Firstly, it is almost impossible to measure the enthalpy at turbine inlet precisely under these conditions, secondly the entropy in timeframe we have obtained an entropy at the inlet of the turbine, which is smaller than at the inlet of the turbine control valve, and according to the second principle this is impossible, the entropy can only increase in the valve, but never decrease. To avoid these calculations with too large errors, the thermodynamically independent properties were measured in places of the plant where they were not close to the critical point, i.e., after the boiler where the calculation error of REFPROP is considerably lower, in order to know the enthalpy and entropy values accurately. Then, by means of heat losses in the pipes it was possible to find the state function of h and then, with the enthalpy and the pressure measured at the inlet of the turbine was possible to calculate the entropy.

A first hypothesis was that increasing the mass flow rate would increase the efficiency. But from the results it has been seen that increasing the mass flow rate decreases the efficiency of the turbine, for certain values of the inlet pressure. This assumption might be due to increased liquid formation at the turbine outlet. In addition, for the turbine efficiency and the Stodola’s law corrections, it is important to operate the formulated equation within the established limits. This means that any point taken outside these limits could cause very large errors.

The turbine performance can be improved by enhancing the turbine inlet conditions. That is, by improving the properties of the fluid at the boiler outlet, either by changing the heat station, which is an expensive solution, by trying to improve the boiler control system or by increasing the heat exchanger efficiency. This would allow to have a pseudo vapour condition with safety margins (because it will be safely located to the right of the peak in the T-s diagram), and it in turn would be further away from the critical point.

8 References

[1] Stanley M. Geothermal energy as a source of electric power thermodynamic and economic design criteria. 1st ed.: The MIT Press; 1976. ISBN: 0-262-13123-4.

[2] Vetter C. Comparison of sub- and supercritical Organic Rankine Cycles for power generation from low-temperature/low-enthalpy geothermal wells, considering specific net power output and efficiency. ELSEVIER 2013;51(1-2):872–873. DOI: 10.1016/j.applthermaleng.2012.10.042.

[3] Gao H. Performance Analysis and Working Fluid Selection of a Supercritical Organic Rankine Cycle for Low Grade Waste Heat Recovery. Energies 2012;5(9):3236–3237. DOI: 10.3390/en5093233.

[4] Luciano J. Gardella. Analysis and evaluation of MoNiKa's first results in baypass configuration. Master Thesis. Karlsruhe Institut für Technologie, Karlsruhe; 2019.

[5] Vetter C. Thermodynamische Auslegung und transiente Simulation eines überkritischen Organic Rankine Cycles für einen leistungsoptimierten Betrieb. Zugl.: Karlsruhe, KIT, Diss., 2014. Karlsruhe: KIT Scientific Publishing; 2014. DOI: 10.5445/KSP/1000041450.

[6] Dr. Kuhn D. Modular Low Temperature Cycle Karlsruhe (MoNiKa). [March 17, 2021]; Available from: https://www.monika.kit.edu/english/.

[7] M+M TURBINE-TECHNIK. Turbinenanlage Propanexpander: Project 1 15 3514 0 2018.

[8] Adrian Bejan. Advanced Engineering Thermodynamics. 3rd ed.: Wiley; 2006. ISBN: 978-0-471-67763-5.

[9] Strauß K. Kraftwerkstechnik: zur Nutzung fossiler, regenerativer und nucklearer Energiequellen. 4th ed.: Springer; 1998. ISBN: 3-540-64750-3.

[10] Korpela SA. Principles of Turbomachinery. 2nd ed.: Wiley; 2020. ISBN: 978-1119518112.

[11] ITES - Institute for Thermal Energy Technology and Safety. GESI - Geothermal Simulation. [March 15, 2018]; Available from: https://www.ites.kit.edu/index.php.

[12] NIST - National Institute of Standards and Technology. REFPROP - Reference Fluid Thermodynamic and Transport Properties Database. [March 15, 2018]; Available from: https://www.nist.gov/.

[13] Beitz W (ed.). Dubbel - Taschenbuch für den Maschinenbau. 19th ed.: Springer; 1997. ISBN: 3-540-62467-8.

[14] NIST. REFPROP 23, 9th Edition. [March 15, 2022]; Available from: https://pages.nist.gov/REFPROP-docs/.

[15] Suman A (ed.). Uncertainty quantification of performance parameter in a small scale ORC test RIG; International Seminar on ORC Power Systems. Athens, Greece. 2019.

[16] MATLAB®. Least-Squares Fitting, R2021a. [March 17, 2021]; Available from: https://de.mathworks.com/help/curvefit/least-squares-fitting.html.

[17] MATLAB®. modelAccuracy: Compute R-square, RMSE, correlation, and sample mean error of predicted and observed LGDs, R2021a. [March 25, 2022]; Available from: https://de.mathworks.com/help/risk/regression.modelaccuracy.html?s_tid=doc_ta.

[18] Karlsruhe Institut für Technologie. Satzung zur Sicherung guter wissenschaftlicher Praxis am 228 Karlsruher Institut für Technologie. [October 05, 2021].

[19] Kehlhofer R. Combined-cycle gas & steam turbine power plants. 3rd ed. Tulsa Oklahoma: PennWell; 2009. ISBN: 978-1-59370-168-0.

[20] MarelliMotori. Phase Synchronous Generator: MJB 250 MA 4. 2015.(References number: 520804-05).

[21] Kreith K. Principle of heat transfer. 7th ed.: CENGAGE Learning; 2011. ISBN: 978-0-495-66770-4.

9 Appendix

This chapter will show the relative information that was not include in the previous section.

9.1 Turbine inlet – piping documents

The following document is the piping system between the boiler and the turbine inlet, provided by Rotan GmbH (see Figure 5):

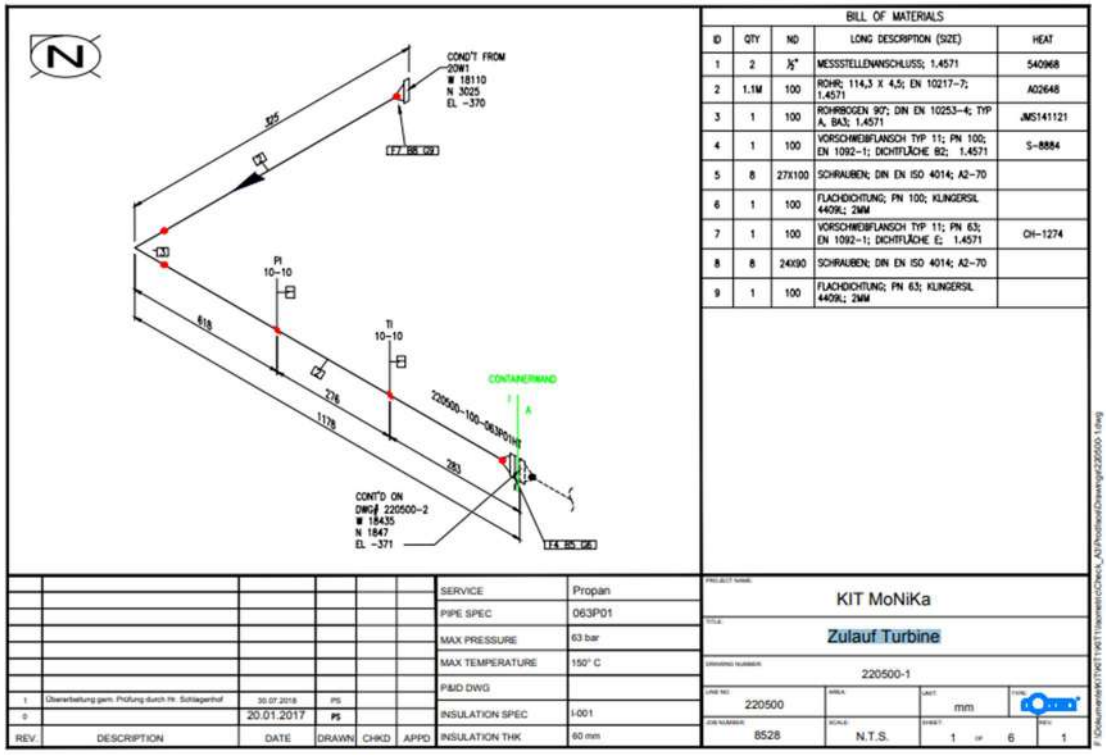

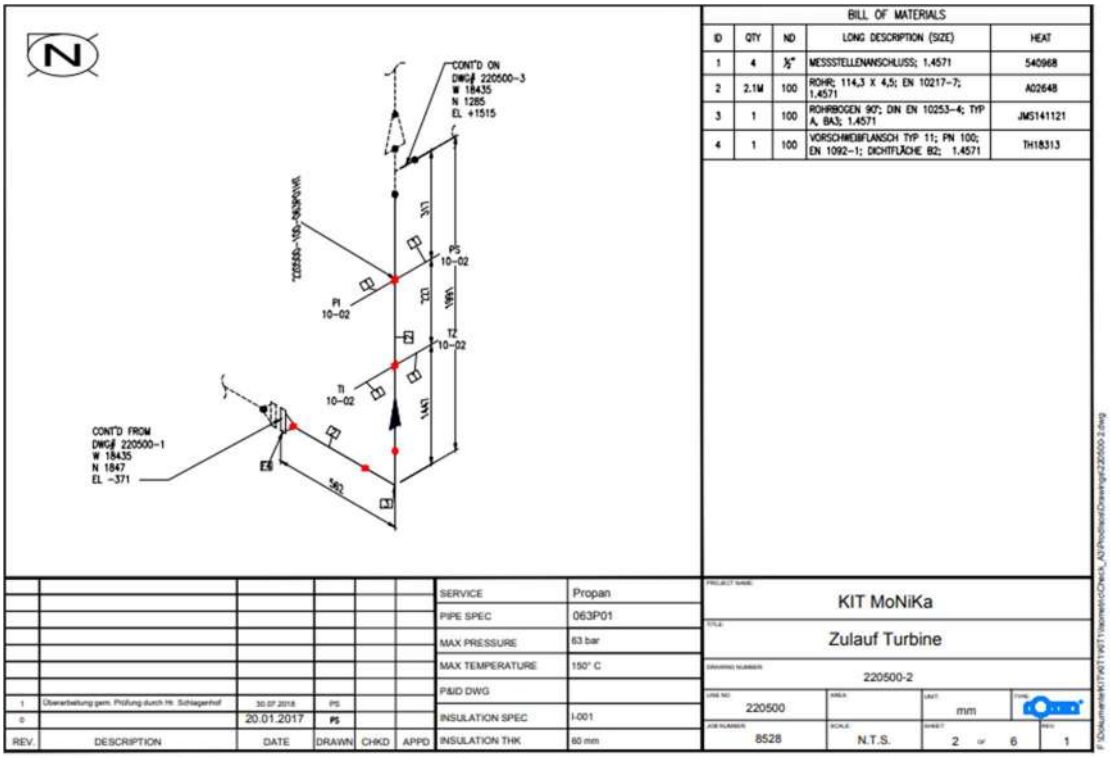

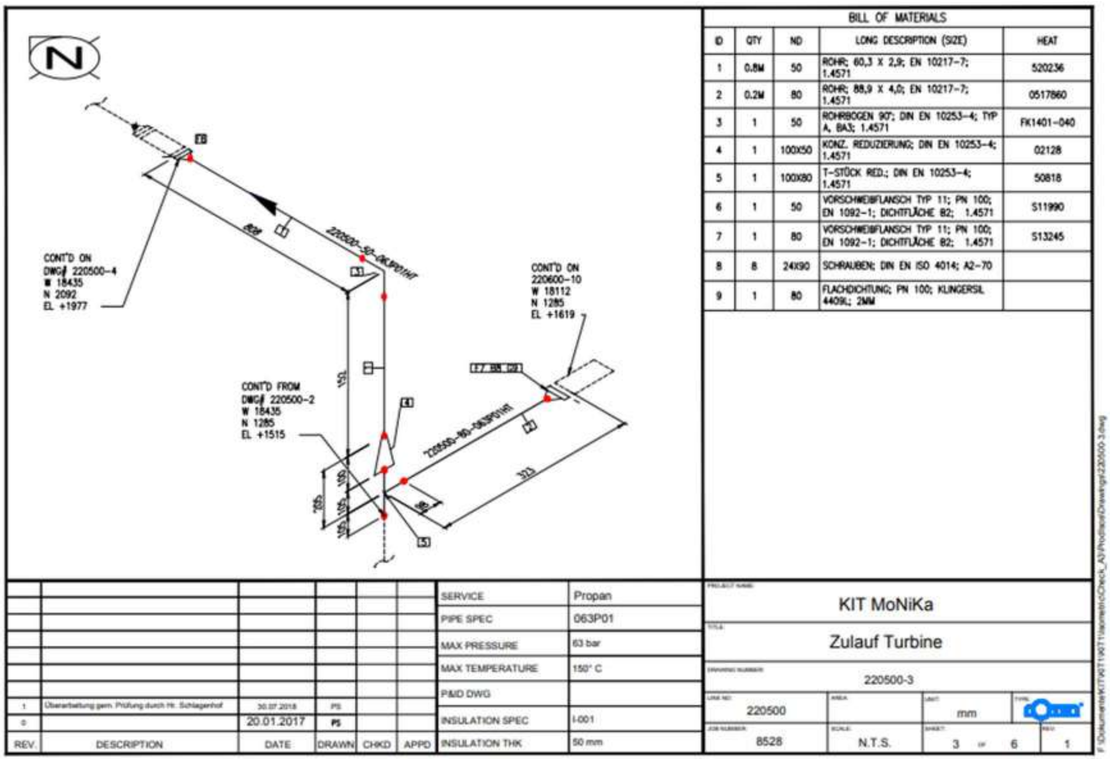
BILL OF MATERIALS
ID | QTY | ND | LONG DESCRIPTION (SIZE) | HEAT
1 | 0.8M | 50 | ROHR; 60,3 X 2,9; EN 10217-7; 1.4571 | 520236
2 | 0.2M | 80 | ROHR; 88,9 X 4,0; EN 10217-7; 1.4571 | 0517860
3 | 1 | 50 | ROHRBOGEN 90°; DIN EN 10253-4; TYP A, BA3; 1.4571 | FK1401-040
4 | 1 | 100X50 | KONZ. REDUZIERUNG; DIN EN 10253-4; 1.4571 | 02128
5 | 1 | 100X80 | T-STÜCK RED.; DIN EN 10253-4; 1.4571 | 50818
6 | 1 | 50 | VORSCHWEIßFLANSCH TYP 11; PN 100; EN 1092-1; DICHTFLÄCHE B2; 1.4571 | S11990
7 | 1 | 80 | VORSCHWEIßFLANSCH TYP 11; PN 100; EN 1092-1; DICHTFLÄCHE B2; 1.4571 | S13245
8 | 8 | 24X90 | SCHRAUBEN; DIN EN ISO 4014; A2-70
9 | 1 | 80 | FLACHDICHTUNG; PN 100; KLINGERSIL 4409L; 2MM
CONT'D ON DWG# 220500-4 W 18435 N 2092 EL +1977
CONT'D ON 220600-10 W 18112 N 1285 EL +1619
CONT'D FROM DWG# 220500-2 W 18435 N 1285 EL +1515
220500-50-063P01HT
220500-80-063P01HT
SERVICE Propan
PIPE SPEC 063P01
MAX PRESSURE 63 bar
MAX TEMPERATURE 150° C
P&ID DWG
INSULATION SPEC I-001
INSULATION THK 50 mm
1 Überarbeitung gem. Prüfung durch Hr. Schlagenhof 30.07.2018 PS
0 20.01.2017 PS
REV. DESCRIPTION DATE DRAWN CHKD APPD
KIT MoNiKa
Zulauf Turbine
220500-3
220500 mm
8528 N.T.S. 3 of 6 1

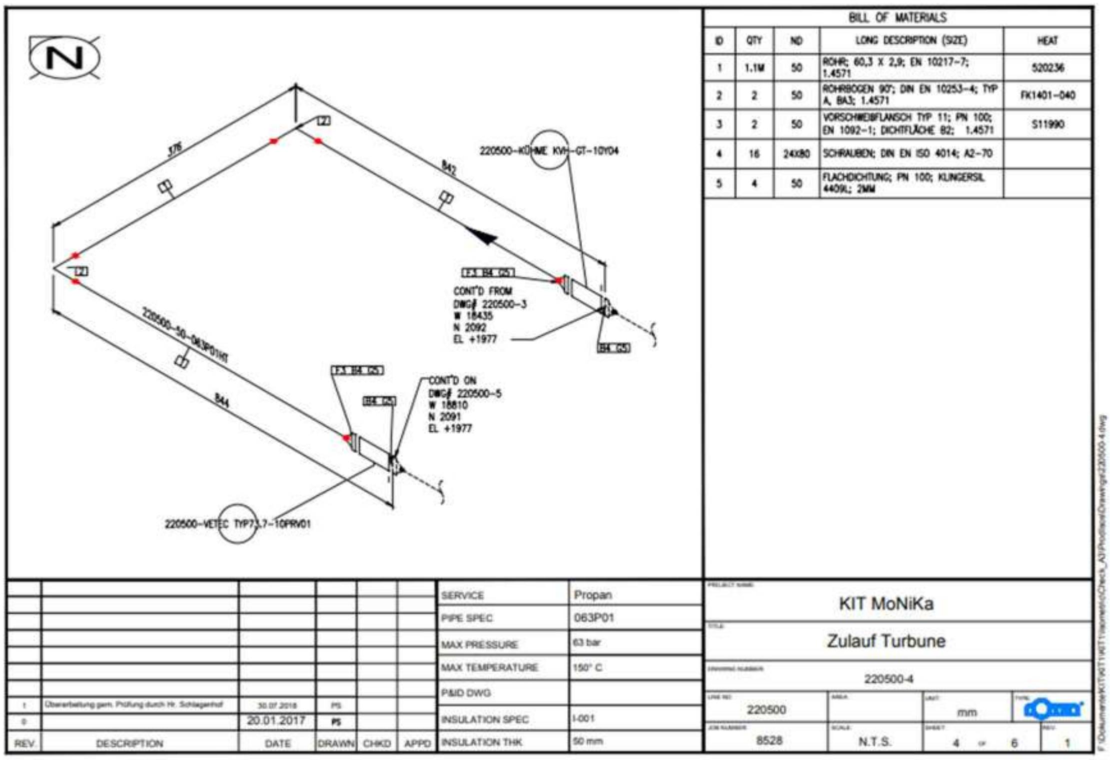
BILL OF MATERIALS
ID | QTY | ND | LONG DESCRIPTION (SIZE) | HEAT
1 | 1.1M | 50 | ROHR; 60,3 X 2,9; EN 10217-7; 1.4571 | 520236
2 | 2 | 50 | ROHRBOGEN 90°; DIN EN 10253-4; TYP A, BA3; 1.4571 | FK1401-040
3 | 2 | 50 | VORSCHWEIßFLANSCH TYP 11; PN 100; EN 1092-1; DICHTFLÄCHE B2; 1.4571 | S11990
4 | 16 | 24X80 | SCHRAUBEN; DIN EN ISO 4014; A2-70
5 | 4 | 50 | FLACHDICHTUNG; PN 100; KLINGERSIL 4409L; 2MM
220500-KÜHME KVH-GT-10Y04
CONT'D FROM DWG# 220500-3 W 18435 N 2092 EL +1977
CONT'D ON DWG# 220500-5 W 18810 N 2091 EL +1977
220500-50-063P01HT
220500-VETEC TYP73.7-10PRV01
SERVICE Propan
PIPE SPEC 063P01
MAX PRESSURE 63 bar
MAX TEMPERATURE 150° C
P&ID DWG
INSULATION SPEC I-001
INSULATION THK 50 mm
1 Überarbeitung gem. Prüfung durch Hr. Schlagenhof 30.07.2018 PS
0 20.01.2017 PS
REV. DESCRIPTION DATE DRAWN CHKD APPD
KIT MoNiKa
Zulauf Turbune
220500-4
220500 mm
8528 N.T.S. 4 of 6 1

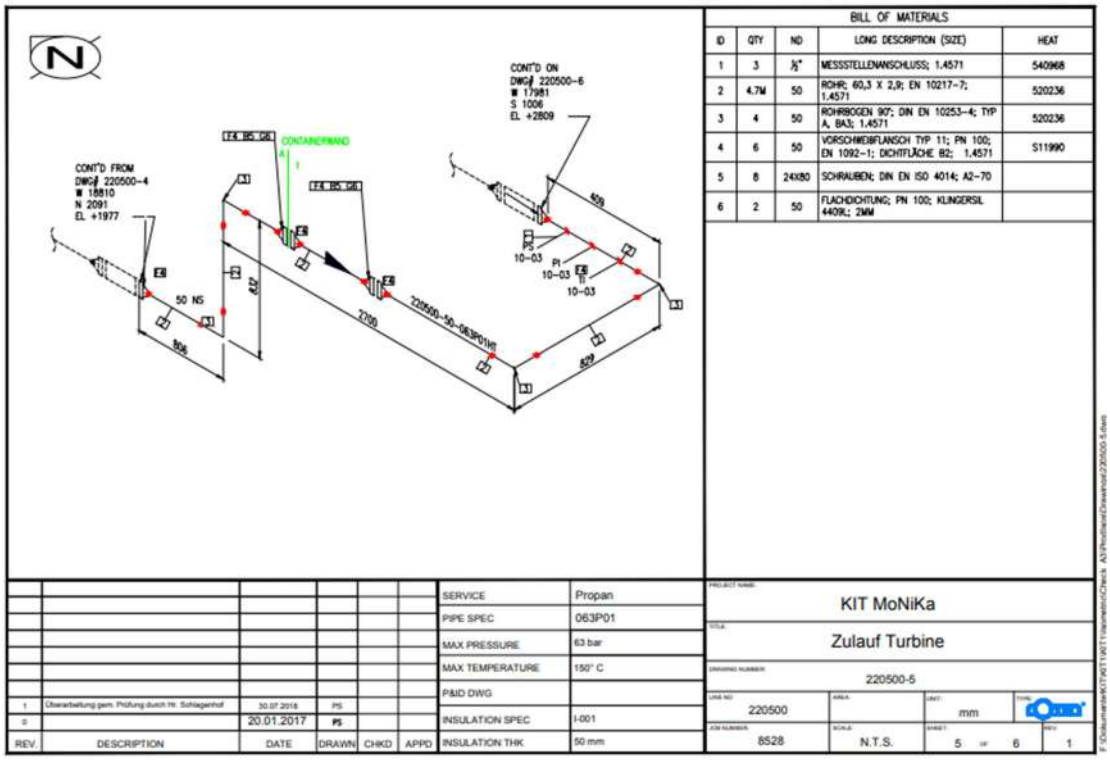

BILL OF MATERIALS				
ID	QTY	ND	LONG DESCRIPTION (SIZE)	HEAT
1	3	½"	MESSSTELLENANSCHLUSS; 1.4571	540968
2	4.7M	50	ROHR; 60,3 X 2,9; EN 10217-7; 1.4571	520236
3	4	50	ROHRBOGEN 90°; DIN EN 10253-4; TYP A, BA3; 1.4571	520236
4	6	50	VORSCHWEIßFLANSCH TYP 11; PN 100; EN 1092-1; DICHTFLÄCHE B2; 1.4571	S11990
5	8	24X80	SCHRAUBEN; DIN EN ISO 4014; A2-70	
6	2	50	FLACHDICHTUNG; PN 100; KLINGERSIL 4409L; 2MM	

REV.	DESCRIPTION	DATE	DRAWN	CHKD	APPD
1	Überarbeitung gem. Prüfung durch Hr. Schlagenhof	30.07.2018	PS		
0		20.01.2017	PS		

SERVICE	Propan
PIPE SPEC	063P01
MAX PRESSURE	63 bar
MAX TEMPERATURE	150° C
P&ID DWG	
INSULATION SPEC	I-001
INSULATION THK	50 mm

KIT MoNiKa

Zulauf Turbine

220500-5

220500 | mm

8528 | N.T.S. | 5 OF 6 | 1

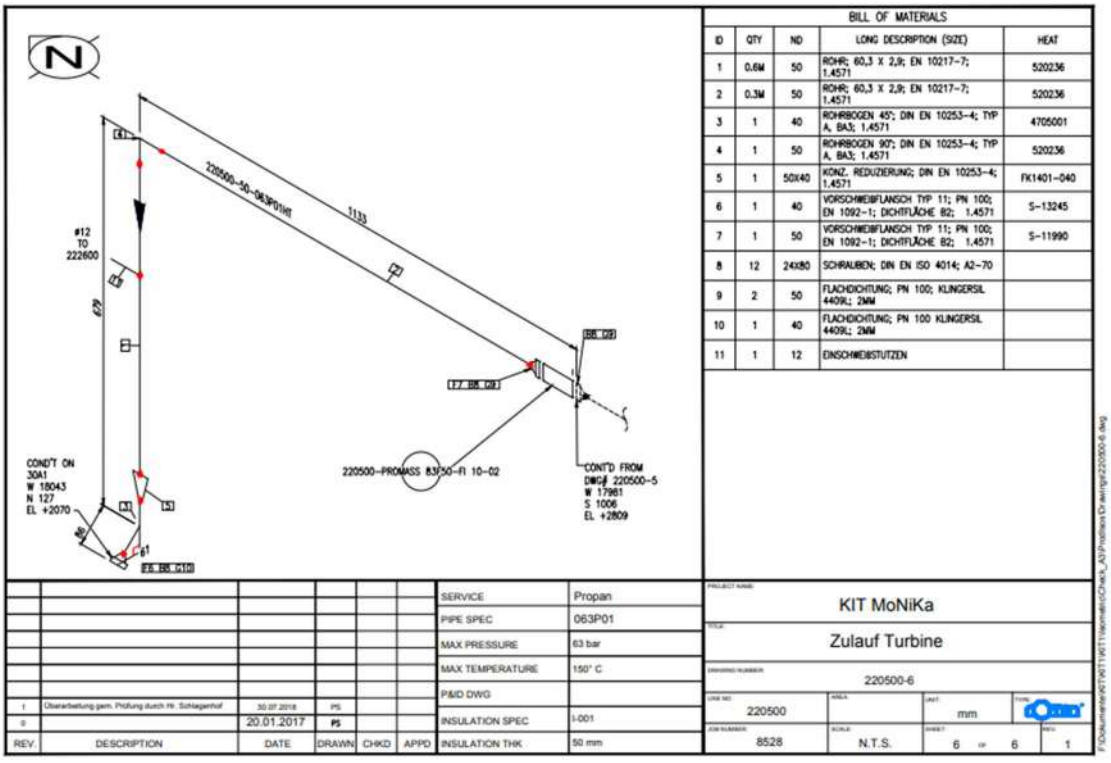

BILL OF MATERIALS				
ID	QTY	ND	LONG DESCRIPTION (SIZE)	HEAT
1	0.6M	50	ROHR; 60,3 X 2,9; EN 10217-7; 1.4571	520236
2	0.3M	50	ROHR; 60,3 X 2,9; EN 10217-7; 1.4571	520236
3	1	40	ROHRBOGEN 45°; DIN EN 10253-4; TYP A, BA3; 1.4571	4705001
4	1	50	ROHRBOGEN 90°; DIN EN 10253-4; TYP A, BA3; 1.4571	520236
5	1	50X40	KONZ. REDUZIERUNG; DIN EN 10253-4; 1.4571	FK1401-040
6	1	40	VORSCHWEIßFLANSCH TYP 11; PN 100; EN 1092-1; DICHTFLÄCHE B2; 1.4571	S-13245
7	1	50	VORSCHWEIßFLANSCH TYP 11; PN 100; EN 1092-1; DICHTFLÄCHE B2; 1.4571	S-11990
8	12	24X80	SCHRAUBEN; DIN EN ISO 4014; A2-70	
9	2	50	FLACHDICHTUNG; PN 100; KLINGERSIL 4409L; 2MM	
10	1	40	FLACHDICHTUNG; PN 100 KLINGERSIL 4409L; 2MM	
11	1	12	EINSCHWEIßSTUTZEN	

REV.	DESCRIPTION	DATE	DRAWN	CHKD	APPD
1	Überarbeitung gem. Prüfung durch Hr. Schlagenhof	30.07.2018	PS		
0		20.01.2017	PS		

SERVICE	Propan
PIPE SPEC	063P01
MAX PRESSURE	63 bar
MAX TEMPERATURE	150° C
P&ID DWG	
INSULATION SPEC	I-001
INSULATION THK	50 mm

KIT MoNiKa

Zulauf Turbine

220500-6

220500 | mm

8528 | N.T.S. | 6 OF 6 | 1

9.2 Calculated efficiency in all the runs

Run 1.1 – Steady state

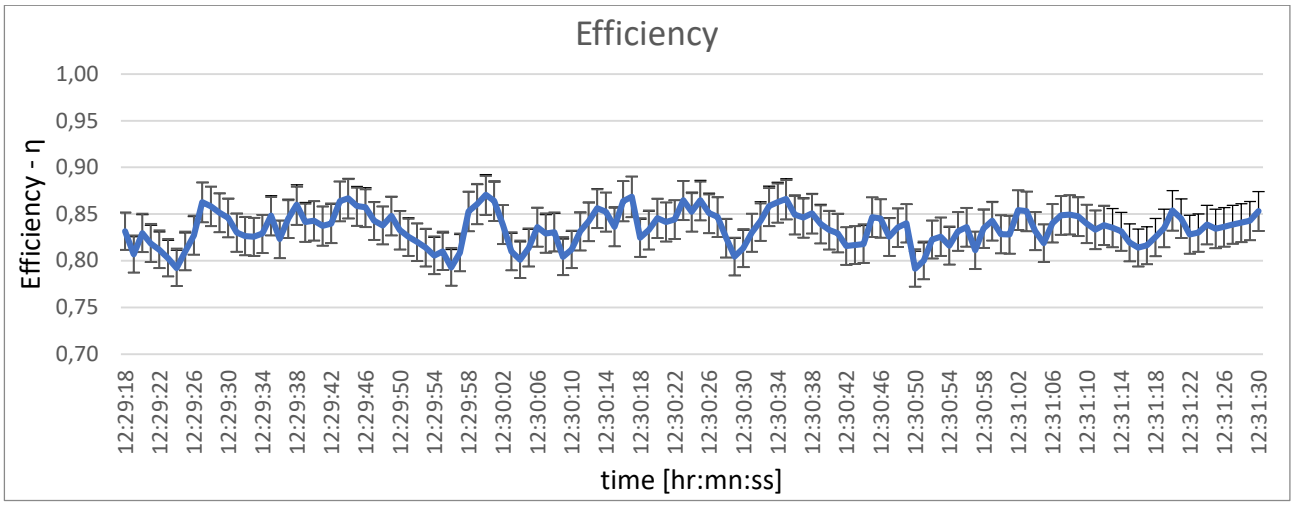

Run 1.2 – Steady state

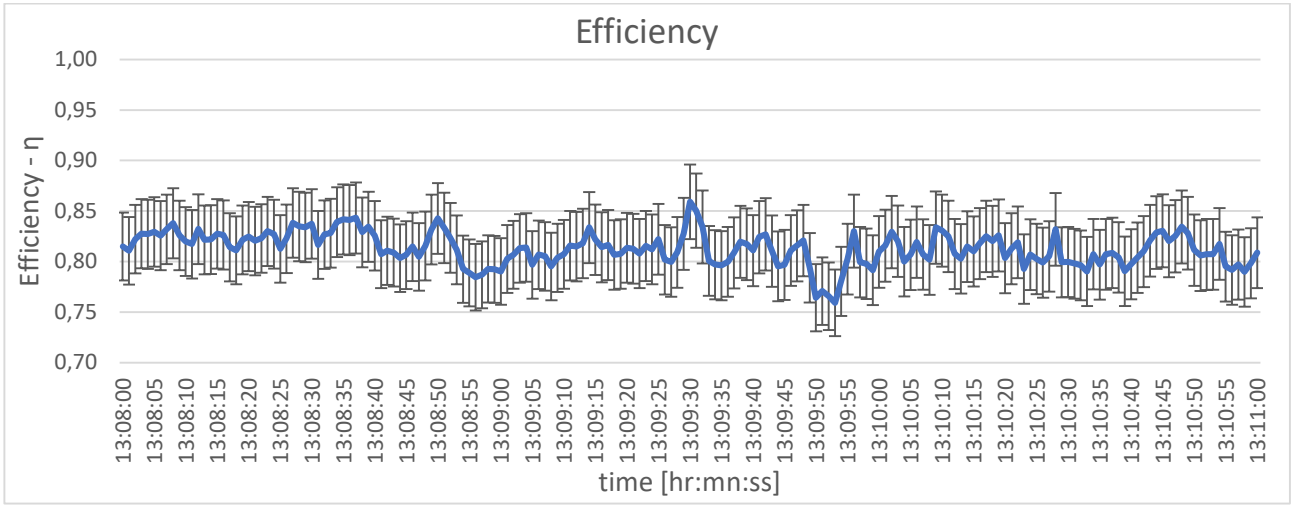

Run 1.3 – Steady state

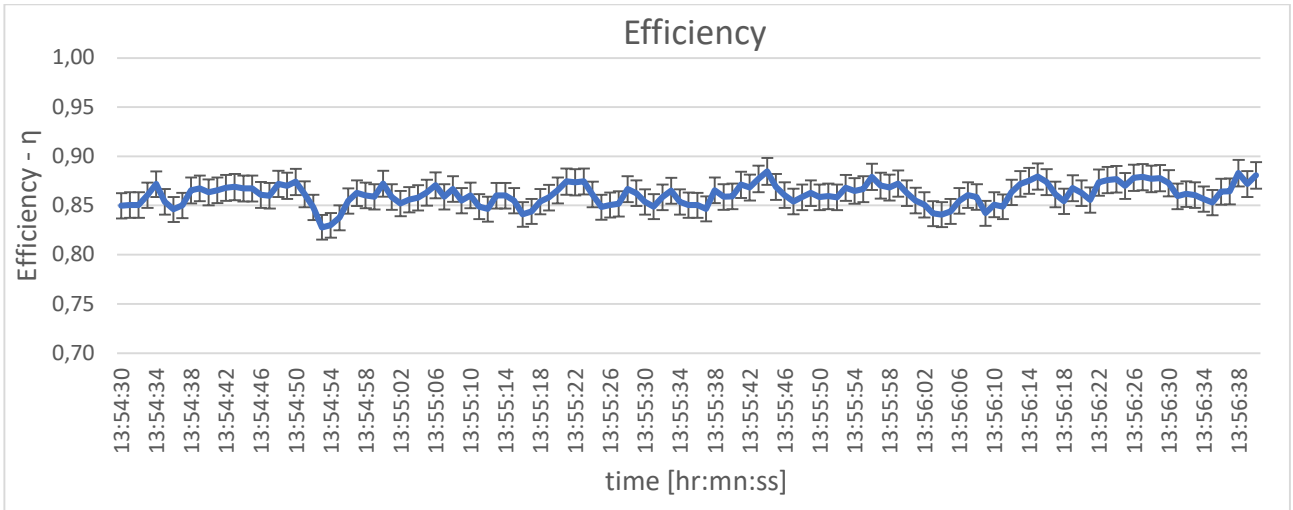

Run 1.4 – Steady state

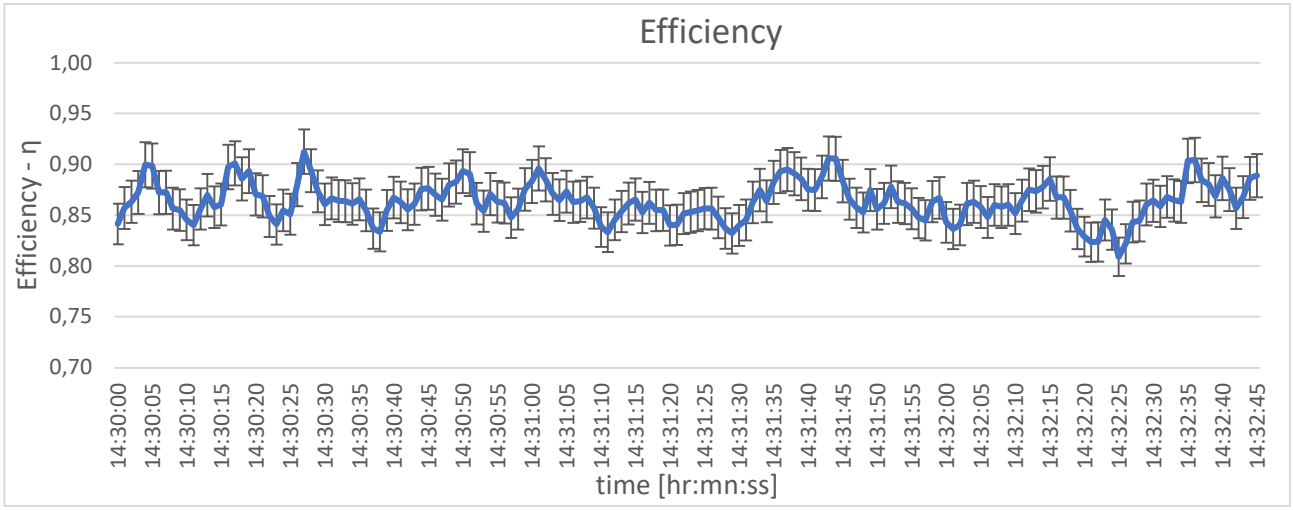

Run 1.5 – Steady state

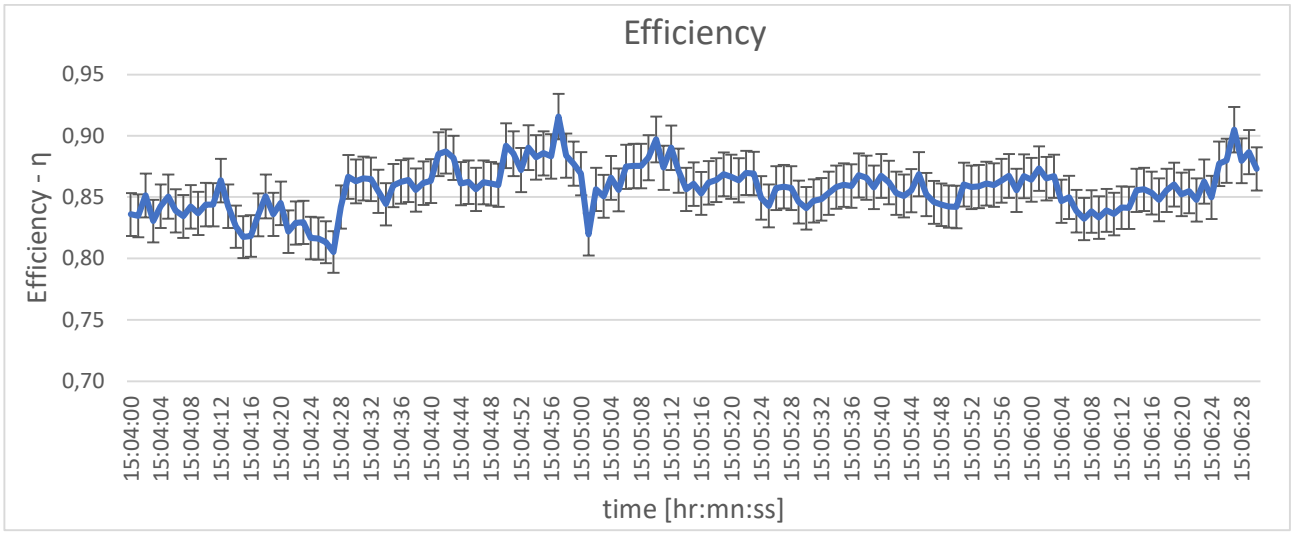

Run 1.6 – Steady state

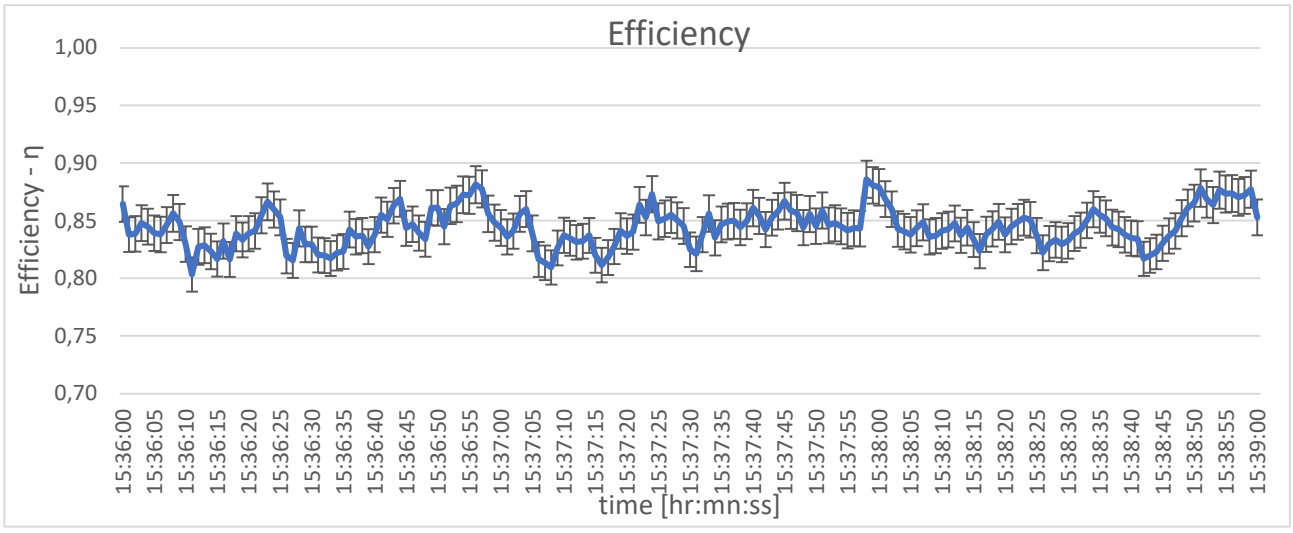

Run 1.7 – Steady state

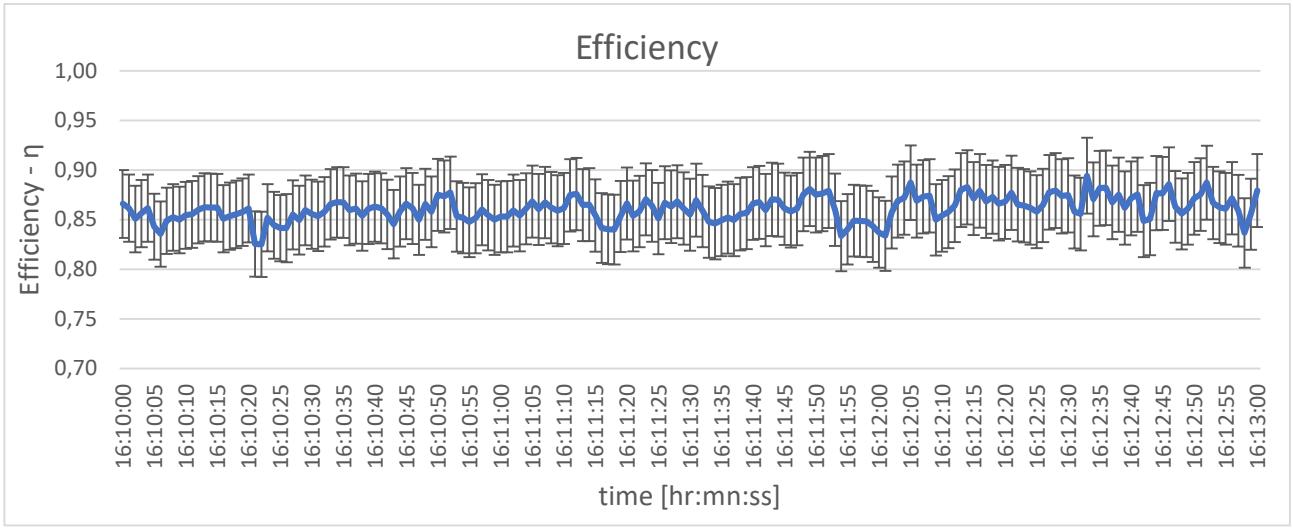

Run 2.1 – Steady state

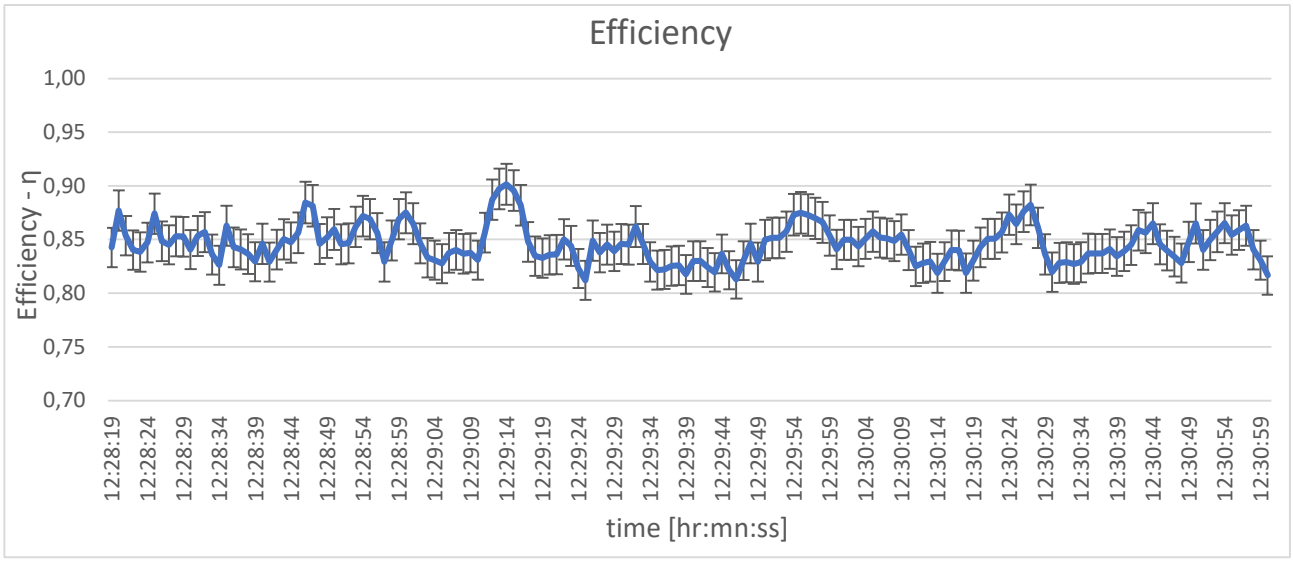

Run 2.2 – Steady state

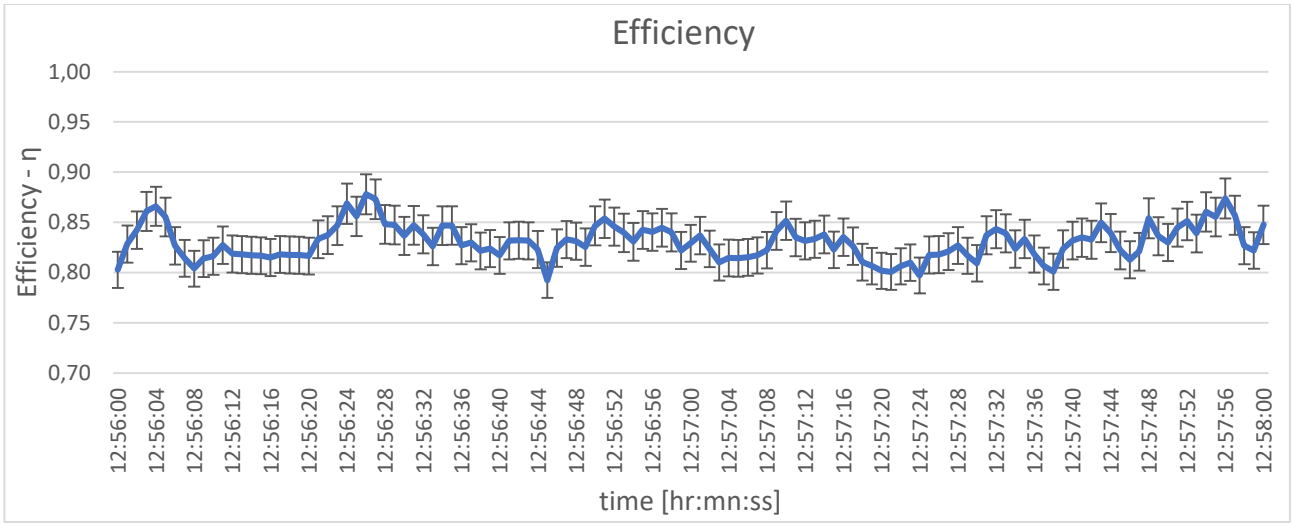

Run 2.3 – Steady state – Already in the work

Run 2.4 – Steady state

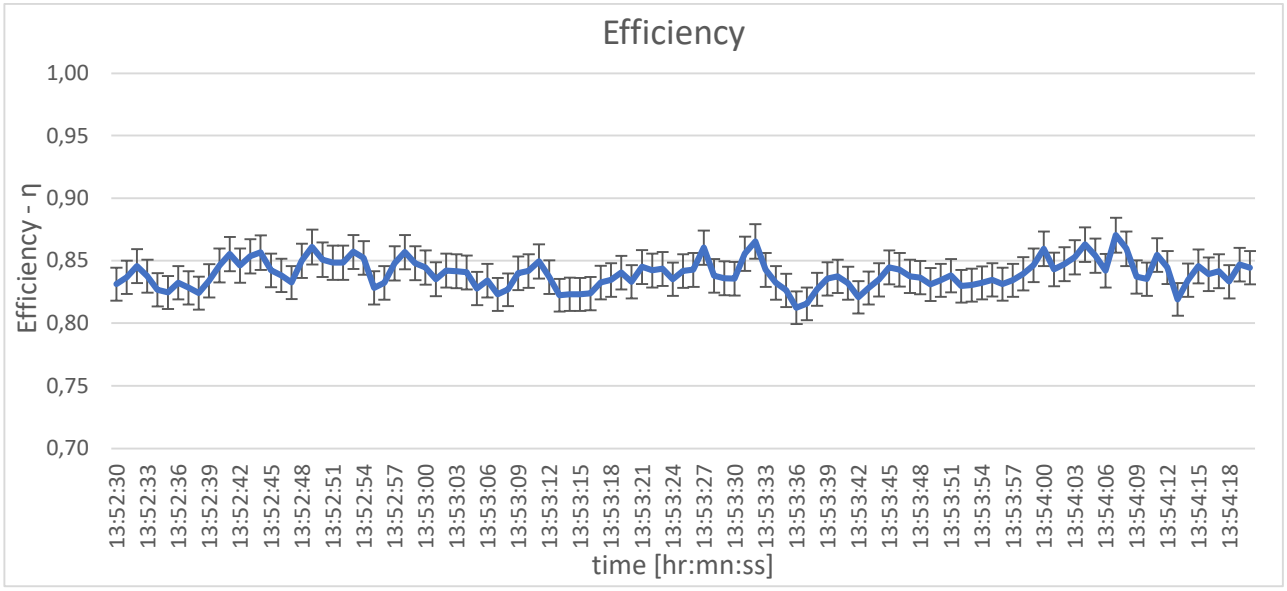

Run 2.5 – Steady state

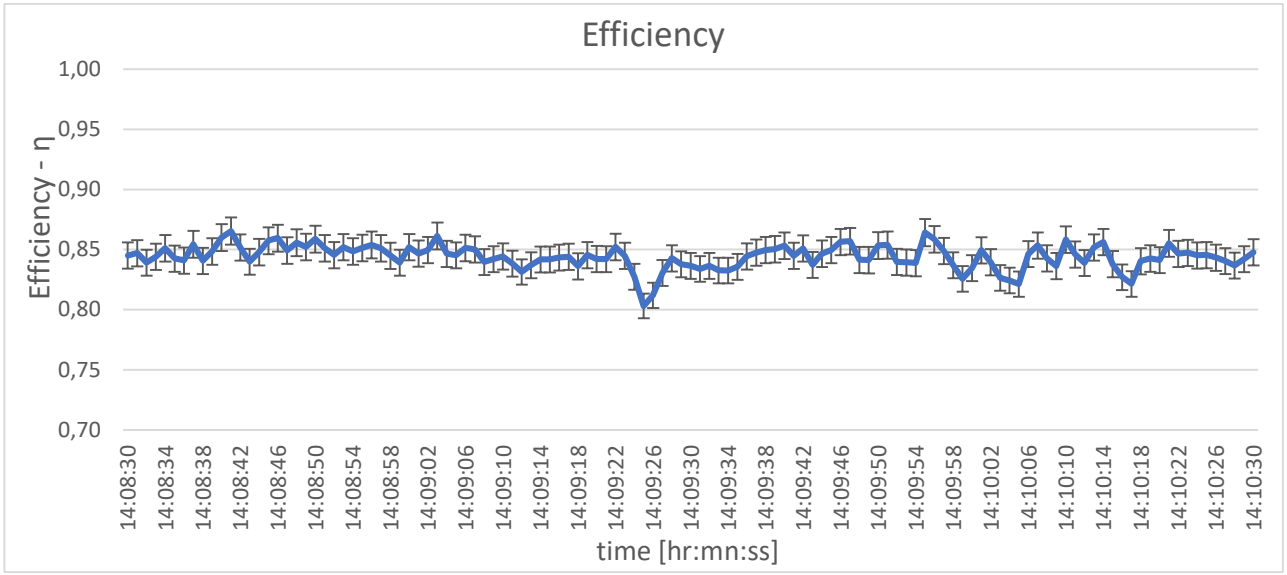

Run 2.6 – Steady state

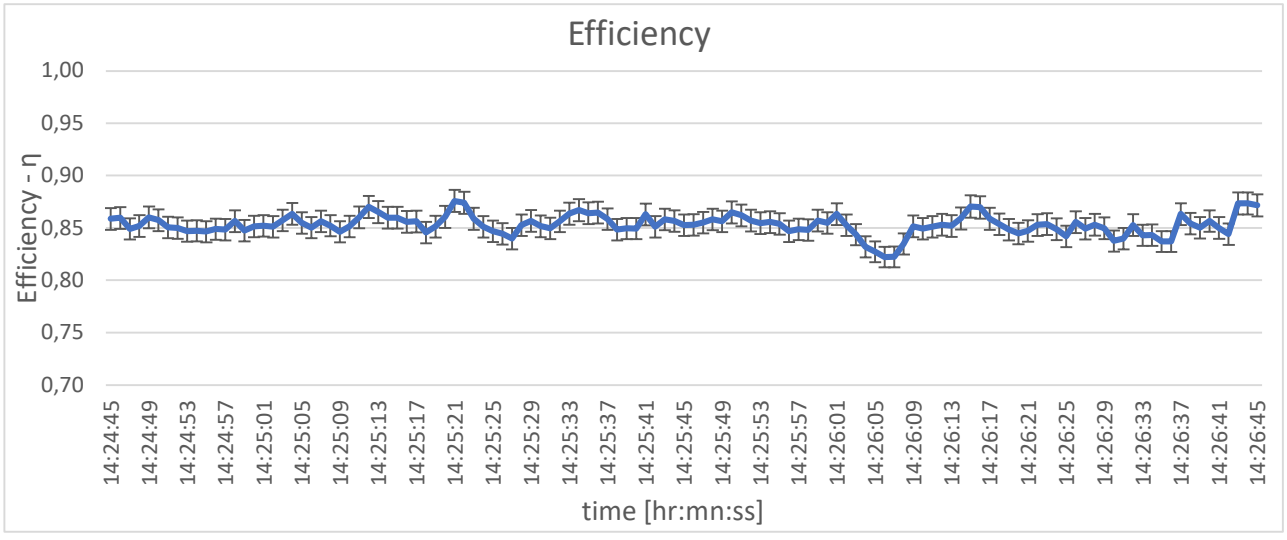

Run 2.7 – Steady state

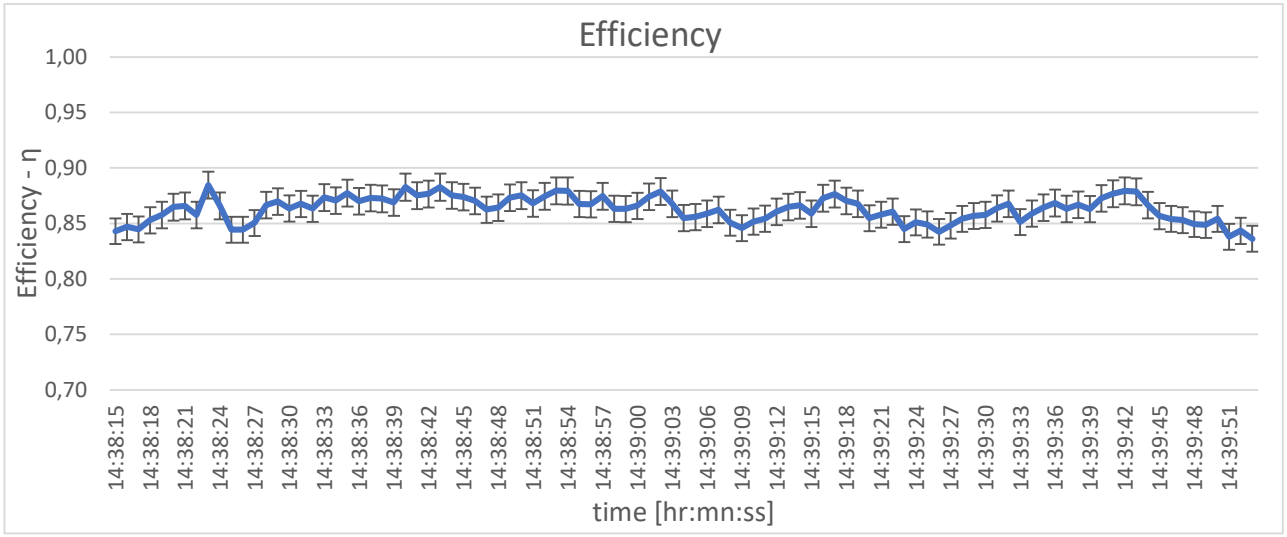

Run 2.8 – Steady state

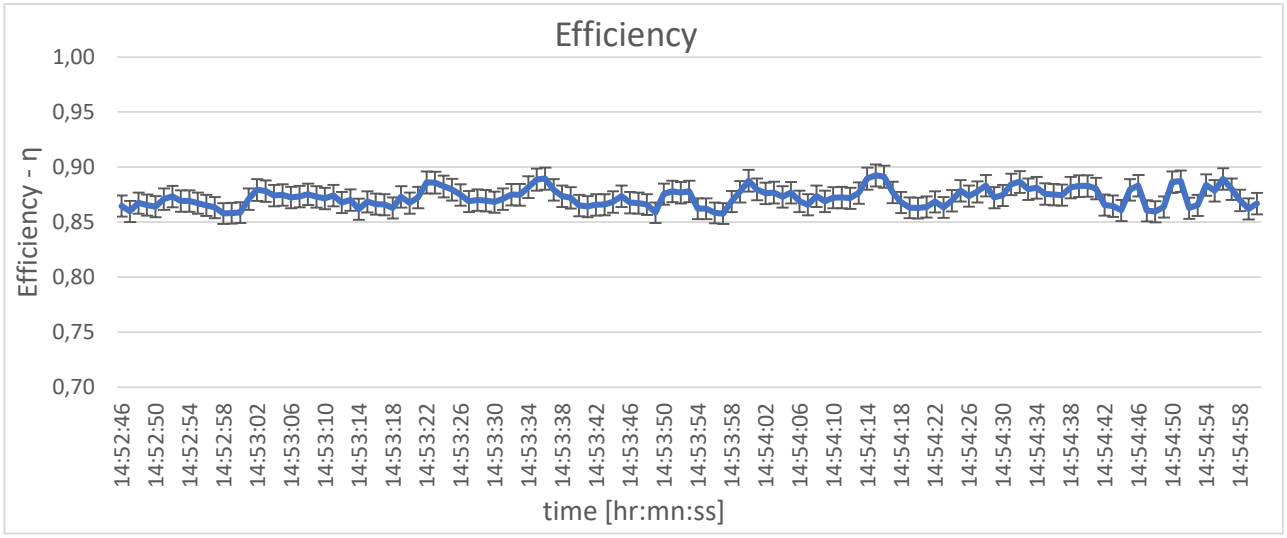

Run 2.9 – Steady state

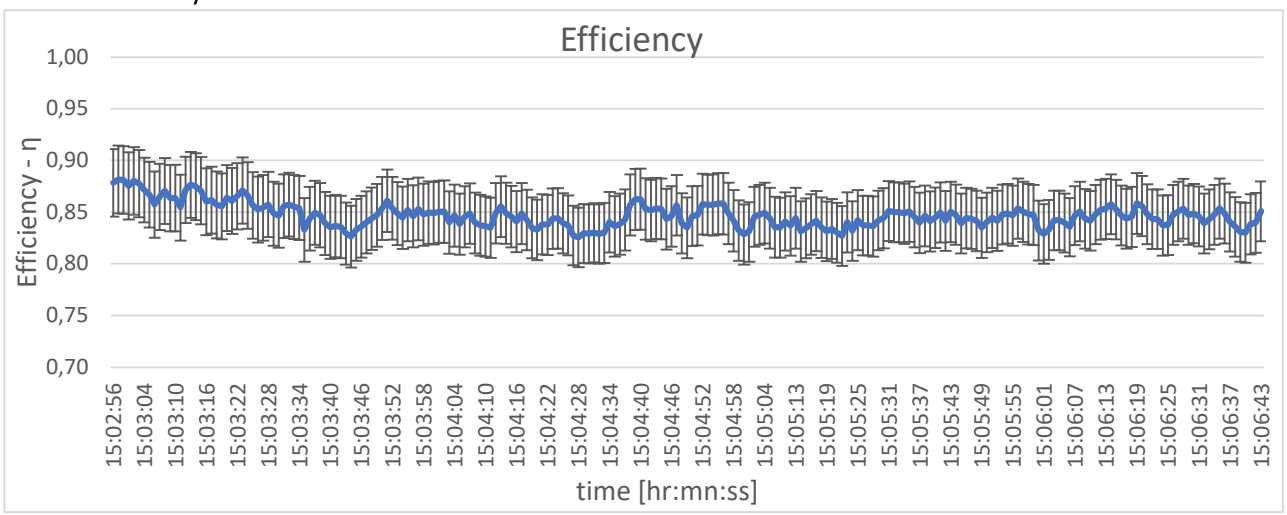

Run 2.10 – Steady state

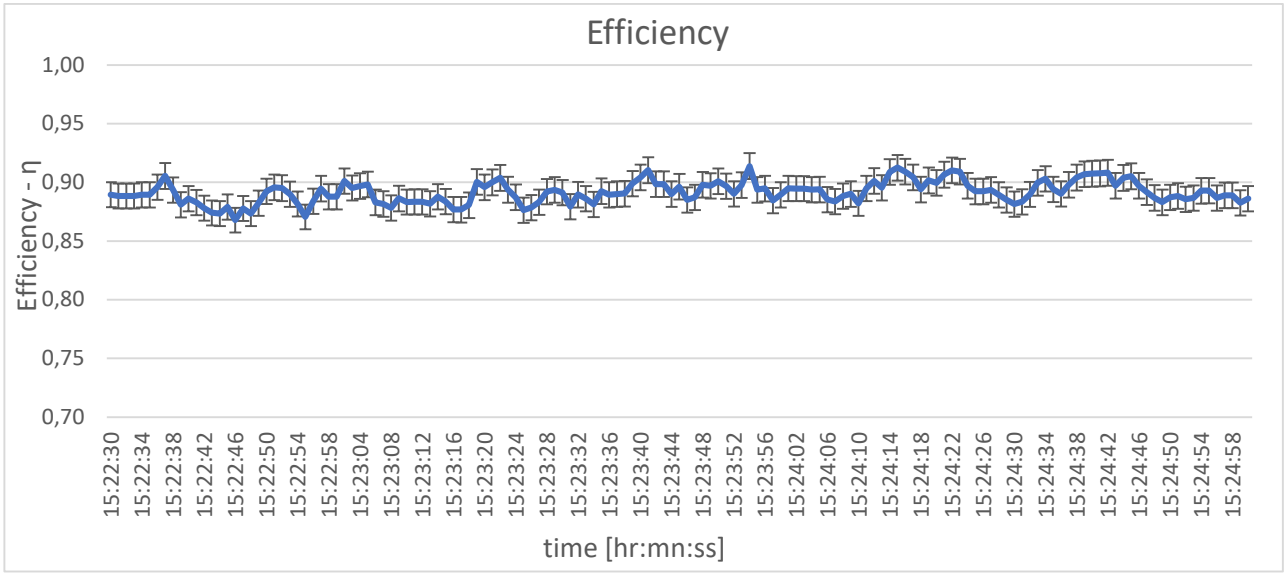

Run 2.11 – Steady state

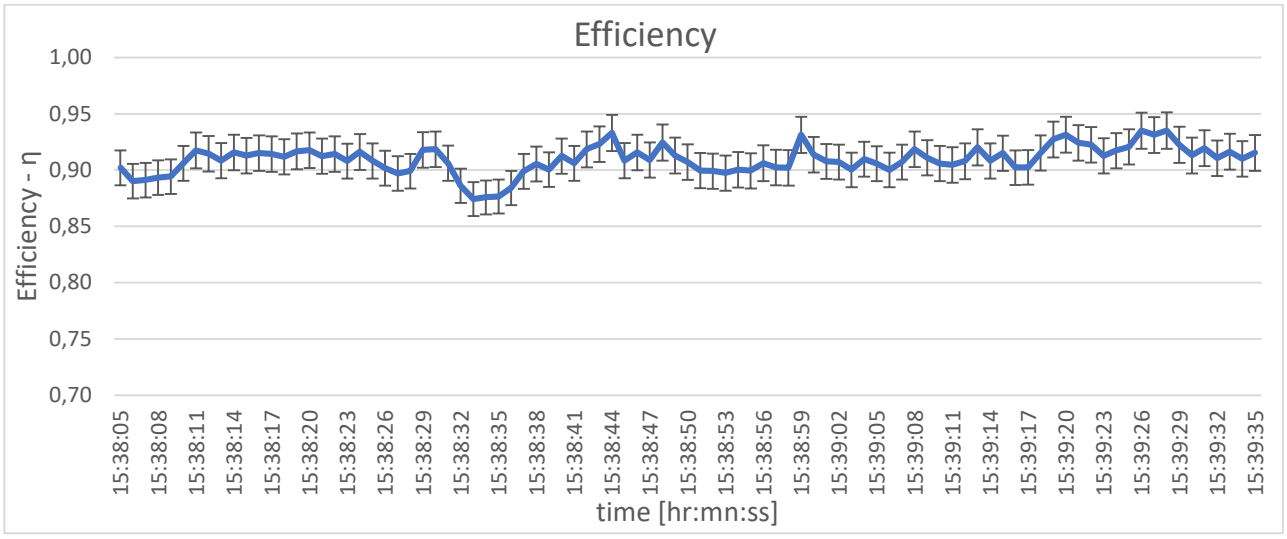

Run 3.1 – Steady state

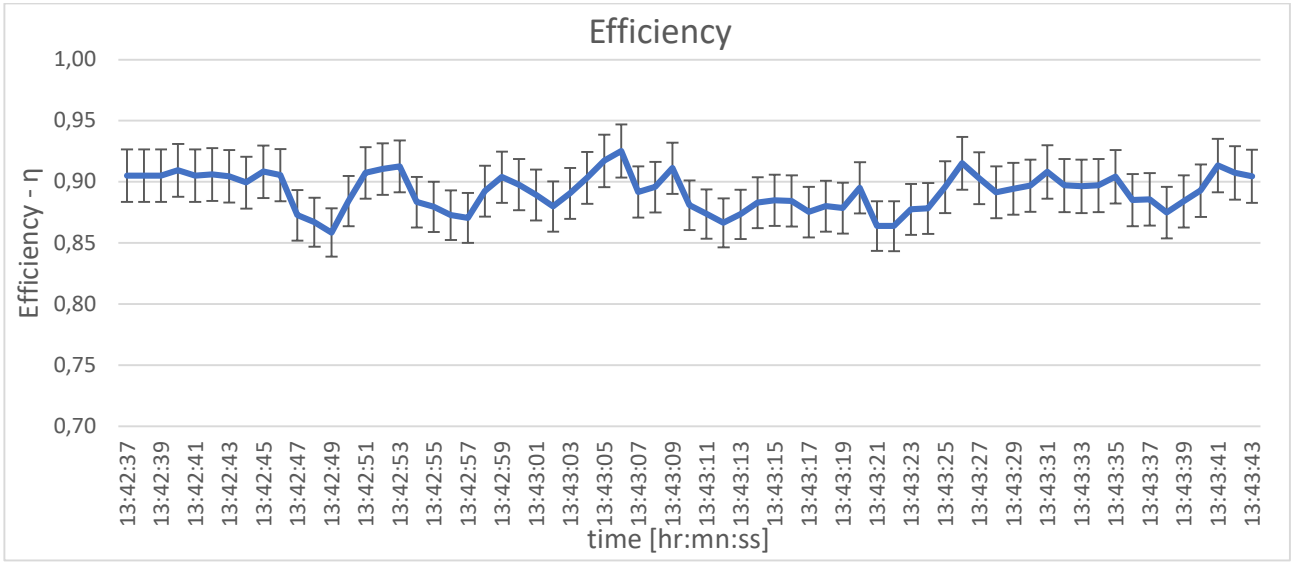

Run 3.2 – Steady state

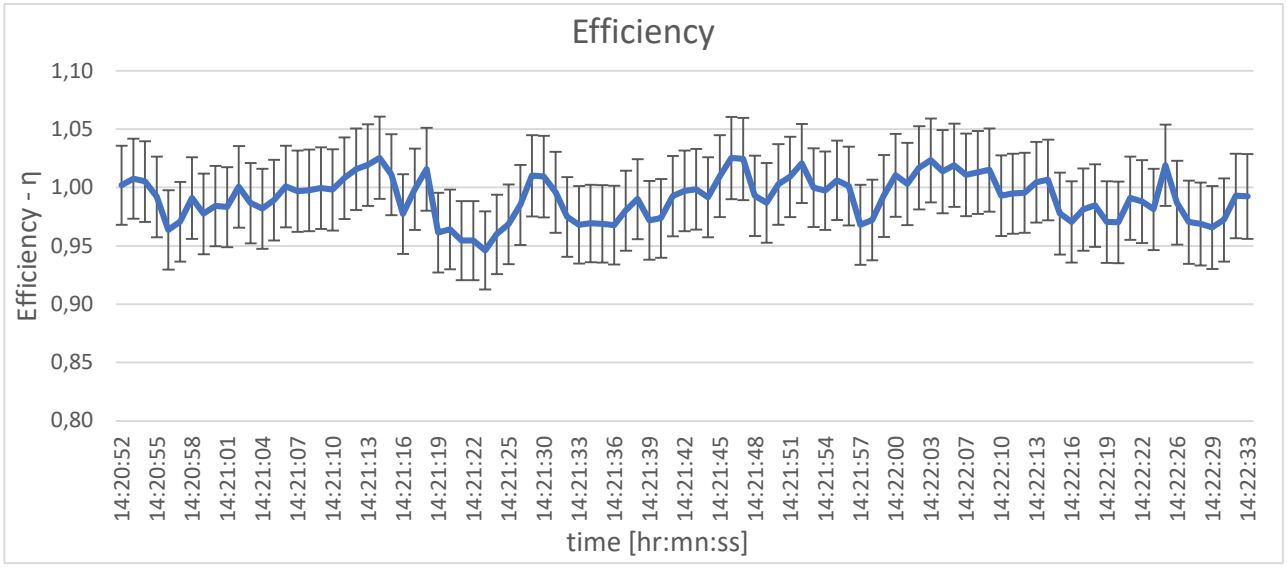

Run 3.4 – Steady state

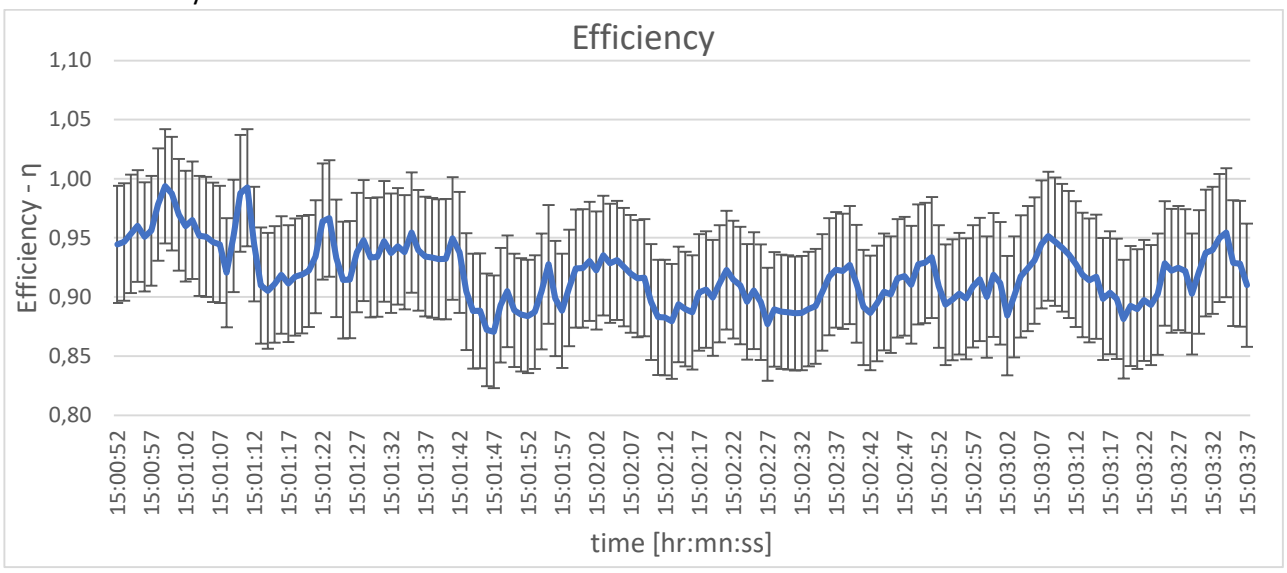

Run 3.5 – Steady state

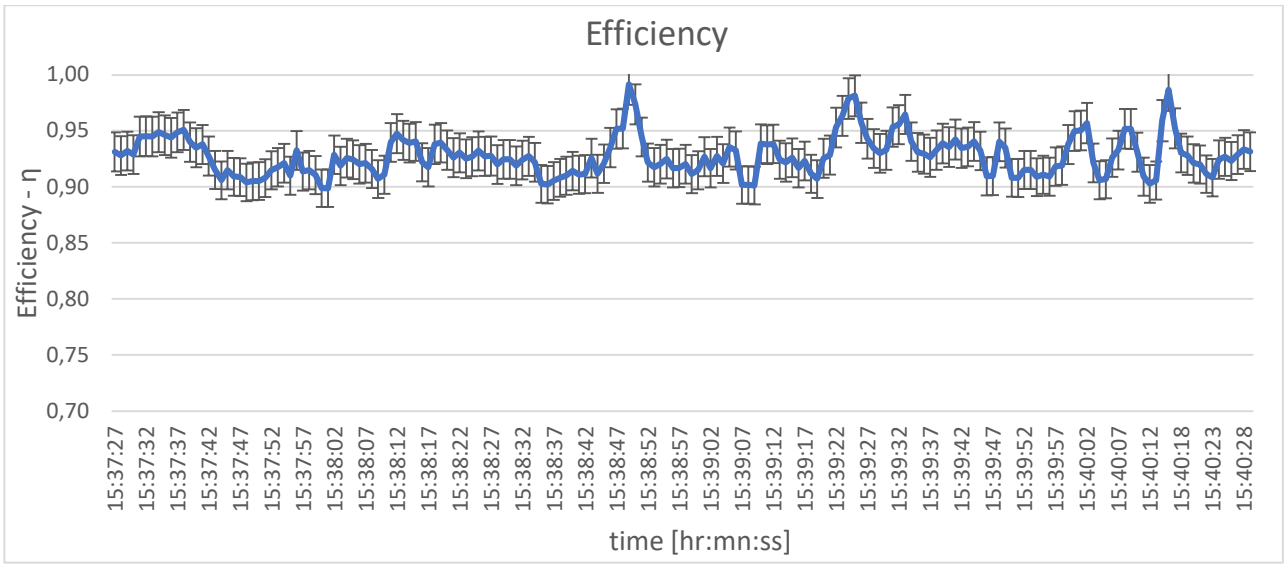

Run 3.6 – Steady state

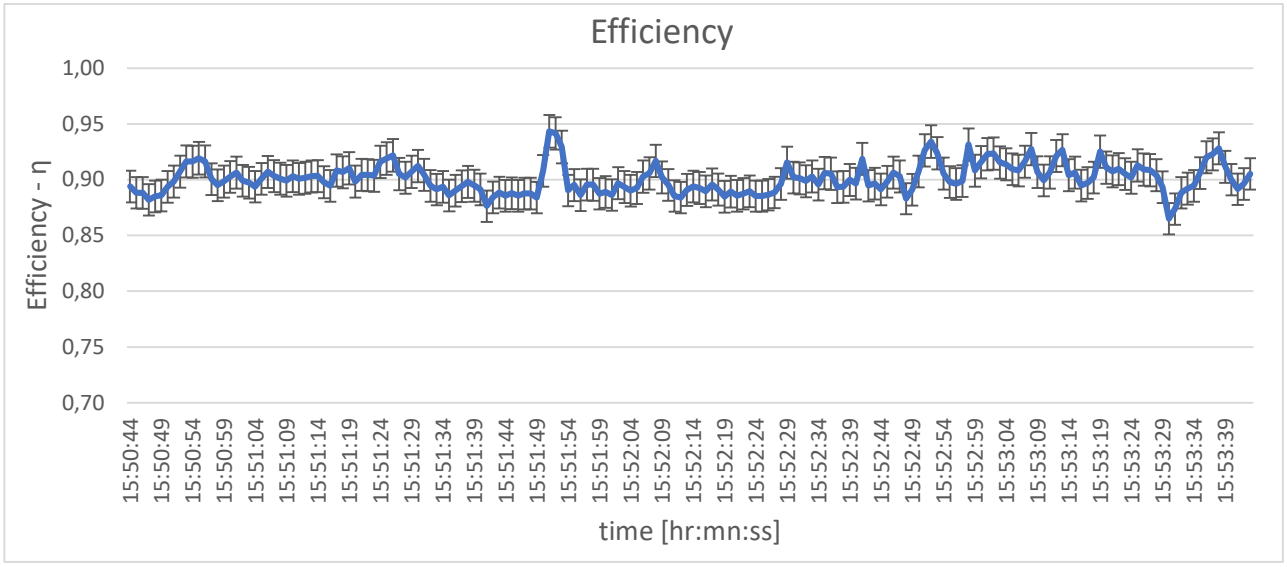

Run 3.7 – Steady state

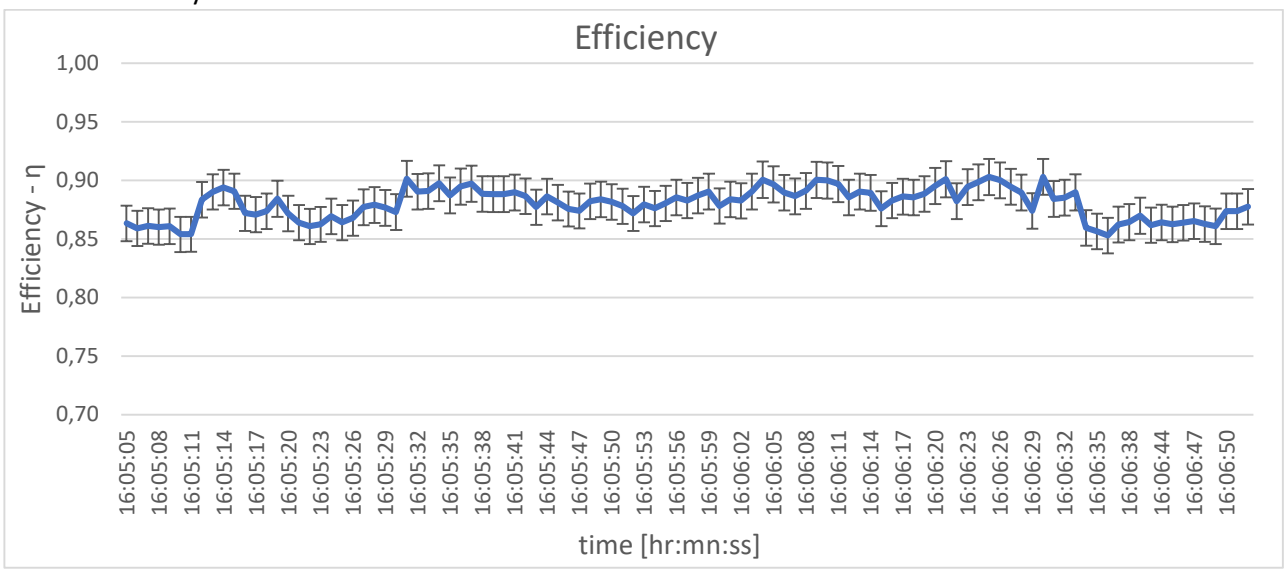

Run 3.8 – Steady state